Impact of LEA29Y expression on myocardial infarction outcome in pigs

von Nadja Theresa Hornaschewitz

Inaugural-Dissertation zur Erlangung der Doktorwürde
der Tierärztlichen Fakultät der Ludwig-Maximilians-Universität
München

Impact of LEA29Y expression on myocardial infarction outcome in pigs

von Nadja Theresa Hornaschewitz

aus Deggendorf

München 2023

Aus dem Veterinärwissenschaftlichen Department der Tierärztlichen Fakultät der Ludwig-Maximilians-Universität München

Lehrstuhl für Molekulare Tierzucht und Biotechnologie

Arbeit angefertigt unter der Leitung

von Univ.-Prof. Dr. Eckhard Wolf

Angefertigt im Klinikum rechts der Isar der Technischen Universität München

Mentor: Prof. Dr. med. Christian Kupatt

Gedruckt mit Genehmigung der Tierärztlichen Fakultät

der Ludwig-Maximilians-Universität München

Dekan:	Univ.-Prof. Dr. Reinhard K. Straubinger, Ph.D.
Berichterstatter:	Univ.-Prof. Dr. Eckhard Wolf
Korreferent/en:	Prof. Dr. Gerhard Wess

Tag der Promotion: 22. Juli 2023

Fia Oma und Opa

und Romeo,

weile ohne eng ned do wa, wo i heid bin und i woas, dassds ollawei vo do om af mi obaschauds, Danke fia Ois!

TABLE OF CONTENTS

INDEX OF ABBREVIATIONS

AAR	Area at risk
Ab	Antibody
ABC	Avidin-biotin complex
APC	Antigen presenting cell(s)
ATP	Adenosine triphosphate
bidest.	Bidistilled
BSA	Bovine serum albumin
bpm	Beats per minute
Ca^{2+}	Calcium ion
CADM1	Cell adhesion molecule 1
CCL	C-C motif chemokine ligand
CD	Cluster of differentiation
cm	Centimeter(s)
cDC	Conventional dendritic cells
Conc.	Concentration
CTLA4	Cytotoxic T-lymphocyte-associated protein 4
Ctr	Control
CX_3CR	CX_3C motif chemokine receptor
CXCl	C-X-C motif chemokine ligand
d	Day(s)
DAB	Diaminobenzidine
DC	Dendritic cells
Dest.	Distilled
DMEM	Dulbecco's Modified Eagle Medium
DMSO	Dimethylsulphoxide
DNA	Deoxyribonucleic acid
dATP	Deoxyadenosine triphosphate
dCTP	Deoxycytidine triphosphate
dGTO	Deoxyguanosine triphosphate
dNTP	Deoxynucleoside triphosphate

dTTP	Deoxythymidine triphosphate
ECG	Electrocardiography
EDTA	Ethylenediaminetetraacetic acid
EDV	End-diastolic volume
EF	Ejection fraction
ELISA	Enzyme-linked-immunosorbent assay
ESV	End-systolic volume
EtOH	Ethanol
F	French
Fc	Fragment crystallizable
FCS	Fetal calf serum
FoxP3	Forkhead-Box-Protein P3
FSC	Forward scatter
g	Gram(s)
h	Hour(s)
H^+	Hydrogen ion, proton
HCl	Hydrochloride acid
HE	Hematoxylin and eosin stain
HLA	Human leucocyte antigen
HRP	Horseradish peroxidase
ICM	Insertable cardiac monitor
ICOS	Inducible T cell costimulator
IFN-γ	Interferon gamma
IgG	Immune globulin G
IgSF	Immunoglobulin super-family
IHC	Immunohistochemistry
IL	Interleukine
I/R	Ischemia/reperfusion
i.v.	Intravenous
J	Joule
KCl	Potassium chloride

kg	Kilogram(s)
l	Liter(s)
LAD	Left anterior descending artery
LCx	Left circumflex artery
LV	Left ventricle
Ly-6C	Lymphocyte antigen 6C
M	Molar
MI	Myocardial infarction
min	Minute(s)
MFI	Median fluorescence intensity
mg	Milligram(s)
MHC	Major histocompatibility complex
ml	Milliliter(s)
mm	Millimeter(s)
mmHg	Millimeter mercury
mmol	Milli mole(s)
Na	Natrium
Na^+	Natrium ion
neg.	negative
ng	Nanogram(s)
nm	Nanometer(s)
ns	Not significant
NSTEMI	Non-ST-segment elevation myocardial infarction
PBMC	Peripheral blood mononuclear cells
PBS	Phosphate-buffered saline
PCR	Polymerase chain reaction
pDC	Plasmacytoid dendritic cells
pH	Negative log of hydrogen ion concentration in a water-based solution
PMA	12-myristate13-acetate
PMN	Polymorphnuclear cells
ROS	Reactive oxygen species

RT	Room temperature
s	Second(s)
SLA	Swine leucocyte antigen
SSC	Side scatter
STEMI	ST-segment elevation myocardial infarction
TAE	Tris acetate buffer
T-bet	T-box expressed in T cells
TBS	Tris buffered saline
TCR	T cell receptor
TGF-β	Transforming growth factor beta
Th1	Type 1 T helper cells
TLR	Toll-like receptor
TMB	Tetramethylbenzidine
TNF-α	Tumor necrosis factor alpha
Tregs	Regulatory T cells
TRIS	Tris(hydroxymethyl)aminomethane
VD	Viability dye
VEGF	Vascular endothelial growth factor
VES	Ventricular extra systoles
VT	Ventricular tachycardia
µl	Microliter(s)
#	Number
-	Negative
+	Positive
°C	Degree Celsius

I. INTRODUCTION

Myocardial infarction (MI), also widely known as heart attack, is a lack in oxygen supply to the myocardium caused by a thrombotic occlusion of a coronary vessel. This ischemia creates a pathological cell death (THYGESEN et al., 2018) and can result in a life-threatening heart failure making MI one of the leading causes of death worldwide (MENSAH et al., 2014). Increased scientific efforts over the years could identify an unhealthy lifestyle as one of the main risk factors for experiencing a heart attack (TIMMIS et al., 2018), as it promotes the often underlying condition of atherosclerosis (LIBBY et al., 2011).

MI causes a complex inflammatory and immune reaction which is crucial for healing and scarring (SWIRSKI & NAHRENDORF, 2018). Already in the first few hours, a large number of immune cells is recruited into the damaged tissue and resident cells in the heart are activated by cytokines and chemokines. Mainly neutrophils and macrophages promote the inflammatory cascade and are responsible for scavenging dead material in the first few days (WAN et al., 2013). After that, it is essential that the inflammatory becomes a reparative phase in the second week after ischemia made up by the disappearance of neutrophils and Ly6C^{low} macrophages (NAHRENDORF et al., 2007). This transition is driven by a reduced production of cytokines and chemokines as well as by T cells (KOLOGRIVOVA et al., 2021). The entire cascade needs to be strictly regulated to achieve a stable scar and the best possible preservation of cardiac function (ERTL & FRANTZ, 2005). It is therefore obvious that interventions or impairments of the immune system can cause disturbances in remodeling. The important role of T lymphocytes in this process has already been demonstrated, since their depletion has led to further heart failure or even a rupture of the left ventricle (WEIRATHER et al., 2014).

While these observations originate from experiments with mice, data on the outcome in immunosuppressed humans are lacking (BOLAD, 2016) although it is possible, for example, that patients after organ transplants suffer an additional myocardial infarction during the subsequent treatment. Belatacept is an often used drug in people after kidney or heart transplantation due to its immunomodulatory effect of blocking the costimulation of T cells (VINCENTI et al., 2016; SHARMA

& SHARMA, 2020). This is a fusion protein, consisting of a modified Fc domain of human IgG and the modified extracellular part of human CTLA4, also known as LEA29Y due to the exchange of two amino acids in this second element (WEKERLE & GRINYÓ, 2012).

It has been successful to generate transgenic pigs that ubiquitously express this protein as a model for general immunosuppression (BÄHR et al., 2016). As swine are one of the most commonly used large animal models for preclinical research based on their high similarity to humans in terms of size and coronary anatomy, these provide the opportunity to investigate effects of an impaired immune system on healing and scarring after myocardial infarction in a high translational manner.

In this work, LEA29Y and wildtype pigs underwent a catheter-based procedure to induce MI followed by reperfusion. Functional and histological measurements in the heart as well as immune cell profiling in the circulation were performed at various time points to detect differences in activation and reaction of the immune system over time.

II. REVIEW OF THE LITERATURE

1. Myocardial infarction (MI)

Cardiovascular diseases (CVD) are the most common cause of death worldwide (MENSAH et al., 2014) and constitute a major challenge for society and the economy, as they are expected to cause costs of up to $47 trillion worldwide between 2010 and 2035 (LASLETT et al., 2012). Alongside strokes, ischemic heart disease account for the largest part of this (GBD 2017 CAUSES OF DEATH COLLABORATORS, 2018) with a total amount of 8.9 million cases in 2019. Therefore the World Health Organization has designated it as the "world´s biggest killer", with the largest increase in deaths since 2000 compared to other illnesses (THE WORLD HEALTH ORGANIZATION, 2023). Myocardial infarction, also referred to as heart attack, often represents the first clinical appearance of ischemic heart disease (MANFROI et al., 2002) and affects over 300000 people in Germany alone every year (DEUTSCHES ZENTRUM FÜR HERZ-KREISLAUF-FORSCHUNG E.V.; 2023).

1.1. Definition and classification

In clinical terms, MI is characterized by acute myocardial injury, as evidenced by abnormal cardiac biomarkers in the presence of acute myocardial ischemia (THYGESEN et al., 2018).

Not least thanks to the discovery of more sensitive biomarkers, this general definition has been repeatedly expanded and adapted to scientific standards since the 1950s to 1970s when the World Health Organization has announced the first electrocardiographic-based declaration (CHAPMAN et al., 2020). Thereby the term acute myocardial injury is used for an elevation of cardiac troponin values (cTn) with at least one value above the 99th percentile upper reference limit (LEDWOCH et al., 2022). Furthermore, an acute MI exists if, in addition to the myocardial injury, at least one of the following criteria is fulfilled:

- symptoms of myocardial ischemia
- new ischemic ECG changes
- pathological Q waves in the ECG
- loss of viable myocardium or regional wall motion abnormalities in imaging

- presence of a coronary thrombus by angiography or autopsy.

Regarding pathological and clinical differences as well as treatment strategies, myocardial infarction is further classified in five different types shown in Table 1 (THYGESEN et al., 2007; THYGESEN et al., 2018).

Type	Clinical classification and pathogenesis
1	Spontaneous MI caused by a rupture or erosion of an atherosclerotic plaque as a consequence of coronary artery disease (CADENAS et al.)
2	MI as a result of an increased oxygen demand or decreased supply caused e.g. by fixed coronary atherosclerosis, coronary spasm, non-atherosclerotic coronary dissection or arrhythmias
3	Spontaneous cardiac death with symptoms of MI before cardiac biomarkers increase or even blood can be sampled or a thrombus is detected by autopsy
	MI associated with coronary revascularization procedures like
4 A	Percutaneous coronary intervention (PCI)
B	Stent thrombosis
C	In-stent restenosis or restenosis after angiography
5	Coronary artery bypass grafting (CABG)

Table 1: Classification of myocardial infarction.

For a quick and optimal treatment, patients in the clinic are often categorized as ST-segment elevation myocardial infarction (STEMI) (IBANEZ et al., 2018) or non-ST-segment elevation myocardial infarction (NSTEMI) (ROFFI et al., 2016) according to ECG measurements. Nowadays NSTEMI is the more common phenotype (MCMANUS et al., 2011) with a less frequently occurring total occlusion of a coronary vessel (WANG et al., 2009). The management of these cases depends on the condition and risk assessment of each patient reaching from a conservative to an urgent angiography treatment for very high-risk patients. In contrast, in the case of a STEMI, immediate reperfusion by primary percutaneous coronary intervention (PCI) or fibrinolytic therapy is indicated due to the complete occlusion (MITSIS & GRAGNANO, 2021). This type further shows a higher risk for early complications, like cardiogenic shock (HOLMES et al., 1999; BAJPAI et al.). At one year follow-up both types show a mortality of about 10% (ROFFI et al., 2016; IBANEZ et al., 2018).

1.2. Epidemiology

The incidence and mortality of myocardial infarction increases with age (BARAKAT et al., 1999). The most common fatal cases are seen at seniority ≥70 years (GBD 2017 CAUSES OF DEATH COLLABORATORS, 2018). This may be related to the fact that these patients due to their age are anyway in a compromised state of health with a higher risk for further disorders. Comorbidities, on the other hand, are also increasingly being observed in younger people as a cause of MI (GULATI et al., 2020). Thereby women are less likely to suffer from MI than men (TIMMIS et al., 2018) but are hospitalized more often and have a higher mortality rate (CANTO et al., 2012). Also the family history can be decisive. Especially if the mother or a sibling is affected and the myocardial infarction occurs before the 50th year of life, such clustering should not be ruled out (NIELSEN et al., 2013).

Basically, the INTERHEART study could identify nine critical points responsible for over 90% of the total risk for MI all over the world (YUSUF et al., 2004). One of them is the importance of psychosocial factors, which should not be underestimated. Personal exceptional situations can increase the risk of a heart attack as is shown, for example, by the Takotsubo syndrome (SUNDARAM et al.). In this case mostly post-menopausal women suffer from myocardial infarction triggered by intense emotional stress why it is also known as “broken heart” syndrome (MANOLIS et al., 2023). External influences can have an impact, too, as observed during environmental disasters or even sporting events (KELLER et al., 2021). All other causes are health behaviours and risk factors associated with an unhealthy lifestyle or other health problems as they occur in our western world and particularly in high-income states.

1.2.1. Health behaviours

A proper diet and physical activity are the cornerstones of a healthy life. The intake of only 375-500 g of fruits, vegetables and legumes per day is associated with lower all-cause mortality (MILLER et al., 2017) and physical activity can reduce the risk of death by 16-30%, with a beneficial effect even with very little activity (EKELUND et al., 2015). Furthermore, any alcohol consumption can immediately increase the cardiovascular risk (MOSTOFSKY et al., 2016) and also smoking should be avoided. Contrary to many opinions, e-cigarettes also carry danger that is less than in traditional smoking but cannot be ignored (SHARMA et al., 2023).

1.2.2. Risk factors

In relation with an unhealthy lifestyle many patients suffering from myocardial infarction show a systolic blood pressure of ≥140 mmHg or diastolic ≥90 mmHg, which is defined as hypertension (PEDRINELLI et al., 2012). Also hypercholesterolaemia with values ≥6.2 mmol/l increases the risk of MI and is most often found in high-income countries. The potential of this problem to reduce the cases of atherosclerosis has already been recognised years ago and thus it is often the topic of awareness programmes and strategies (GLANZ, 1988). Closely related to this is obesity which is occurring more and more frequently in all age groups worldwide (WANG & BEYDOUN, 2007). Rising prevalence is also recorded for diabetes as a further risk factor and associated disease (DAL CANTO et al., 2019).

1.3. Pathophysiology

MI is pathologically defined as myocardial cell necrosis as a result of a significant and sustained ischemia. As described above, it is mostly caused by atherosclerosis-related coronary heart disease (MENDIS et al., 2011). Atherosclerosis is a multifocal, immunoinflammatory, chronic disease of the wall of large and medium-sized arteries fuelled by lipid. Initially, the endothelium becomes leaky due to damage or dysfunction (LIANG et al., 2020) so that it is possible for cholesterol-containing low-density lipoproteins (LDL) in the blood to extravasate into the subendothelial space. These are retained and modified (e.g. oxidized) and become cytotoxic, proinflammatory and chemotactic. Monocytes are directed into the lamina intima and mature into macrophages which assimilate the lipids and become foam cells. During development of a plaque, smooth muscle cells (SMCs) and extracellular matrix macromolecules, like collagen, migrate and proliferate in the intima. An advanced plaque often contains lipid from dead macrophages in its core or even cholesterol crystals or microvessels (LIBBY et al., 2011). During atherogenesis, erosion and healing occur repeatedly, exposing subendothelial tissue and triggering platelet binding. This leads to fibrin formation and gives the plaque a fibrous cap, which is important for stabilization. Atherosclerosis can be asymptomatic for years or plaques can become confluent over a longer period of time and gradually narrow the vessel lumen. The greatest danger, however, is the rupture of fibrous plaques causing 76% of all fatal cases of MI (FALK, 2006). For a variety of reasons related to the plaque itself, such as a thinning of the fibrous cap or also related to enhanced shear stresses, the plaque may rupture. Thereby a tear in

the cap exposes the highly thrombogenic core to the blood (BENTZON et al., 2014) and platelets can bind, activating the blood coagulation cascade and leading to acute atherothrombosis (BADIMON & VILAHUR, 2014). The resulting thrombus induces coronary occlusion which causes myocardial cell death in a transmural wave front beginning in the subendocardium and extending towards the epicardium (REIMER et al., 1977). Besides apoptosis (CHEN et al., 2021), mainly necroptosis also occurs as a form of regulated necrosis (ZHANG et al., 2016).

1.4. Immune response and remodeling

Of course, the ischemia and the resulting cell death trigger an extensive immune reaction in response to sterile inflammation (DEBERGE et al., 2021) which is divided into different phases (PRABHU & FRANGOGIANNIS, 2016). Additionally, the reperfusion, which is established as therapy to revert the coronary occlusion, poses a risk to the affected cardiac tissue itself.

1.4.1. Ischemia/reperfusion injury

Efforts in the treatment of myocardial infarction are usually aimed at a quick reperfusion of the ischemic area in order to keep tissue loss as low as possible and to preserve the myocardium in the border area of the ischemia, the so-called border zone (SINGH & COHEN, 2014). Indeed, this can also cause additional tissue damage and dysfunction and counteract the positive aspect of recirculation (HAUSENLOY & YELLON, 2013). This phenomenon is therefore called ischemia/reperfusion (I/R) injury and can determine up to 50% of the final infarct size.

It is caused by a number of metabolic changes aimed at compensating for the acidosis developed during ischemia. Seconds after the occlusion of a coronary vessel, cardiomyocytes switch to anaerobic glycolysis to ensure the minimum energy supply necessary for their survival and maintenance of contractility. In this process, the energy-providing pyruvate is converted into lactate with the production of H^+, which accumulates intracellularly. The resulting pH change in ischemia should be compensated during reperfusion, hence H^+ is transported out of the cells in exchange for Na^+ (FRANK et al., 2012). To avoid again an increased level of Na^+ within cardiomyocytes, the sarcolemmal $2Na^+/Ca^{2+}$ exchanger becomes activated and brings Ca^{2+} ions into the cells which in turn can lead to a Ca^{2+} overload and cell death (HAUSENLOY & YELLON, 2013). Furthermore, calcium

phosphate complexes can form, which are counted among the group of damage-associated molecular patterns (DAMPs). These can bind to toll-like receptors (TLR) as well as intracellular protein complexes, so called inflammasomes that induce the secretion of interleukin-1β (IL-1β) and thus constitute the basis for the triggered inflammatory reaction following myocardial infarction and reperfusion. The activation of these intracellular protein complexes is also due to emerging reactive oxygen species (ROS) (ZWEIER et al., 1987; KAWAGUCHI et al., 2011). The resulting oxidative stress can affect mitochondrial function and thereby further disrupt respiratory chain activity (PETROSILLO et al., 2003; PARADIES et al., 2004).

In the worst case, the reperfusion associated damage can lead to further cell death called lethal myocardial reperfusion injury (IBANEZ et al., 2011). There the above-mentioned metabolic changes lead to the opening of the mitochondrial permeability transition pore (MPTP). Opening of this nonselective channel leads to membrane depolarization and finally cell death due to uncoupling of oxidative phosphorylation and ATP loss (HEUSCH et al., 2010).

Clinically, the reperfusion injury can manifest in the form of reversible arrhythmias (MANNING & HEARSE, 1984) or a prolonged contractile dysfunction after ischemia called myocardial stunning (BRAUNWALD & KLONER, 1982). In addition, an irreversible microvascular obstruction (MVO) can occur (KRUG et al., 1966), caused by capillary damage (KLONER et al., 2018) or occlusion due to plaque material or blood cells like platelets or neutrophils (ARAKAWA et al., 2009). In the latter case, this happens as a result of the already present immune reaction. The secretion of a variety of cytokines (e.g. IL-1β, IL-6 or TNF-α) and chemokines (e.g. CCL-2, CXCL-2) after stimulation of inflammasomes and TLR (NEWTON & DIXIT, 2012) triggers leucocyte influx into the affected myocardium and activates a polyphasic cascade of inflammation and immune response (HINKEL et al., 2012).

1.4.2. Inflammation phase

The inflammatory phase in the first hours to days after the ischemia is characterized by the recruitment of neutrophils and monocytes. They come from different sources, first of all, cells of the patrolling cells in the peripheral blood are attracted (SWIRSKI & NAHRENDORF, 2018). Further, cardiac fibroblasts produce

haematopoietic growth factors like the granulocyte/macrophage colony-stimulating factor (GM-CSF) and promote the maturation of haematopoietic stem and progenitor cells (HSPCs) in the bone marrow (ANZAI et al., 2017). In addition, angiotensin-2 signalling induces the release from extramedullary reservoirs, like the spleen, into the circulation (SWIRSKI et al., 2009). However, not only are additional cells recruited, but existing ones are also activated. The heart muscle of a healthy adult mouse, for example, shows all major leukocyte classes and numerical even 12-fold more compared to a skeletal muscle (RAMOS et al., 2017). The most prominent population of it are macrophages with a portion of 7-8% of all leucocytes (HEIDT et al., 2014). In addition to cardiomyocytes (GWECHENBERGER et al., 1999), resident macrophages in turn attract further monocytes and drive the inflammation through the secretion of pro-inflammatory cytokines and chemokines such as CC-chemokine ligand 2 (CCL2) (SHI et al., 2011; BAJPAI et al., 2019), IL-6, IL-1β and TNF-α (SHAPOURI-MOGHADDAM et al., 2018). Polymorphnuclear cells (PMN) are the first to accumulate in the inflammatory site (approximately 10^5 cells/mg tissue) (NAHRENDORF et al., 2007). They contain granules with a variety of proteins and enzymes (MA et al., 2013) and are followed by monocytes that differentiate into cardiac macrophages (COILLARD & SEGURA, 2019). It is known that there are two different subtypes of macrophages, so called M1 or lymphocyte antigen 6C high (Ly-6C^{high}) and M2 or Ly-6C^{low} and both play a key role in infarct healing. While either are released from the spleen, only Ly-6C^{high} are immediately recruited to the ischemic myocardium (SWIRSKI et al., 2009) due to CCL2 expression. They predominate with a share of 75% of all monocytes from day 1 to 4 within the damaged tissue (NAHRENDORF et al., 2007) and produce pro-inflammatory cytokines as described above (SHAPOURI-MOGHADDAM et al., 2018). The main function of these leucocytes during the first inflammation phase is the phagocytosis of dead cells in combination with the degradation of extracellular matrix (KOLOGRIVOVA et al., 2021), which is determined as efferocytosis (YOSHIMURA et al., 2020). This is an active process with the formation of proteolytic enzymes and the contribution of various receptors such as the macrophage efferocytosis tyrosine- kinase (MERTK) (WAN et al., 2013).

1.4.3. Reparation and proliferation phase

As they are the first to appear, neutrophils are also the first to disappear from the inflammation. While the number already declines from the third day, they have almost completely vanished one week after MI (SWIRSKI & NAHRENDORF, 2018). During this lifespan, there is continuous shift in their proteome starting with a prevailing production of metalloproteinases on day one through an increase of apoptosis on day three up to a reparative character on day seven, expressing fibronectin, galactin-3 and fibrinogen. By that, neutrophils enable a reorganization in the extracellular matrix and contribute on the one hand because of this to scar formation (DASEKE et al., 2019). On the other hand, they polarize macrophages towards the reparative M2 subpopulation (HORCKMANS et al., 2017) that are the predominant monocytes from day five on (NAHRENDORF et al., 2007). This switch is further driven by a variety of factors with a suspected participation of T cells (SAXENA et al., 2014). Intrinsic factors such as nuclear receptor subfamily 4 group A member 1 (Nr4a1) limit the influx of M1 macrophages as well as their production of pro-inflammatory cytokines (HILGENDORF et al., 2014). In addition, the ischemic myocardium specifically recruits M2 macrophages by the expression of fractalkine, a chemokine which receptor is CX_3CR1 that is highly expressed by Ly-$6C^{low}$ macrophages. The result of this transition is the production of IL-10, TGF-β and VEGF. In addition to preventing further inflammation, this leads to activation of cardiac fibroblasts, hence collagen synthesis, as well as angiogenesis and thus forms the basis for a sufficient healing and scarring (NAHRENDORF et al., 2007).

1.4.4. Maturation phase

During the weeks after ischemia the aim is to replace lost tissue to prevent myocardial rupture and preserve heart function as well as possible. The problem with this is that cardiomyocytes cannot regenerate and replacement can only take place in the form of a scar (FURTADO et al., 2016). For a proper formation of this, a balanced turnover of extracellular matrix is crucial. Therefore, matrix metalloproteinases remove, while activated, α-smooth muscle actin (α-SMA) positive myofibroblasts produce collagen type I (CHOU et al., 2018; NOTOHAMIPRODJO et al., 2022). These cells also provide a contractile potential that can lead to shrinkage of the scar and thus influence the recorded infarct size (HOLMES et al., 1994; YOKOTA et al., 2020).

1.4.5. Remodeling

The totality of these reactions to the damage of the heart is summarized as remodeling. First used in the 20th century, the meaning of this term has changed and developed over time and describes nowadays complex changes in myocardial structure and function as a result of damage (KOLOGRIVOVA et al., 2021). Clinically it is defined as an increase of the left ventricular end diastolic pressure (LVEDV) of at least 20% and can take months (VAN DER BIJL et al., 2020). Despite the attempt to compensate injury by fibrosis, LV dilatation or hypertrophy, pump failure and arrhythmias may develop. Since a scar is only a replacement and cannot substitute myocardial functions due to lack of contractile elements (CHOU et al., 2018), adverse remodeling and heart failure may occur (ERTL & FRANTZ, 2012).

The whole event of healing and remodeling is a very complex process that needs to be highly regulated (ERTL & FRANTZ, 2005). If the inflammatory reaction is too strong and the switch to the proliferation phase does not work properly, the myocardium thins (PANIZZI et al., 2010). This would implement anti-inflammatory agents, like corticosteroids, as a feasible treatment approach (GIUGLIANO et al., 2003). But on the other hand, an unstable scar due to granulation tissue as the result of an insufficient inflammatory clearance reaction may also cause ventricular rupture (SILVERMAN & PFEIFER, 1987; SWIRSKI & NAHRENDORF, 2018).

1.4.6. The role of T cells

An increasing role in remodeling after myocardial infarction has been ascribed to T lymphocytes in recent years (HOFMANN & FRANTZ, 2016). FACS experiments have revealed decreased numbers of $CD4^+$ (HOFFMANN et al., 2012) and $CD8^+$ (HOFFMANN et al., 2015) cells in the peripheral blood in patients with STEMI. Moreover, these cells, and in particular $Foxp3^+$ regulatory T cells (Tregs), have been found within the first week in heart-draining lymph nodes (HOFMANN et al., 2012) and in peri-infarct tissue (CURATO et al., 2010) in mice. These results have implied the assumption that an MI also activates T cells for the inflammatory and healing processes which has subsequently been confirmed in several studies. First, $CD4^+$ cells have been studied in general. CD4 and MHC class II deficient mice as well as animals with a transgenic impaired T cell receptor or a lack in $CD11c^+$ antigen-presenting cells have proven an intact T cell activation as crucial

for myocardial healing. Corresponding experiments have resulted in higher numbers of proinflammatory Ly-6C^{high} macrophages and impaired collagen formation, leading to LV dilatation and impaired survival caused by deteriorated LV function or even ventricular rupture (ANZAI et al., 2012; HOFMANN et al., 2012). Corresponding observations have also been made in studies of transgenic mice with a depletion of the subpopulation of regulatory T cells due to knockout or antibodies (SAXENA et al., 2014; WEIRATHER et al., 2014). However, therapeutic activation as well as injection of Tregs have resulted in a decrease of infarct size and improvement of scar formation following an enhanced polarization of macrophages towards the M2 phenotype (MATSUMOTO et al., 2011; SHARIR et al., 2014). Further, also in the ischemic myocardium detected CD8$^+$ cells have been investigated in more detail and have been defined as an angiotensin II receptor type 2 positive (AGTR2$^+$) and IL-10 (CURATO et al., 2010) producing subclass that are therefore also discussed to contribute to the switch to Ly-6C^{low} macrophages during the reparative healing phase (SWIRSKI & NAHRENDORF, 2018). In summary, these results demonstrate the important role of T lymphocytes in the complex process of remodeling.

1.5. Comorbidities and exceptional cases

With this sophisticated, multifactorial processes of atherothrombosis and repair, it is obvious that inflammatory comorbidities can have a significant impact on both risk and outcome of MI. It has been shown that further diseases have a strong impact on mortality after myocardial infarction with a linear increase with each additional comorbidity (BAECHLI et al., 2020). These are often diseases that are associated with inflammation and thereby address the immune system. For example Diabetes mellitus is well known for its inflammatory potency (LONTCHI-YIMAGOU et al., 2013) and listed as one of the most common risk factors (YUSUF et al., 2004). Pneumonia is also considered to be such, since several studies have shown an increased number of heart attacks after this (CORRALES-MEDINA et al., 2015) and prove the role of infections triggering coronary syndromes (CORRALES-MEDINA et al., 2010). This leads to the suggestion that a stable and safely regulated immune system is crucial for preventing or withstanding myocardial infarction.

1.5.1. Myocardial infarction in immunocompromised conditions

Of course, this implements the question of the effects of a compromised immune system on MI incidence and healing and respectively the question of an optimal management and treatment of corresponding patients.

Research indicates a higher risk of developing a heart attack for patients who are positive for human immunodeficiency virus (HIV) (ALSHEIKH & ALSHEIKH, 2022) or who are treated against cancer targeting the bone marrow cells (LOZAHIC et al., 2021), whereas immunomodulatory medication of arthritis shows different effects (OZEN et al., 2021). In particular, the drug Abatacept is associated with a lower likelihood of MI (JIN et al., 2018; KANG et al., 2018).

Closely related to this is Belatacept, a drug that is often used after kidney or heart transplantations (VINCENTI et al., 2016; SHARMA & SHARMA, 2020) as a further situation that requires immunosuppression. Apart from HIV and immunomodulatory cancer therapy, also for this clinical picture an increased risk for myocardial infarction is described with cardiovascular disease in general as the leading cause of death (BRIGGS, 2001; BOLAD, 2016). One of the reasons for that discussed is the administration of immunosuppressants (SOLOMON et al., 2006). Belatacept affects the costimulation and activation of T cells (WEKERLE & GRINYÓ, 2012). Concurrent to the pivotal role of these cells in myocardial healing, this would suggest an impaired remodeling and scar formation in Belatacept treated persons. However, data concerning outcome and infarct repair of this is missing (BOLAD, 2016) as well as general clinical data to prove the beneficial role of T cells in humans (HOFMANN & FRANTZ, 2016). Further research is therefore needed, not only to provide the best possible treatment for affected patients, but also to gain more general information in a more translational setup.

2. Research on myocardial infarction

As the example of immunosuppressed patients demonstrates, treatment and therapy strategies remain still unsatisfactory in some cases and several interactions are not yet fully clarified (CAHILL et al., 2017), although a lot of research is carried out on myocardial infarction. It covers a very broad and rapidly changing field that has developed over the last three decades (ERTL & FRANTZ, 2012) but further

investigation is still needed. This preferably requires translational, reproducible and replicable experimental models.

2.1. Animal models

2.1.1. Advantages and limitations

Various *in vitro* and *ex vivo* models such as myocyte cell culture or the perfusion of isolated hearts have been established but animal models are obviously the most translational ones (LINDSEY et al., 2018), although an ultimate model for myocardial infarction has not been found so far (KUMAR et al., 2016). Apart from the basic species differences, it is not possible to adequately represent the heterogeneity and gradual evolution of this disease, since it is the result of multiple interactions. As described, several factors like age, gender or family history in combination with health behaviours such as alcohol consumption or smoking contribute to the development of myocardial infarction, which is additionally influenced by possible comorbidities and psychosocial stress (SHIN et al., 2021). Another drawback of the use of animals for experimental purposes is further the increasingly shrinking appreciation in society (CAVAGNARO & SILVA LIMA, 2015). Nevertheless, as a whole organism, these are considered as the best option to mimic biological processes as closely as possible to humans as well as to overcome the lack of available samples from patients (DE VILLIERS & RILEY, 2020).

2.1.2. Animals used

While large animals were used in the early days, the methods of using small animals in research have evolved immensely over the past 25 years (LINDSEY et al., 2021a), so that rodents are now the most commonly used models for inducing myocardial infarction.

Mice in particular have many advantages in this respect, such as a short generation time and well-defined genetics. Their small body size enables low costs for maintenance and interventions as well as very easy and practical handling only by a single person. However, the anatomic mismatch compared to humans is also the biggest limitation of this model. Differences in cardiac kinetics, like a fivefold higher heart rate and an incongruent myosin expression of cardiomyocytes, question the transferability of experimental results. Moreover sample number and

size is quite restricted and the short lifespan of mice disqualifies them for use in long-term evaluations. The drawbacks of small animals open up the necessity for alternate models, e.g. in large animals. Anatomical and physiological similarities of pigs, sheep and goats allow the use of human devices and imaging methods. The proportions resemble more the human (patho-)physiology and enable easier manipulation of individual coronary vessels to create more defined ischemic damage and greater translational potential. However, higher effort and costs must be invested in interventions and care (MILANI-NEJAD & JANSSEN, 2014; LINDSEY et al., 2018).

In addition to the animals already mentioned, others such as non-human primates (CHONG et al., 2014), dogs (JUGDUTT, 2002), cats (RITCHIE et al., 1979), guinea pigs (CAMERON et al., 1985) and even ferrets (GOMOLL, 1996) are also used as models for myocardial infarction.

2.1.3. Strategies

Various methods for inducing an MI have been developed, which are mostly used in different model animals regardless of size and are described below for the pig.

Basically, they can be categorized by the location of the ischemic impact. Especially in large animals it is feasible to see or display the various coronary vessels, which offers the possibility to address different parts of it. The most common ones are the left anterior descending artery (LAD) which is known for the induction of an anterior wall infarction (SKYSCHALLY et al., 2019) and the left circumflex artery (LCx) that causes damage at the posterior wall (ISHIKAWA et al., 2018).

Different experimental setups can further be classified according to whether the ischemia is followed by reperfusion or not. Although both cases are based on the same damage, the cellular and molecular cascades triggered in each case differ. Therefore the two strategies should not be used synonymously, but the respective characteristics must be taken into account for study designs and the best one should be chosen according to the research hypothesis.

Non-reperfused MI causes clearer effects with large infarct sizes (40-60% of LV). An excessive loss of myocytes leads to LV dilatation, thinning and dysfunction that results in heart failure and fatal ventricular rupture. The inflammation response is enormous and can even affect further organs like kidney or spleen (HALADE et al., 2018). This approach can be used to investigate mechanisms or possible

therapeutics addressing poor scar formation or adverse remodeling. A benefit is that due to the strong damage, a smaller number of samples is sufficient to prove outcomes but at the same time a greater loss of animals is to be expected caused by lethal arrhythmias. Further, this approach only represents the proportion of MI patients with around 30% for whom reperfusion is not or only poorly possible because of delay, anatomical issues or microvascular obstruction (RIBICHINI et al., 2004).

Reperfusion strategies limit the extent of myocardial infarction and allow for access of blood perfusion into the area at risk (AAR). The peri-infarct border zone can be salvaged and the loss of LV function attenuated. Infiltrating immune cells can reach the affected myocardium through the reinfused vessel which allows for a fast and short, but potentially overwhelming inflammatory response (FRANGOGIANNIS et al., 1998). I/R injury can cause several problems like lethal arrhythmias and the procedure to induce this is technically more challenging. This experimental setup should be chosen for refinement of currently prophylactic and therapeutic strategies. Although only partial recirculation is usually observed in patients, reperfused MI represents the clinical situation best (LINDSEY et al., 2018; LINDSEY et al., 2021a; LINDSEY et al., 2021b).

2.2. Pig models of myocardial infarction

The pig as model for myocardial infarction research is designated as an opportunity of "unique translational value" (HEUSCH et al., 2011). Even though there are some disadvantages, such as the high susceptibility to cardiac arrhythmias or the increase in weight during aging, the advantages of this animal clearly outweigh in experiments. Swine show rapid wound healing, are resistant to infection and have anatomical and hemodynamic conditions of the heart comparable to humans. Both species have a similar cardiac output as well as a right dominant coronary circulation. Furthermore, the left coronary vessel presents larger in diameter and longer than the right one and forms only few collaterals, as is also the case in most patients (SHIN et al., 2021). Owing to these conditions, the pig is a very well suited model to induce defined myocardial infarctions by various methods.

2.2.1. Coronary artery ligation

The most commonly used option in MI research is the direct ligation of a coronary artery.

Pigs are subjected to a midsternal or left thoracotomy in the fourth intercostal space to expose the heart and identify vascular conditions and collaterals. These may vary among individuals and the ligation should be placed in order to perform experiments as reproducible and comparable as possible, hence most often it is defined to constrict the LAD distal to the first diagonal branch or, in case of the LCx, in its proximal part (SHIN et al., 2021). Thereby the respective vessel is prepared for about 3 mm and tied with a surgical suture to create a permanent or temporal occlusion. The latter is achieved by tying a piece of rigid polyvinyl tubing along with the artery, that allows the ligature to be removed before closing the chest by layers to provide reperfusion after a certain period of time (DU TOIT et al., 2001; TIMMERS et al., 2011; XIONG et al., 2012).

The possibility of direct presentation and observation allows very precise induction of MI in terms of location, ischemia duration and extent, which can be carried out in multiple species. On the other hand, it is a highly invasive method and a severe procedure, that, due to the high risk of complications and reactions after the intervention, not only places a high burden on the animals, but also carries the potential to influence the experimental results, as it can alter and mask the inflammatory and healing processes of the heart (SHIN et al., 2021).

2.2.2. Percutaneous Transluminal Coronary Angioplasty (PTCA)

In order to overcome the issues of a surgical technology, further approaches have been investigated leading to the development of catheter-based strategies.

In percutaneous transluminal coronary angioplasty, reperfused myocardial ischemia can be induced by a balloon catheter in a close-chest setup. The only operative intervention required is the insertion of an arterial sheath into the common carotid or femoral artery, serving as access for all catheters and guidewires under radiographic control (OKURA et al., 2012). First, a Judkins right catheter is placed in the ostium of the left main stem to visualize the coronary anatomy in a left ventricular angiography and choose the best position for the occlusion (in accordance with the challenges that are already discussed above). A guidewire is then advanced through the Judkins catheter into the artery and a balloon catheter is

mounted on that and brought into the desired location. These are available in various dimensions with different diameters and lengths that should be selected based on the size of the respective vessel obtained in the X-ray image. Once checked for the correct balloon position, myocardial infarction is induced by gently inflating it to a pressure between 4 and 6 bar using a pump. At the end of the desired ischemia time coronary as well as LV angiography can be repeated to ensure the reperfusion of each vessel after the balloon has been deflated and removed with the guidewire (BÄHR et al., 2021).

Although the localisation and extension of necrosis cannot be controlled as precisely as in coronary ligation, the advantages of a close-chest approach clearly prevail. The minimally invasive procedure reduces the risk of complications and infections, so the animals need less medication and generally experience lower distress. This kind of intervention also offers the opportunity to react quickly to possible changes in balloon localisation or arrhythmia problems by simple deflation, as well as to apply further manipulations or therapeutics directly via catheters. Furthermore, the significance of a reperfused model of cardiac ischemia is particularly high in this case, since patients are also treated with PTCA in the clinic to restore blood flow after myocardial infarction. In conclusion, catheter-induced myocardial infarction in pigs represents an excellent translational model for preclinical research (CAMACHO et al., 2016; SHIN et al., 2021).

2.2.3. Percutaneous intracoronary embolization

However, this can be performed not only by a balloon, but also by various other materials or reagents that are inserted into coronary vessels via catheters, such as coils (MAKKAR et al., 2005) or polystyrene microspheres (HANES et al., 2015) and also homogenized gelatine sponges (LI et al., 2000; SAKAGUCHI et al., 2003). All these methods result in MI caused by embolization and are discussed as reperfusion assessments due to the possibility of washing off the materials in the blood stream.

2.2.4. Alternative means of inducing myocardial infarction

In addition to those described, there are also other, less common methods for experimentally triggering heart attack. Amyloid (POTZ et al., 2018; ISHIDA et al., 2019) or hydraulic constrictors (SJAASTAD et al., 2000) can mimic chronic myocardial infarction by their gradual occlusion, but require an invasive

intervention. This is also the case for cryoinjury procedures, in which a rod frozen in liquid nitrogen is pressed against the exposed heart after thoracotomy (YANG et al., 2012; HIRANO et al., 2017). This creates a scar with composition similar to ischemia and is therefore used for the study of cellular therapies. Another strategy to induce MI is the rather simple application of chemical reagents. For instance, isoproterenol can be injected subcutaneously, but this is a very indirect method that is difficult to validate (KIM et al., 2014; SHIN et al., 2021).

2.3. Pig models of immunodeficiency

The inflammatory reaction and subsequent scarring following MI are tightly regulated processes and it has been shown that disturbances of the immune system can significantly affect those, leading to a poorer outcome, which this work aimed to investigate further. Therefore, it is of course crucial to have appropriate heart attack models, but to study its healing under immunosuppressed conditions, animals are required that adequately represent this situation. Several immunodeficient pigs have been developed for research purposes to date which are described and characterised below.

2.3.1. The operational immunodeficient pig (OIDP)

In this model, the immunodeficiency is caused by the surgical removal of the thymus as well as the spleen as major immune organs. This technique can be performed in wildtype animals and has already been validated for its efficiency in a setup for transplantation of humanized tissue into the OIDP (ITOH et al., 2019). Nevertheless, it is quite impractical due to its invasive character with two different surgical fields.

2.3.2. The SCID pig

Therefore, it is much more convenient to replicate a model at the genomic level without further intervention, as is the case with pigs mimicking severe combined immunodeficiency (SCID). This is a group of congenital disorders compromising T lymphocyte development and thus also affecting B and NK cells, which occur with an incidence of 1 in 40000 to 75000 in humans. Newborns suffer from a total absence or reduced immune functions leading to an early death unless treated as soon as possibly with hematopoietic stem cells or gene therapy. However, this is often difficult, since the disease usually presents without clinical symptoms at birth and is only diagnosed between the fourth and seventh month of life.

Currently, mutations in more than 30 genes are suspected to cause SCID and display a variety of different phenotypes. Some have already been successfully reproduced or even found natively in pigs (IQBAL et al., 2019; PABST, 2020).

2.3.2.1. *Artemis* pig model

Severe combined immunodeficiency is known to affect various species and in 2015 it has been described for the first time as also occurring naturally in pigs. Two spontaneous mutations within the *Artemis* gene (*DCLR1EC*) have been identified to cause a phenotype similar to the one in humans, as the animals develop functional NK cells but neither B nor T lymphocytes (WAIDE et al., 2015). Therefore, they are considered appropriate recipients of xenografts as well as models for oncological research (POWELL et al., 2017).

2.3.2.2. *IL2Rγ* knockout pig model

The interleukin-2 receptor subunit gamma is a part of the receptor complexes recognizing several interleukins (LEONARD et al., 2019). Its gene is located on the X-chromosome, so mutations within this provoke the X-linked SCID form. *IL2Rγ* knockout swine have been established performing several genome editing techniques (WATANABE et al., 2013; CHOI et al., 2016). All exhibit the same phenotype with B lymphocytes but lower numbers of T and NK cells as well as the complete absence of the thymus (IQBAL et al., 2019).

2.3.2.3. *RAG1/2* knockout pig model

The Recombination Activating Gene (*RAG*) *1* and *2* encode for a protein complex that is crucial for the V(D)J rearrangement of antibodies and receptors of B and T lymphocytes. More than 20 mutations are possible within these genes causing an immune disorder that is called Omenn syndrome (ALEMAN et al., 2001). Initially, a biallelic mutation in both genes has been applied, but since the two encoded proteins work synergistically (HUANG et al., 2014) and the impairment of one is already sufficient to create the disease profile, models affecting only a single gene are more common now (CHOI et al., 2017). Animals facing this modification lack T and B lymphocytes and have only few NK cells as well as hypoplastic immune organs (IQBAL et al., 2019).

The last two models of SCID can even be combined for several approaches that require the total absence of T and B cells as well as NK cells, as it is the case, for

example, with transplantation of human hepatocytes into pigs. Since one of the knockouts already causes serious reproductive and survival problems under sterile conditions, these are even more severe in the double affected animals (REN et al., 2022; ZHAO et al., 2022).

2.3.3. LEA29Y transgenic pigs

As mentioned above, the previously characterized immunodeficient models entail various disadvantages that can be avoided by the administration of LEA29Y transgenic pigs (henceforth referred to as LEA29Y). First described in 2016, these have also been established by a genetic modification affecting T cells by the ubiquitous expression of an immunomodulatory fusion protein (BÄHR et al., 2016).

2.3.3.1. Background

The adaptive immune system has evolved as the specific response to a broad spectrum of pathogens with T lymphocytes being a very important cellular component of this (BONILLA & OETTGEN, 2010).

It is known that the activation of these cells requires two distinct signals. First, the T cell receptor (TCR) recognises epitopes on its ligand, a cell surface marker called major histocompatibility complex (MHC), expressed by antigen presenting cells (APC), such as dendritic cells and macrophages. APC process uptaken proteins and present peptides to the T lymphocytes via their MHC, which is also known as human leukocyte antigen (HLA) or swine leukocyte antigen (SLA) depending on the different species (THÉRY & AMIGORENA, 2001; SZETO et al., 2020). When T cells identify the antigen as exogenous and pathogenic they become activated in a first step and if it remains with this single signal, they fail to react further but enter an anergic state or undergo apoptosis (Figure 1A). For a sufficient immune reaction a second trigger in the form of costimulatory events of other cell surface receptors is essential (SMITH-GARVIN et al., 2009). So far, a large repertoire of these has been discovered, the best known of them being CD28 (CHEN & FLIES, 2013).

CD28 is a member of the immunoglobulin super-family (IgSF), a subgroup of cosignalling receptors characterized by a variable extracellular immunoglobulin-like domain. It is expressed constitutively on the cell surface of T lymphocytes and binding of its ligands CD80 (B7-1) and CD86 (B7-2) on APC leads to T cell priming and activation (Figure 1B). To avoid an excessive immune reaction, this simultaneously induces cytotoxic T lymphocyte antigen-4 (CTLA4) on the T cells,

which is also part of the IgSF, but shows a higher affinity to CD80 and CD86 (RUDD et al., 2009). As a resulting feedback mechanism CD28 is therefore displaced from its costimulatory binding and downregulated by endocytosis, preventing further T lymphocyte activation, as shown in Figure 1C (CHEN & FLIES, 2013; ESENSTEN et al., 2016).

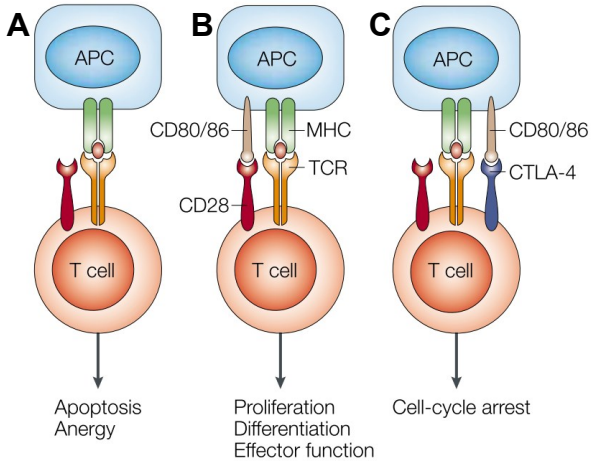

Figure 1: T cell activation. (A) Single recognition of MHC by the TCR. **(B)** MHC-TCR binding with an additionally costimulatory signal. **(C)** Downregulating feedback mechanism by CTLA4 (adapted from ALEGRE et al., 2001).

This signalling cascade is the best-studied costimulatory signalling pathway and is considered to have great potential as a target for immunomodulatory therapies. While initial interest was centred on modulating the binding of CD28 (WEISS et al., 1986), the focus is now increasingly on CTLA4-agonists so that two corresponding drugs have been developed so far, known as Abatacept (CTLA4-Ig) and Belatacept.

Belatacept is a fully human immunoglobulin fusion protein, consisting of an extracellular domain of CTLA4 and a fragment of the Fc domain of IgG1. It is also known as LEA29Y due to the exchange of two amino acids compared to the natural CTLA4 structure as well as CTLA4-Ig. Leucine at position 104 is replaced by glutamic acid and tyrosine instead of alanine at position 29. This results in a slower dissociation from CD80 and CD86, leading to a higher immunosuppressive efficacy compared to the previously developed Abatacept (LARSEN et al., 2005; LATEK et al., 2009). Its effect on blocking costimulation of T cells has been well demonstrated in patients after kidney or liver transplantation (KLINTMALM et al., 2014; VINCENTI et al., 2016) and was further used for the development of the

animal model, as LEA29Y transgenic pigs ubiquitously express the fusion protein controlled by a CAG-promoter.

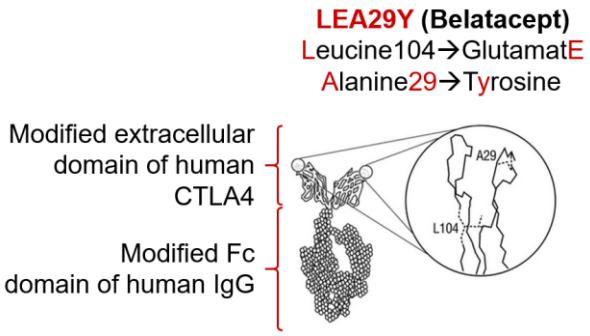

Figure 2: Structure of the fusion protein LEA29Y (adapted from LATEK et al., 2009).

2.3.3.2. Benefits

Compared to the other options, these pigs represent the best functional and practical large animal model for immunosuppression. It is based on a very well-studied and frequently targeted pathway in humans and could be reproduced in swine by genetic modification. This facilitates the onset of immunodeficiency from birth, without the need for further measures, so that corresponding animals can be generated simply by mating. Although a certain level of hygiene should be observed, the pigs can be kept for the usual lifetime under conventional farming conditions without further costs, which overall make transgenic LEA29Y animals well suited for use in the experiments in this thesis.

The aim therefore was to investigate the effects of blocking T cell costimulation on cardiac healing and scar formation following myocardial infarction using this model. For this purpose, an MI with subsequent reperfusion was induced by percutaneous transluminal coronary angioplasty in both transgenic LEA29Y as well as wildtype pigs and experiments with follow-up periods of 3, 9 and 14 days were compared to control animals without any previous intervention. Tissue from the left ventricle was systematically sampled, and studies were conducted on functional and histological measurements in the heart as well as immune cell profiling in the circulation.

III. ANIMALS, MATERIALS AND METHODS

1. Animals

In this work, pigs expressing the CTLA4-Ig derivate LEA29Y as well as wildtype (WT) controls were used to investigate the effect of a compromised immune system on infarct progression in the heart. All pigs were generated and housed at the Chair for Molecular Animal Breeding and Biotechnology, LMU Munich. Experimental interventions took place either at the Center for Innovative Medical Models or at the "Zentrum für Präklinische Forschung" (Klinikum rechts der Isar, TUM, Munich, Germany). Pigs of both sexes and genotypes were subjected to a procedure of catheter-based induction of myocardial infarction with subsequent reperfusion or were used as untreated controls. All animals were at an age of 2.5-4 months and weighed between 13 and 50 kg. Whenever possible, pigs were housed in groups. They received rationed amounts of a commercially available pig fodder and had tap water ad libitum at their disposal. They were also offered a variety of enrichment materials.

All animal experiments were carried out in compliance with the German Animal Welfare Act and with the approval of the government of Upper Bavaria (AZ ROB-55.2-2532.Vet_02-19-195 and ROB-55.2-2532.Vet_02-18-134).

2. Material

2.1. Devices

Accu-jet™ pro pipette controller	Brand, Wertheim
Analytik Jena US UVP GelStudio Plus	Thermo Fisher Scientific, USA
Angiomat Illumena contrast agent pump	Liebel-Flarsheim Company LLC, France
ARC 400 electric knife	BOWA-electronic GmbH & Co. KG, Gomaringen
Autoclav Varioklav 400	H+P Labortechnik, Oberschleißheim
BioMat2 microbiological safety cabinet	Contained Air Solutions, UK

BD LSRFortessa™ Cell Analyzer	BD Biosciences, USA
Benchtop 96 Tube working rack	Stratagene, USA
CardioMessenger Smart	Biotronik, Berlin
CARESCAPE Monitor B450	GE, USA
Centrifuge 5417 R	Eppendorf, Hamburg
Centrifuge 5424	Eppendorf, Hamburg
Centrifuge 5804 R	Eppendorf, Hamburg
Centrifuge 5910 R	Eppendorf, Hamburg
Centrifuge Rotina 380 R	Hettich Lab Technology, Tuttlingen
Chyo Petit Balance MK-2000B	YMC CO, Japan
CoolCell® container	BioCision, USA
CO_2 incubator SHEL LAB, Model TC2323	Sheldon Manufacturing Inc., USA
Daewoo KOC-154K microwave	Daewoo, South Korea
DMi1 inverted microscope	Leica Microsystems, Wetzlar
Embedding molds premium	Medite, Burgdorf
EPIQ 7G Ultrasound machine	Philips, Netherlands
Erbe ICC 200 electric knife	Erbe Elektromedizin GmbH, Tübingen
Excelsior AS A82310100	Thermo Fisher Scientific, USA
FiveEasy pH meter F20	Mettler-Toledo, USA
Grant JB Nova 5 water bath	Grant Instruments Ltd, UK
Heating plate with magnetic stirrer RH basic	IKA-Werke, Staufen im Breisgau
Heraeus Megafuge 16R	Thermo Fisher Scientific, USA
HLC Cooling-ThermoMixer MKR 13	Ditabis, Pforzheim
Incision and injection tool for ICM	Biotronik, Berlin

inoLab® pH meter 7110	WTW, Weilheim
Insertable cardiac monitor BioMonitor 2, BIOMONITOR III	Biotronik, Berlin
Labcycler thermocycler	SensoQuest GmbH, Göttingen
Laboratory Centrifuge 4-15C	SIGMA-ALDRICH CHEMIE GmbH, Steinheim
Lamina flow HB 2448K	Heraeus, Hanau
Leica DMi8 microscope with Thunder Imaging System	Leica Microsystems, Wetzlar
LIFEPAK 20	Stryker Corporation, USA
LogiCal® Pressure Transducer	Smiths Medical, Inc, USA
Microm HM 325 rotary microtome	Thermo Fisher Scientific, USA
Multipipette E3	Eppendorf, Hamburg
Multitip pipette (300 µl)	Eppendorf, Hamburg
MyLab X8 ultrasound machine	Esaote, Italy
Neptune ventilator	Medec, Belgium
Neubauer improved cell counting chamber	Assistent, Sondheim von der Rhön
Owl™ gel electrophoresis systems (EasyCast™ B1A and B2 mini, A2)	Thermo Fisher Scientific, USA
PC-EKG 2000	EIKEMEYER®, Tuttlingen
Pipettes (1000 µl, 200 µl, 20 µl, 10 µl, 2 µl)	Gilson Inc, USA
Polymax 2040 shaker	Heidolph Instruments, Schwabach
Power Pac 300 gel electrophoresis unit	Bio-Rad Laboratories, Munich
Primus Ventilator	Drägerwerk AG & Co. KGaA, Lübeck
Renamic programmer	Biotronik, Berlin
Rotilabo® mini centrifuge	Carl Roth, Karlsruhe
Select Vortexer	Select BioProducts, USA

SimpliNano™ spectrophotometer	Biochrom GmbH, Berlin
Spectrafuge 24D Microcentrifuge	Labnet International, USA
Tecan Sunrise Elisa reader	Tecan, Austria
TES 99 modular paraffin embedding system	Medite, Burgdorf
Thermo-Shaker TS-100	bioSan, Lativa
Tissue cool plate COP 30	Medite, Burgdorf
Tissue float bath 1052	GFL, Burgwedel
Ultrasound probe P 1-5, P 2-9	Esaote, Italy
Ultrasound probe X5-1	Philips, Netherlands
Ultrasound table	EIKEMEYER®, Tuttlingen
Vismo patient monitor	Nihon Kohden, Japan
Ziehm Vision RFD mobile C-arm X-ray	Ziehm Imaging, Nuremberg

2.2. Consumables

Angiodyn Hahnbank-Baugruppe 3-Fach OFF	B. Braun Melsungen AG, Melsungen
Angiograhic catheter, 110 cm, 6F/7F PIG (pigtail catheter)	Cordis, USA
Angiograhic catheter, 100 cm, 6F, JR 4 SH (Judkins right catheter)	Cordis, USA
AVANTI™ Sheath 7F, 8F, 9F, 10F	Cordis, USA
BasixTouch™, 35 atm/bar 30 ml inflation device	Merit Medical GmbH, Eschborn
Careflow™ Central Venous Catheter Kit	Argon Medical Devices, USA
Cellstar® serological pipettes (5 ml, 10 ml, 25 ml)	Greiner BioOne, Austria
Cellstar® tubes (15 and 50 ml)	Greiner BioOne, Austria
Cover slips for histology	Carl Roth, Karlsruhe
Cryovials (1.5 ml)	TPP, Switzerland

Discofix® Hahnbank	B. Braun Melsungen AG, Melsungen
Disposable scalpel #21	Henry Schein, Munich
Feather® microtome blades S35	pfm medical, Cologne
Fielder FC 0.36 mm, 180 cm coronary guide wire	ASAHI INTECC CO., LTD, Japan
Glass pasteurpipettes	Brand, Wertheim
Immuno plates maxisorp C96	Thermo Fisher Scientific, USA
Intrafix® SafeSet	B. Braun Melsungen AG, Melsungen
Individual reaction tubes 1.2 ml	STARLAB, Hamburg
LogiCal® Pressure Monitoring Kit	Smiths Medical, Inc, USA
Microplate U-bottom 96 well	Eppendorf, Hamburg
Microscope slides Star Frost®	Engelbrecht, Edermünde
Monocryl™ Plus	Ethicon, Inc., USA
Monovette® (K3 EDTA, Serum, Lithium-Heparin Gel+)	Sarstedt AG & Co. KG, Nümbrecht
NitriSense nitrile gloves	Süd-Laborbedarf, Gauting
Parafilm® M	Carl Roth, Karlsruhe
PCR reaction tubes (0.2 ml)	Brand, Wertheim
Petri dish 94×16	Greiner BioOne, Austria
Pipette tips	Eppendorf, Hamburg
Pipette tips with filter	Greiner BioOne, Austria
Pressure transducer	Smiths Medical, Inc, USA
Prolene™ 3-0	Ethicon, Inc., USA
PROWATER 0.36 mm, 180 cm coronary guide wire	ASAHI INTECC CO., LTD, Japan
Qualitative filter paper	VWR, USA
Reagent reservoir	Thermo Fisher Scientific, USA

Safe-Lock reaction tubes (1.5 ml, 2 ml)	Eppendorf, Hamburg
Silk	RESORBA® Medical GmbH, Nuremberg
Stapler	Henry Schein, Munich
Tesa tape 4541 50 m x 50 mm	Tesa SE, Norderstedt
Tesa tape 4651 50 m x 50 mm	Tesa SE, Norderstedt
Test tube round bottom 5 ml	Scientific Laboratory Supplies, UK
Tissue-Tek® O.C.T.™	Sakura, Staufen
Tissue-Tek® Cryomold® 25 × 20 × 5 mm	Sakura, Staufen
TREK RX™ balloon catheter (different sizes)	Abbott, USA
Uni-link embedding cassettes	Engelbrecht, Edermünde
Vasofix® Braunüle®	B. Braun Melsungen AG, Melsungen

2.3. Drugs

Adrenaline	InfectoPharm Arzneimittel u. Consilium GmbH, Heppenheim
Amiodarone	Ratiopharm GmbH, Ulm
Atropine sulfate	B. Braun Melsungen AG, Melsungen
Azaperone	Elanco GmbH, Cuxhaven
Cefuroxim 750 mg	Dr. Friedrich Eberth Arzneimittel GmbH, Ursensollen
Fentanyl	Eurovet Animal Health BV, AE Bladel
Heparine	B. Braun Melsungen AG, Melsungen
KCl	B. Braun Melsungen AG, Melsungen
Ketamine	CP-Pharma Handelsgesellschaft mbH, Burgdorf

Magnesiumsulfate 50%	Inresa Arzneimittel GmbH, Freiburg
Midazolame 15 mg	Hexal AG, Holzkirchen
NaCl	B. Braun Melsungen AG, Melsungen
Propofol 20 mg/ml	B. Braun Melsungen AG, Melsungen
Ringer-Lactate	B. Braun Melsungen AG, Melsungen
Tauro Lock™-HEP500	TauroPharm GmbH, Waldbüttelbrunn
Ultravist-370 contrast agent	Bayer AG, Leverkusen

2.4. Chemicals and reagents

10x CoralLoad PCR Buffer	Qiagen, Hilden
Acetic acid (glacial)	Carl Roth, Karlsruhe
Acetic acid	Carl Roth, Karlsruhe
Agarose	Bio&SELL, Nuremberg
Avidin-biotin complex	Vector Laboratories Inc., USA
Bovine serum albumine (BSA)	SIGMA-ALDRICH CHEMIE GmbH, Steinheim
Brefeldin A	BD Biosciences, USA
Bromophenol blue	Carl Roth, Karlsruhe
Citrat	Merck, Darmstadt
Diaminobenzidine (DAB)	Vector Laboratories Inc., USA
Dimethylsulphoxide (DMSO)	SIGMA-ALDRICH CHEMIE GmbH, Steinheim
Direct Red 80	SIGMA-ALDRICH CHEMIE GmbH, Steinheim
dNTPs (dATP, dCTP, dGTP, dTTP)	ThermoFisher Scientific, USA
EDTA 0.5 M	AppliChem GmbH, Darmstadt
Ethanol	Carl Roth, Karlsruhe

Eosin Y powder	Merck, Darmstadt
Fetal calf serum (FKS), low endotoxin	PAN-Biotech, Aidenbach
Formaldehyde 37%	Carl Roth, Karlsruhe
Gelatine from cold water fish skin	SIGMA-ALDRICH CHEMIE GmbH, Steinheim
GelRed® Nucleic Acid Gel Stain	Biotium, USA
GeneRuler™ 1-kb Plus DNA Ladder	Thermo Fisher Scientific, USA
Gibco DMEM	Thermo Fisher Scientific, USA
H_2O_2 30%	AppliChem GmbH, Darmstadt
HCl 25%	Merck (Darmstadt, Germany)
Histokit	Glaswarenfabrik Karl Hecht G mbH & Co KG, Sondheim
HotStarTaq® Plus DNA Polymerase (5 U/µl)	Qiagen, Hilden
Ionomycin	Merck, Darmstadt
Mayer´s Hemalum	SIGMA-ALDRICH CHEMIE GmbH, Steinheim
Na-Azid	Merck, Darmstadt
NaCl	neoFroxx GmbH, Einhausen
NaH_2PO_4, H_2O	Carl Roth, Karlsruhe
NaH_4PO_5	Carl Roth, Karlsruhe
Na_2HPO_4, $2H_2O$	Carl Roth, Karlsruhe
Pancoll density gradient	PAN- Biotech, Aidenbach
PBS (without calcium and magnesium)	SIGMA-ALDRICH CHEMIE GmbH, Steinheim
Penicillin/Streptomycin	Thermo Fisher Scientific, USA
Phorbyl-12-myristate-13-acetate	Merck, Darmstadt
Picric acid 1.3%	SIGMA-ALDRICH CHEMIE GmbH, Steinheim
RPMI 1640	PAN-Biotech, Aidenbach

Sulphuric acid 0.5 mol/l	Carl Roth, Karlsruhe
Tetramethylbenzidine	Agilent Technologies, Denmark
TRIS	neoFroxx GmbH, Einhausen
Triton X-100	SERVA Feinbiochemica, Heidelberg
Türk´s solution	Merck, Darmstadt
Tween 20	Agilent Technologies, Denmark
Weigert´s Hematoxylin	Carl Roth GmbH & Co. KG, Karlsruhe
Xylol	Liquid Production GmbH, Flintsbach am Inn

2.5. Kits

Avidin/ Biotin Blocking Kit	Vector Laboratories Inc., USA
BD Cytofix/Cytoperm™ Kit	BD Biosciences, USA
DNeasy® Blood & Tissue Kit (250)	Qiagen, Hilden
EZ-Link™ Sulfo-NHS-LC-Biotinylation Kit	Thermo Fisher Scientific, USA
Intracellular Fixation & Permabilization Buffer Set eBioscience™	Thermo Fisher Scientific,USA

2.6. Buffers and solutions

When necessary, water, deionized in Barnstead™ EASYpure™ II ultrapure water system (Wilhelm Werner GmbH, Leverkusen), was used as Aqua bidest. for solution.

2.6.1. Genotyping

TAE buffer (50x):

242 g 2 M Tris

100 ml 0.5 M EDTA (pH 8.0)

57 ml acetic acid (glacial)

Mixed in 1 l Aqua bidest. and stored at RT after filtration and autoclavation. For usage the buffer was diluted to single concentration with Aqua bidest.

2 mM dNTP-mix:

2 mM dATP, dCTP, dGTP, dTTP

Mixed in Aqua bidest. and stored in aliquots at -20°C.

2.6.2. ELISA

Coating Buffer pH 7.2:

0.175 g NaH_2PO_4, H_2O

0.67 g Na_2HPO_4, $2H_2O$

4.235 g NaCl

Mixed in 0.5 l Aqua bidest. and stored at 4°C.

Washing and Dilution Buffer pH 7.2:

0.35 g NaH_2PO_4, H_2O

1.34 g Na_2HPO_4, $2H_2O$

29.22 g NaCl

1 ml Tween 20

Mixed in 1 l Aqua bidest. and stored at 4°C.

2.6.3. PBMC analyses

5% Wash medium:

50% 10% Wash medium for PBMC isolation

50% PBS (without calcium or magnesium)

Mixed and stored at 4°C.

10% Wash medium:

90% DMEM

10% FCS

Mixed and stored at 4°C.

Culture medium:

RPMI

1% Penicillin/Streptomycin

10% FCS

Stored at 4°C.

Freezing medium:

90% FCS

10% DMSO

Mixed directly before use and stored on ice.

2.6.4. Histology

1% Eosin for HE:

10 g Eosin Y powder

1000 ml Aqua dest.

1.5 ml Acetic acid (glacial)

Eosin was solved in hot Aqua dest. and then let cool down. Filtered and stored in darkness at room temperature.

Blocking Buffer for IHC:

1% BSA

0.1% Triton X-100

0.2% Gelatine from cold water fish skin

0.02% Na-Azid

Mixed in TBS and stored at 4°C.

Citrat Buffer 10 mM pH 6.0 for IHC:

4.2 g Citrat

NaOH 2 M until pH reaches 6.0

Mixed in 2 l Aqua dest. Stored at 4°C.

Formalin 4%:

100 ml Phosphate Buffer

100 ml Formaldehyde 37%

Mixed in 800 ml Aqua bidest. Stored at room temperature.

Picro-Sirius Red Solution:

0.5 g Direct Red 80

Mixed in 500 ml Picric acid (1.3%) at least 1 week before use.

Filtered and stored at room temperature.

Phosphate Buffer:

40 g NaH_4PO_5

65 g Na_2HPO_4

Mixed in 1l Aqua bidest. and stored at room temperature.

Stock solution HCl-Ethanol for HE:

1000 ml EtOH 96%

14.3 ml HCl 25%

357 ml Aqua bidest.

Stored at room temperature. The stock solution was diluted 1:1 with EtOH 70% to get a working solution.

Stock solution TBS Buffer pH 7.6 for IHC:

121.0 g TRIS

90 g NaCl

HCl 25% until pH reaches 7.6

Mixed in 2 l Aqua dest. Stored at room temperature.

The stock solution was diluted 1:10 with Aqua dest. to get a working solution.

Tris/EDTA Buffer pH 9.0 for IHC:

4 ml EDTA 0.5 M

2.42 g TRIS

HCl 25% until pH reaches 9.0

Mixed in 2 l Aqua dest. Stored at 4°C.

2.7. Antibodies and proteins

2.7.1. ELISA

Anti-CTLA4 antibody [KT56] ab110650	abcam, UK
Anti-CTLA4 antibody [KT50] (HRP) ab106490	abcam, UK
Recombinant human CTLA4 protein (Active) ab167727	abcam, UK

2.7.2. PBMC analyses

Antibody/Reagent	Clone	Producer
goat anti-mouse anti-IgG2b-Alexa488	polyclonal	Jackson Immuno Research, UK
chicken IgY anti-human Anti-SynCAM (TSLC1/CADM1)	3E1	MBL International, USA
mouse IgG1 anti-human CD2-BV605	RPA-2.10	BD Biosciences, USA
mouse IgG1 anti-human CD2-BV711	RPA-2.10	BD Biosciences, USA
mouse IgG1 anti-pig CD3-PerCP-Cy5.5	BB23-8E6-8C8	BD Biosciences, USA
mouse IgG2b anti-pig CD4	74-12-4	Southern Biotech, USA
mouse IgG2b anti-pig CD4-PerCP-Cy5.5	74-12-4	BD Biosciences, USA
mouse IgG2a anti-pig CD8α-Biotin	76-2-11	Southern Biotech, USA
mouse IgG1 anti-pig CD8β-biot[1]	PPT23	Pirbright Institute[2]
mouse IgG1 anti-pig CD8β-PE	PPT23	Bio-Rad, USA
mouse IgG2a anti-human CD14-PE-Vio615	Tük4	Miltenyi Biotec B.V. & Co. KG, Bergisch Gladbach,
mouse IgG1 anti-pig CD16-AF647	G7	Bio-Rad, USA
mouse IgG1 anti-pig CD27-APC	b30c7	Bio-Rad, USA
mouse IgG1 anti-pig CD27-PE	b30c7	Bio-Rad, USA
mouse IgG1 anti-pig CD163-PE	2A10/11	Bio-Rad, USA
mouse IgG1 anti-pig CD172a-FITC	74-22-15	Bio-Rad, USA
donkey anti-chicken-IgY-Biotin	polyclonal	Jackson Immuno Research, UK
rat IgG2a anti-mouse Foxp-3-PE	FJK-16s	eBioscience (Thermo Fisher Scientific, USA)
goat anti-mouse IgG2b-BV421	polyclonal	Jackson Immuno Research, UK
hamster IgG anti-human ICOS-BV605	C398.4A	BioLegend, USA
mouse IgG1 anti-human IL-17A PerCP-Cy5.5	eBio64DEC17	eBioscience (Thermo Fisher Scientific, USA)
mouse IgG1 anti-bovine IFN-γ A647	CC302	Bio-Rad, USA
mouse IgG1 anti-human Ki-67 PE-Dazzle 594	Ki-67	BioLegend, USA
mouse IgG2b anti-pig MHC-II	2E9/13	Jackson Immuno Research, UK
Streptavidin BV421	/	BioLegend, USA
Streptavidin BV605	/	BD Biosciences, USA
mouse IgG1 anti-human T-bet-AF647	4B10	BD Biosciences, USA
mouse IgG1 anti-human T-bet-BV421	4B10	BioLegend, USA

mouse IgG2b anti-pig TCR-gd	PPT16	Pirbright Institute[2]
mouse IgG1 anti-human TNF-α-BV711	MAb11	BioLegend, USA
whole mouse IgG	/	Jackson Immuno Research, UK
Fixable Viability Dye eFluor780	/	Thermo Fisher Scientific, USA

Table 2: Antibodies and reagents for PBMC analyses.
[1] conjugated to Biotin using the EZ-Link™ Sulfo-NHS-LC-Biotinylation Kit (Thermo Fisher Scientific).
[2] In house production of The Pirbright Institute.

2.7.3. IHC

Anti-Iba1 antibody	abcam, UK
Goat Anti-Mouse IgG (H+L), biotinylated	Vector Laboratories Inc., USA
Goat Anti-Rabbit IgG (H+L), biotinylated	Vector Laboratories Inc., US
Neutrophils, mouse anti porcine, clone PM1	BMA Biomedical, Switzerland
Polyclonal Rabbit Anti-Human CD3	Agilent Technologies, Denmark
Rabbit Anti-Goat IgG (H+L), biotinylated	Vector Laboratories Inc., USA

2.8. Oligonucleotides

Oligonucleotides were purchased from Biomers.net GmbH, Ulm.

CAGf 5′-CTC TGC TAA CCA TGT TCA TG-3′

LEAr 5′-GGC TTT GTC TTG GCA TTA TG-3′

2.9. Software

FACSDiva™ software version 9.0.1.	BD Biosciences, USA
FlowJo™ v10.8.1	BD Biosciences, USA
ImageJ	Java, Sun Microsystems, USA
Leica Application Suite X	Leica Microsystems, Wetzlar
Microsoft® Excel® 2013	Microsoft Corporation, USA
MyLabDeskEvo	Esaote, Italy

Online random number generator	https://zufallsgenerator.net/, Switzerland
PC-EKG Software 64-bit-version	EIKEMEYER®, Tuttlingen
Prism 5	GraphPad Software, USA

3. Methods

3.1. Animal experiments

3.1.1. Genotyping of experimental animals

In order to select the correct animals for the experimental groups, offspring from LEA29Y x WT matings were genotyped for the presence of the LEA29Y transgene. Genomic DNA was isolated from tail biopsies, taken shortly after birth, using the DNeasy® Blood Tissue Kit (Qiagen) following the manufacturer´s instructions. The concentration of extracted DNA was measured in a spectrophotometer to equilibrate it to 20 ng/µl and used as template for genotyping PCRs. Previously identified DNA of WT and LEA29Y pigs served as controls. The established primers CAGf and LEAr for the specific detection of the transgene were mixed with the other reagents to a volume of 20 µl on ice in 0.2 ml reaction tubes. For a non-template control, master mix was left without DNA. The compositions of this as well as the cycler protocol can be found in Table 3 and 4. To check presence and size of the PCR product, electrophoresis on 1% (1 g Agarose/ 100 ml 1x TAE buffer) agarose gel was subsequently performed. 2.5 µl of a 1:250 mixture of GelRed® and bromophenol blue was added to the samples before pipetting these and 6 µl of GeneRuler™ DNA ladder into the gel slots. The electrophoresis chamber was filled with 1x TAE buffer and connected to an electrical voltage. The resulting DNA fragments could then be visualized under UV light as bands.

Reagent	Amount [µl]
10× CoralLoad PCR buffer	2.0
dNTPs (2 mM)	2.0
Forward primer (10 µM): CAGf	0.4
Reverse primer (10 µM): LEAr	0.4
HotStarTaq (5 U/ µl)	0.2
Aqua bidest.	14
DNA template	1

Table 3: Master mix for genotyping PCR.

Step	Temperature	Duration	Repetitions
Denaturation	95°C	5 min	
Denaturation	94°C	30 s	35x
Annealing	56°C	30 s	
Elongation	72°C	45 s	
Final Elongation	72°C	5 min	
Termination	4°C	5 min	

Table 4: Cycler protocol for genotyping PCR.

3.1.2. Experimental setup and groups

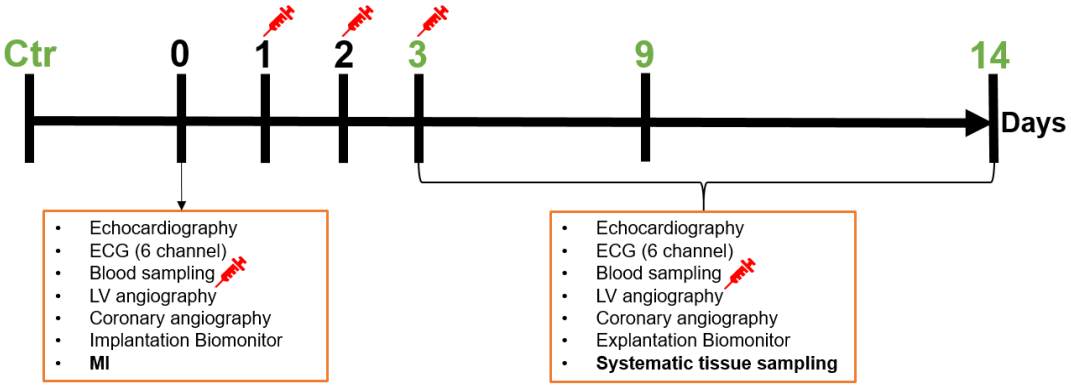

Figure 3: Experimental setup.

Figure 3 depicts the experimental time line starting with induction of MI. Animals were assigned to three different experimental groups with follow-up periods of 3, 9 or 14 days. Untreated pigs of both genotypes were used as controls. Functional measurements (echocardiography, 6 channel ECG, LV and coronary angiography) were performed before myocardial infarction as baseline values and were repeated at the end of every experiment. In addition, insertable cardiac monitors were implanted to continuously monitor arrhythmic events. Lithium heparin blood samples were taken at several time points to isolate PBMC. After euthanasia, the hearts were explanted and systematically sampled.

	Control	3 days	9 days	14 days	Σ
LEA29Y	3	4	2	1	10
WT	3	3	1	/	7

Table 5: Experimental groups and n numbers.

3.1.3. Anaesthesia

Pigs were anaesthetised on the day they underwent the MI protocol as well as on the last day of the experiment. Before each anaesthesia, the animals were fasted overnight. For sedation, they received an intramuscular injection of 10 mg/kg Azaperone, 0.02 mg/kg Atropin sulfate and 20 mg/kg Ketamine. An intravenous catheter was then placed in an ear vein. After a 2 mg/kg Propofol bolus, an endotracheal tube was inserted into the trachea. Anaesthesia during intervention was maintained by continuous i.v. injection of Propofol at a rate of 10 mg/kg/h and 0.001-0.0015 mg/kg of Fentanyl every 30 minutes. Ringer's lactate mixed with 150 mg Amiodaron and 1 g Magnesium sulfate per 500 ml as well as Gelafundin 4% were administered for volume substitution and prevention of arrhythmias. The pigs were connected to a volume-controlled ventilator (Dräger; Medec) and were continuously monitored by capnography, 3-channel ECG (LIFEPAK 20, Stryker Corporation), pulse oximetry and invasive blood pressure measurement (CARESCAPE Monitor, GE; Vismo Monitor, Nihon Kohden) throughout the intervention. To end the anaesthesia the Propofol perfusion was stopped. For infection prevention, the animals received 30 mg/kg Cefuroxime i.v. Analgesia was facilitated by application of 0.4 mg/kg Meloxicam i.v., which was continued orally for up to four days post intervention.

3.1.4. Functional heart measurements

3.1.4.1. Echocardiography

All animals underwent echocardiography before ischemia and at the end of each experiment. To detect affected areas of the heart, short-axis and long-axis images were taken with the pig lying laterolateral on an ultrasound table (EIKEMEYER®), the right front leg stretched out and the examiner pressing the phase array probe (X5-1, Philipps; P 2-9/P 1-5, Esaote) onto the right side of the thorax. This was performed with the EPIQ 7G (Philips) or MyLab X8 (Esaote) ultrasound machine.

3.1.4.2. 6 channel ECG

6 channel ECG examination was done with the PC-EKG 2000 (EICKEMEYER®). The pigs were in dorsal recumbency and 5 alligator electrodes were clipped to all 4 legs and the left thorax.

3.1.4.3. Insertable cardiac monitor

Insertable cardiac monitors (ICM) are small implantable devices for long-term ECG monitoring. After myocardial infarction either the BioMonitor 2 or the BIOMONITOR III (Biotronik) was implanted subcutaneously on the left side of the thorax using an incision and injection tool. The devices were programmed with the desired parameters (Figure 4C) via the Renamic programmer and monitoring device (Biotronik). For the BIOMONITOR III the home monitoring application was activated which sends daily ECG measurements to a cloud by the CardioMessenger Smart (Biotronik) via mobile phone network. At the end of the experiment the ICM was deactivated, explanted and data was retrieved by the Renamic appliance.

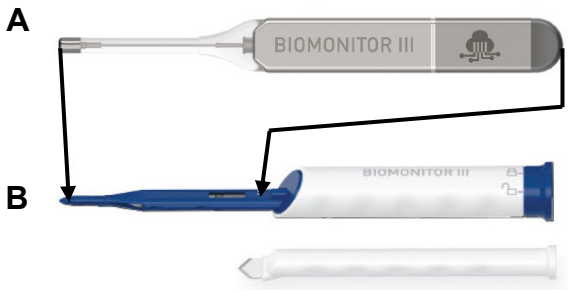

C

Hohe ventrikuläre Frequenz (HVF)	
HVF	EIN
HVF-Limit [bpm]	200
HVF-Zähler	16
Bradykardie	
Bradykardie	EIN
Brady-Limit [bpm]	50
Brady-Dauer [s]	10
Plötzlicher Frequenzabfall (PFA)	
Plötzlicher Frequenzabfall (PFA)	EIN
Verringerung der Frequenz bei PFA [%]	50
PFA-Empfindlichkeit	Mittel
Vergleichsintervalle	64
Frequenzabfallinterv.	16
Dauer Asystolie	
Dauer Asystolie [s]	3

Figure 4: Implantation of an ICM. (A) The BIOMONITOR III with a length of 7.75 cm and a silicon tip. **(B)** The incision and insertion tool (pictures adapted from Biotronik). **(C)** Parameters programmed on the Biomonitors.

3.1.5. Cather-based heart intervention

For all catheter-based heart interventions and functional measurements, a sheath is required to gain access to the arterial circulation. For this, a short skin incision was made in the jugular groove using an electric knife (BOWA-electronic GmbH & Co. KG; Erbe) to expose the musculus sternocleidomastoideus. The medial located right arteria carotis communis was exposed by blunt dissection. Anticoagulation with 10000 IE i.v. Heparine was given before the subsequent ligation cranial to the insertion point of the sheath. The vessel wall was then opened with a small incision and the sheath (Cordis) was advanced via a guide wire. For fixation during the procedure, the sheath was fixed in its position in the vessel with another ligature caudal to the insertion point. This vascular access was then used both as an introducer for catheters and for invasive blood pressure measurement for which it was connected to a fluid-filled electronic pressure transducer (Smiths Medical, Inc.). Ultravist-370 (B. Braun) was used as a contrast agent to visualize structures

on a mobile C-arm X-ray (Ziehm Imaging). Left ventricular angiography was performed using a 6F pigtail catheter. The left ventricle was flushed with 30 ml of contrast agent by a pump (Liebel-Flarsheim) at a rate of 12 ml/s to assess the ejection fraction of the heart. Then, a Judkins right coronary catheter (6F) was used to visualise the vessels in a coronary angiography and as a guiding catheter for coronary wires as well as the catheter for MI induction. LV and coronary angiography were performed before and immediately following myocardial infarction as well as at the end of the experiment.

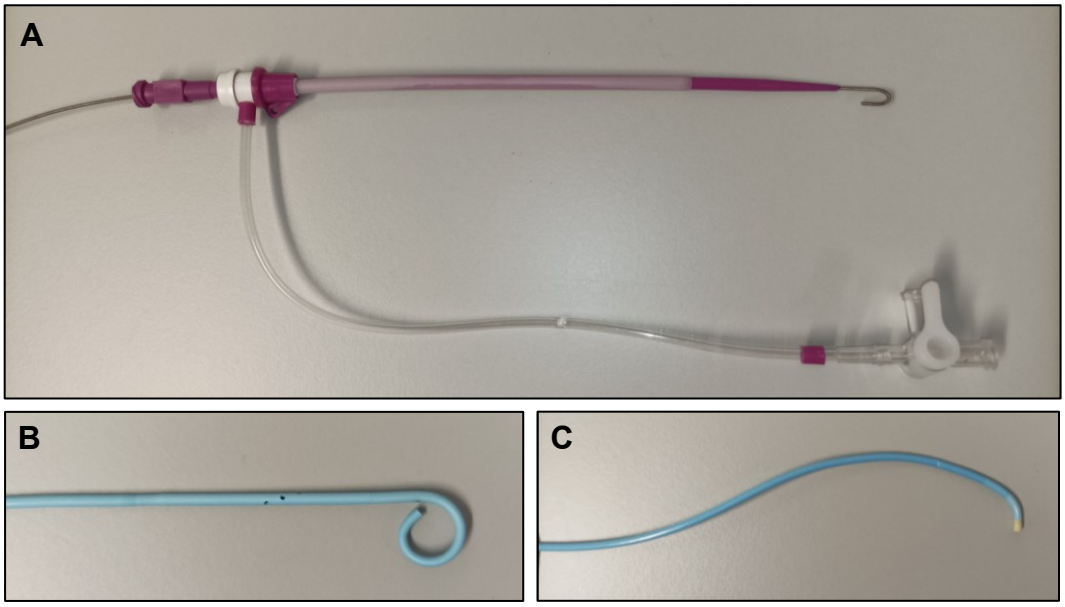

Figure 5: Equipment for catheter-based heart intervention. (A) Sheath. **(B)** Tip of 6F pigtail catheter (110 cm). **(C)** Tip of 6F Judkins right catheter (100 cm).

3.1.6. Induction of myocardial infarction

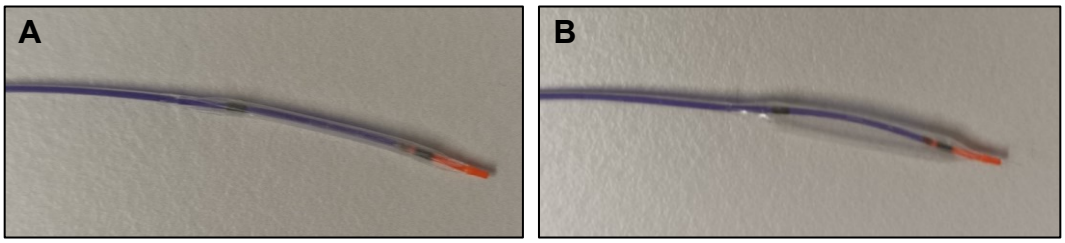

Figure 6: PCTA catheter. (A) Deflated. **(B)** Inflated.

MI was induced via a percutaneous transluminal coronary angioplasty (PCTA) balloon-catheter. For this, a Fielder FC or PROWATER (ASAHI INTECC CO., LTD) coronary guide wire was inserted through the Judkins guiding catheter down into the distal LAD. A PCTA catheter was then advanced over the guide wire to the

correct position within the LAD and inflated using a BasixTouch™ inflation device (Merit Medical GmbH) to block the blood flow through the LAD (Figure 6). Depending on the individual vascular situation, the coronary vessel was blocked mostly in its proximal third after the first big branching (Figure 7).

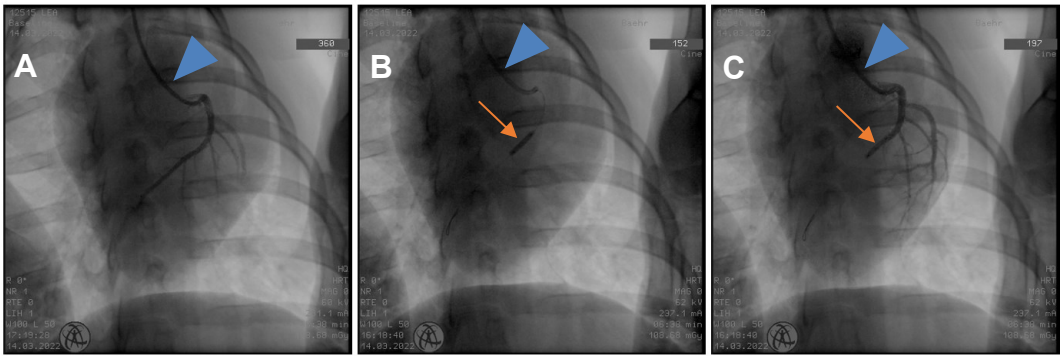

Figure 7: Coronary angiography of LEA29Y 12515. (A) Before MI. Contrast agent injected through a Judkins catheter ▶ visualized the coronary situation and their normal perfusion. **(B)** Induction of myocardial infarction. The balloon → was advanced through the catheter and inflated in the proximal part of the LAD. Therefore blood flow was no longer possible distal to it as shown in **(C)**.

During ischemia, hemodynamics were closely monitored. To counteract arrhythmias, 50 mg Amiodarone was administered i.v. at intervals of 5 minutes for up to three times. Adrenalin was as required to maintain blood pressure. In case of ventricular fibrillation, pigs were defibrillated with up to 360 J by LIFEPAK 20 (Stryker Corporation), initially without releasing the PCTA catheter. Positioning of the balloon catheter was reconfirmed after each defibrillation. If sinus rhythm could not be re-established after three consecutive shocks, the balloon was briefly deflated to facilitate reperfusion and aid resuscitation. It was then re-inflated in the same position for completion of total ischemia time. After 45 or 60 minutes, the PCTA balloon was deflated and removed together with the guide wire. Coronary as well as LV angiography were repeated to visualize re-established blood flow in all vessels and detect initial heart injury through ischemia. After completion of all procedures, the sheath was removed and the vessel and wound closed. For subsequent intervention, the contralateral side was used.

3.1.7. Blood sampling

Blood was drawn into suitable containers, S-Monovetten® K3 EDTA, Lithium-Heparin Gel+ and Serum (Sarstedt AG & Co. KG), either during anaesthesia via the arterial sheath or post intervention through a central venous catheter (Merit

Medical GmbH) that had been inserted through an ear vein using Seldinger technique. For this purpose, a guide wire was first placed into the vessel through a new puncture or via the existing intravenous catheter. This or the puncture cannula was removed and the central venous catheter was advanced over the wire. It was sewn to the skin and protected from contamination or damage by the animals with tape (Tesa SE). After each blood collection, the catheter was rinsed with NaCl and blocked with Heparin diluted 1:10 or Tauro Lock™-HEP500 (TauroPharm GmbH).

Serum samples were centrifuged after 20 min and frozen at -80°C together with EDTA samples. Lithium-Heparin samples were used to isolate PBMC.

3.1.8. Euthanasia and tissue sampling

At the end of each experiment the pigs were euthanized by an intracardial injection of 60 ml KCl in deep anaesthesia. Then a medial sternotomy was performed to explant the heart. The heart was weighed, photographed and underwent a systematic tissue sampling to obtain 36 defined pieces of the left ventricle (LV) as described below:

1. Starting from below- the valve level the heart was cut in 5 equidistant slices.
2. The right ventricle was removed from each slice.
3. The slice was opened to a strand at the point the right ventricle was removed in the area of the Sulcus interventricularis subsinuosus.
4. The strand was cut in 8 (last slice: 4) equisdistant pieces.
5. Additionally, samples of the right ventricle and the atrias were taken.

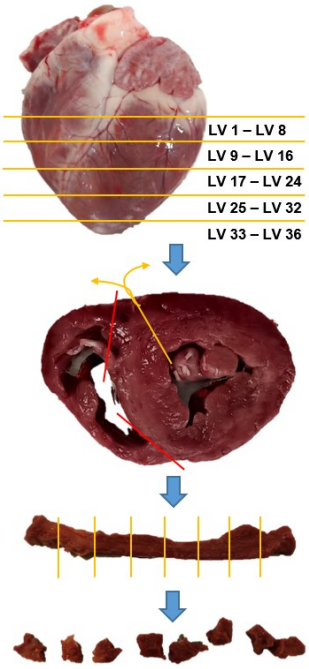

Figure 8: Systematic sampling of the heart tissue. The procedure is described in detail opposite.

Each piece was macroscopically evaluated and classified as MI, Area at risk (AAR) or remote area. The AAR is the still viable part directly adjacent to the infarct region. Each sample was then transmurally divided into three parts. One was frozen

on dry ice as soon as possible, one was frozen in Tissue-Tek® and one was fixed in 4% Formalin. All other tissue samples (right ventricle, right and left atrium, lung, liver, kidney, spleen, lymph node) underwent the same procedure.

3.2. Functional analyses

3.2.1. Infarct size

The infarct size was calculated in two different ways using photographs of the five heart slices of each animal and ImageJ. Firstly, the area share of infarction in the entire left ventricle was determined for one slice and was repeated for all slices (Figure 9A). The percentage of the infarct on the left ventricle was then calculated from the quotient of the sum of all infarct areas by the sum of all areas of the left ventricle. Secondly, the same calculation was repeated with the circumferences instead of the area shares (Figure 9B). Strictly only those areas where the infarct was visible at the outer edge were taken into account as the infarct perimeter.

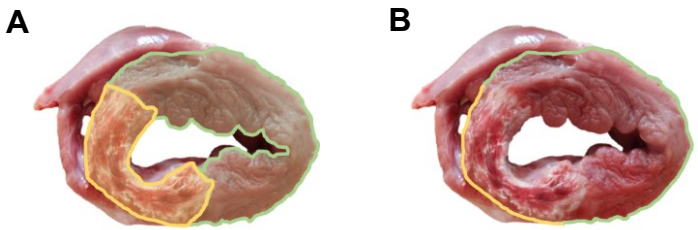

Figure 9: Calculation of infarct size using proportion of (A) area or (B) circumference.

3.2.2. Ejection fraction

The ejection fraction (EF) is an important parameter to assess the pump function of the heart. It describes the volume of blood that is ejected from the LV with each heartbeat and can be examined in different ways. In this experiment LV angiography was used as described above and EF was calculated with the following formula:

$$EF(\%) = \frac{EDV - ESV}{EDV} x100$$

End-diastolic (EDV) and end-systolic (ESV) volumes were calculated as the contrast filling in the respective heart phase, examined in ImageJ (Figure 10).

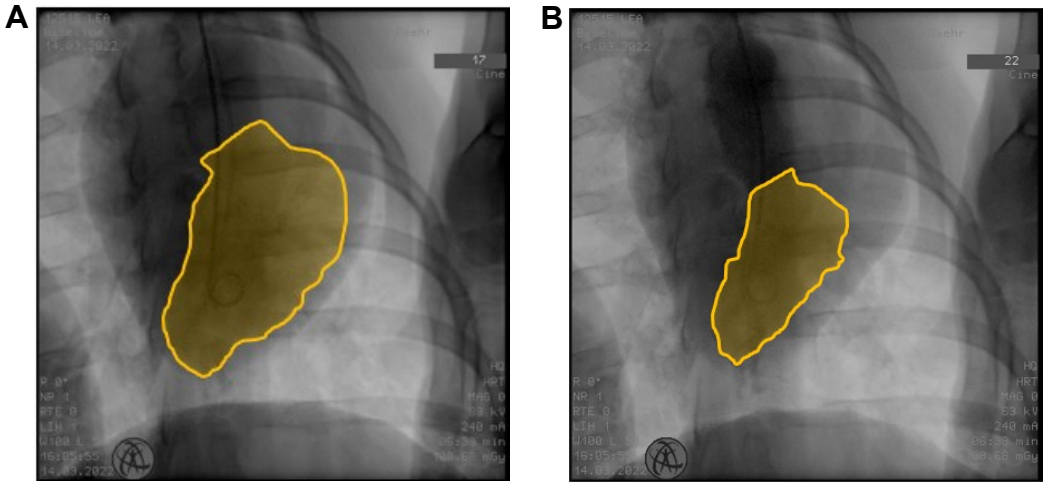

Figure 10: Calculation of EF using X-ray pictures of LV angiography. (A) End-diastolic volume. **(B)** End-systolic volume.

3.3. Molecular analyses

3.3.1. ELISA

A sandwich ELISA was established and performed to detect CTLA4-levels in frozen serum of LEA29Y transgenic animals. For all samples duplicates were tested and plates were read out in an ELISA reader (Tecan). The protocol is provided in Table 6.

Procedure	Reagent	Time
Coating of the plate with primary antibody	0.5 µg anti-CTLA4 antibody in 100 µl coating buffer per well	Stored at 4°C overnight
Washing	200 µl washing and dilution (WD) buffer per well	3x
Application of the antigen	Dilutions of standard, samples, negative control or WD buffer (as blank) in 100 µl washing buffer per well	Stored at room temperature (RT) and light-protected for 2 h
Washing	200 µl WD buffer per well	3x
Application of the second antibody	Dilution of 1:1000 of anti-CTLA4 antibody (HRP) in 100 µl WD buffer per well	Stored at RT and light-protected for 1 h
Washing	200 µl WD buffer per well	3x
Application of substrate	200 µl TMB per well	5.5 min, stored at RT and light-protected
Reaction stop	Sulphuric acid 0.5 mol/l	Response-dependent

Table 6: CTLA4-ELISA protocol.

Used Antigen Dilutions:

Standard (Recombinant human CTLA4 protein, abcam):	6; 4; 2; 1; 0.5; and 0.25 ng/ml
Negative control (serum of WT):	1:10 and 1:20
Samples (Serum of LEA29Y):	1:2000 and 1:4000

3.3.2. PBMC analyses

3.3.2.1. PBMC isolation

Peripheral blood mononuclear cells (PBMC) were isolated from heparinised blood under sterile conditions by density gradient centrifugation according to the following protocol:

1. Heparinised blood was diluted 1:2 with PBS (without calcium and magnesium) at RT.
2. 15 ml of density gradient was carefully overlaid with 25 ml of blood suspension in a 50 ml tube.
3. Density gradient centrifugation: 900g, 30 min, acceleration 4, deceleration 1, 20°C.
4. PBMC (accumulated in the interphase) were collected into a new pre-cooled 50 ml tube.
5. Washing was repeated twice with cooled PBS and hereafter with cold 5% wash medium, consisting of centrifugation (450g, 10 min, acceleration and deceleration 9, 4°C), discarding supernatant and resuspending.
6. Cells were counted: isolated PBMC were resuspended in 5 ml of cold 10% wash medium and 10 µl of this suspension were mixed with 90 µl of Türk´s solution. A Neubauer improved cell counting chamber was used for manual counting.
7. The last washing step was finished with cold 10% wash medium as described in step 5.
8. The isolated PBMC were resuspended with freezing medium and distributed in pre-cooled cryovials in portions of 1 ml each.

Samples were then slowly cooled in CoolCell® container (BioCision) at -80°C over night and transferred to liquid nitrogen the next day for storage.

3.3.2.2. Flow cytometry staining

Flow cytometry staining and analyses were performed at the Pirbright Institute in cooperation and with the kind help of Prof. Wilhelm Gerner und Selma Schmidt.

The cryopreserved samples were thawed in a 37.5°C water bath and transferred to pre-warmed culture medium in 15 ml falcons. After centrifugation (1500g, 8 min, 20°C) the supernatant was discarded, cells were resuspended in 8 ml culture medium and counted as described above. All steps were done under sterile conditions because in addition to *ex vivo* staining, intracellular staining was planned to investigate cytokine production. For this purpose, at least $6x10^6$ cells were divided and cultured overnight at 37°C in a microtiter plate. The remaining cells were centrifuged again, resuspended in PBS and also transferred to microtiter plates, prepared for the *ex vivo* staining. Three different staining panels were performed to identify $CD4^+$ cells, $CD8\beta^+$ and $\gamma\delta^+$ T cells as well as myeloid cells. The labelling of cell surface markers took up to three incubation steps whereby subsequently the eBioscience™ Buffer Set (Thermo Fisher Scientific) was used to fixate and permeabilise cells. Dilutions and labelling strategies are provided in Table 7. For each step, 10 µl of the antibody diluted in PBS+10% porcine plasma was placed in a well on the cells and incubated at 4°C for 20 minutes. To avoid interactions, antibodies were diluted only in PBS in steps where viability dye eFluor™ 780 (Thermo Fisher Scientific) was used. Dilution buffers were also applied for the two washing steps after every incubation. For this, 200 µl were added in each well, cells were centrifuged (470g, 4 min, 4°C), the supernatant discarded and cells resuspended. The following day, cultured cells were stimulated with 20 µl of a mixture consisting of 50 ng/ml phorbyl-12-myristate-13-acetate (Merck), 500 ng/ml Ionomycin (Merck) and 0.22 µl/well Brefeldin A (BD Biosciences) to enhance cytokine production and prevent secretion via the golgi apparatus and before culturing for another 4 hours. Two different intracellular staining panels were performed to detect cytokine levels in $CD4^+$ cells as well as in $CD8\beta^+$ and $\gamma\delta^+$ T cells. Therefore, cell surface markers were again labelled in two steps according to the previously described procedures and after fixation and permeabilisation via the BD Cytofix/Cytoperm (BD Biosciences) antibodies to detect IFN-γ, TNF-α and IL-17A were added. At the end of every staining, samples were washed and finally resuspended in 200 µl of the provided buffer of respective fixation and permeabilisation kit and transferred to tubes (STARLAB) for flow cytometry

analysis. All samples were also processed without staining and measured as controls for auto fluorescence. Additionally, all colours were assessed as single stain controls for the several fluorochromes in a panel.

Antigen	Fluorochrome	Amount per well [µl]	Labelling strategy, possibly following antibodies (and amount [µl])
***Ex vivo* CD4 panel**			
CD3	PerCP-Cy5.5	1	Directly conjugated
ICOS	BV605	0.5	Directly conjugated
FoxP3	PE	0.2	Directly conjugated
Ki-67	PE-Dazzle594	2	Directly conjugated
T-bet	AF647	2	Directly conjugated
CD4	Alexa488	0.2	Secondary antibody: Anti-IgG2b (0.025)
CD8α	BV421	0.1	Secondary antibody: Streptavidin (0.025)
Viable dye (VD)	eFluor780	0.025	Directly conjugated
***Ex vivo* CD8β/γδ panel**			
CD8β	PE	0.5	Directly conjugated
CD27	APC	10	Directly conjugated
CD2	BV711	0.5	Directly conjugated
ICOS	BV605	0.5	Directly conjugated
Ki-67	PE-Dazzle594	2	Directly conjugated
T-bet	AF647	1	Directly conjugated
TCR- γδ	Alexa488	0.025	Secondary antibody: Anti-IgG2b (0.025)
VD	eFluor780	0.025	Directly conjugated
***Ex vivo* myeloid cell panel**			
CD172a	FITC	0.5	Directly conjugated
CD163	PE	3	Directly conjugated
CD14	PE-Vio615	0.2	Directly conjugated
CD16	AF647	0.5	Directly conjugated
CD4	PerCP-Cy5.5	1	Directly conjugated
MHC-II	BV421	0.025	Secondary antibody: goat anti-mouse-IgG2b (0.1)
CADM1	BV605	0.2	Tertiary antibody: donkey anti-chicken-IgY-biotin (0.05), Streptavidin (0.05)
VD	eFluor780	0.025	Directly conjugated
Intracellular staining CD4 panel			
ICOS	BV605	0.5	Directly conjugated
CD27	PE	2	Directly conjugated
IFN-γ	Alexa647	0.025	Directly conjugated
IL-17A	PerCP-Cy5.5	0.75	Directly conjugated
TNF-α	BV711	1	Directly conjugated

CD4	Alexa488	0.2	Secondary antibody: Anti-IgG2b (0.025)
CD8α	BV421	0.1	Secondary antibody: Streptavidin (0.025)
VD	eFluor780	0.025	Directly conjugated
Intracellular staining CD8β/γδ panel			
CD2	BV605	2	Directly conjugated
CD27	PE	2	Directly conjugated
IFN-γ	Alexa647	0.025	Directly conjugated
IL-17A	PerCP-Cy5.5	0.75	Directly conjugated
TNF-α	BV711	1	Directly conjugated
TCR- γδ	Alexa488	0.025	Secondary antibody: Anti-IgG2b (0.025)
CD8β	BV421	0.05	Secondary antibody: Streptavidin (0.025)
VD	eFluor780	0.025	Directly conjugated

Table 7: Flow cytometry staining strategies.

3.3.2.3. Flow cytometry analyses

Stained PBMC samples were analysed in a BD LSRFortessa™ Cell Analzyer (BD Biosciences) with 5 lasers (355 nm, 405 nm, 488 nm, 561 nm, 640 nm) and were processed by FACSDiva™ software. Anlaysis of the data was done by using FlowJo™. In a first step lymphocytes as well as myeloid cells were identified based on their forward (FSC) and side scatter (SSC) properties. After exclusion of not single as well as dead cells (see Figure 11), different subpopulations could be visualized by hierarchically gating for certain markers as shown in Figures 12-16 for the different panels.

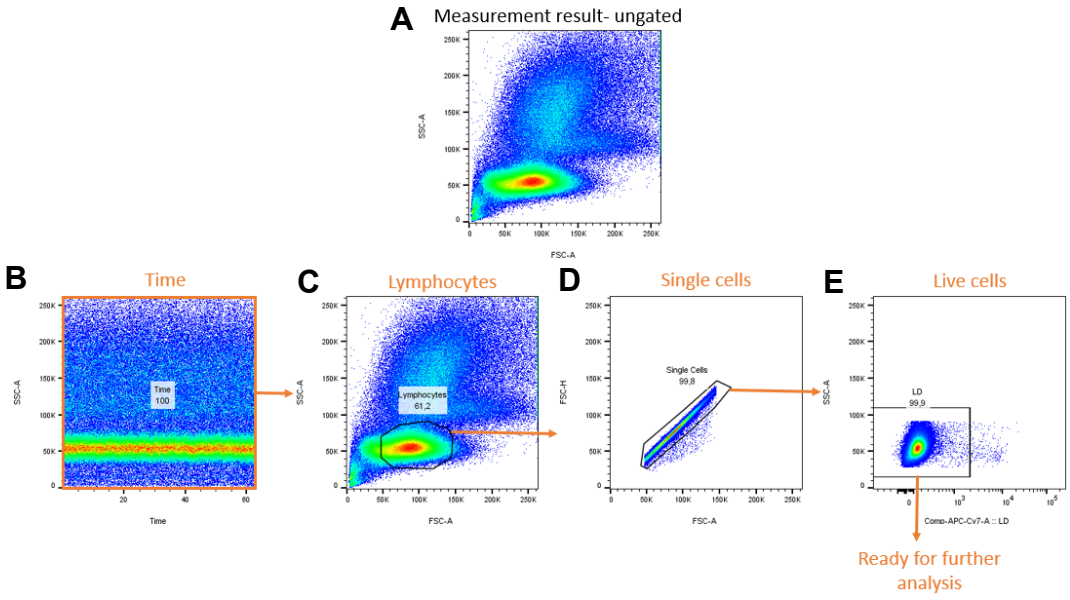

Figure 11: Common starting gates for all lymphocyte panels. (A) Ungated result of all detected cells. **(B)** The consistency of the measurement was checked by a time gate. As many cells as possible were included. **(C)** Lymphocytes were detected as medium-sized cells with low internal granularity. **(D)** Single cells were identified by plotting FSC-area against FSC-height. **(E)** The viability Dye eFluor780 accumulated in dead cells. These were excluded of further analyses.

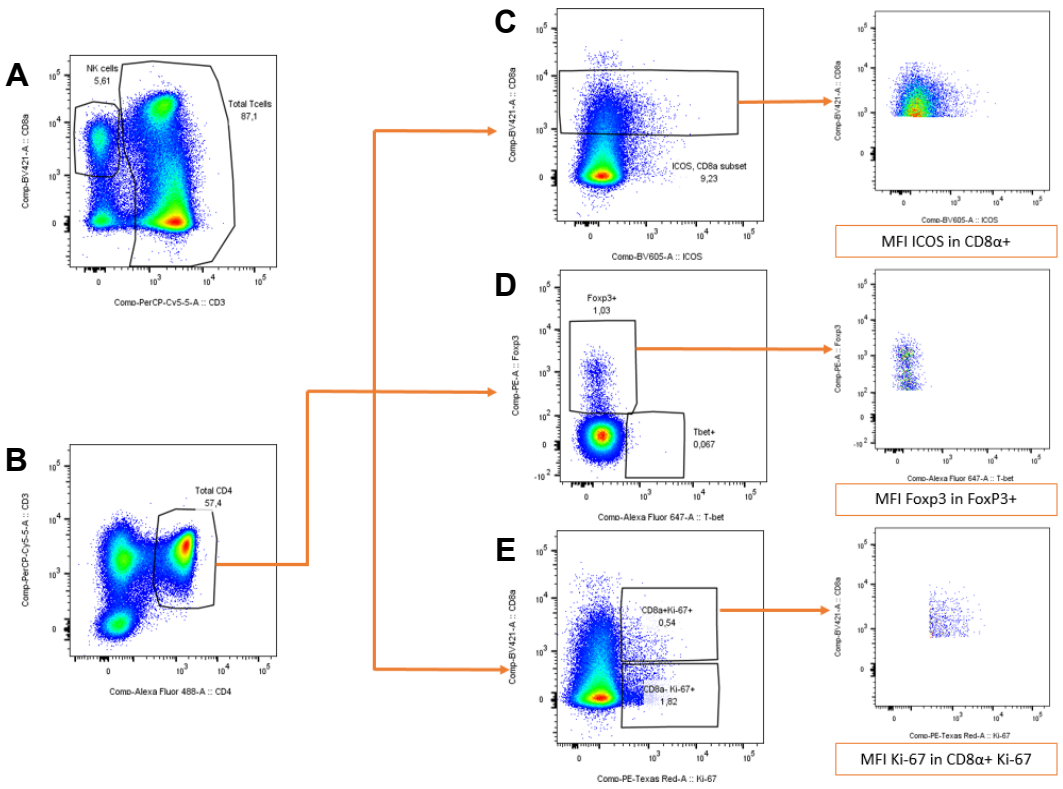

Figure 12: Gating strategies for the *ex vivo* CD4 panel. (A) NK cells were identified by the expression of CD8α but lack of CD3. Positive cells for this were determined as total T cells. **(B)** $CD4^+$ T lymphocytes. **(C)** The activated subpopulation of these was gated as $CD8\alpha^+$ and was further examined by the calculation of the MFI of ICOS. **(D)** Additionally, Tregs were identified by positive staining for FoxP3 as well as, in the case of Th1 cells, for T-bet. The MFI of FoxP3 was calculated within the $FoxP3^+$ subset. **(E)** $CD4^+$ cells were tested for proliferation, characterized by Ki-67, in its CD8α positive and negative subsets.

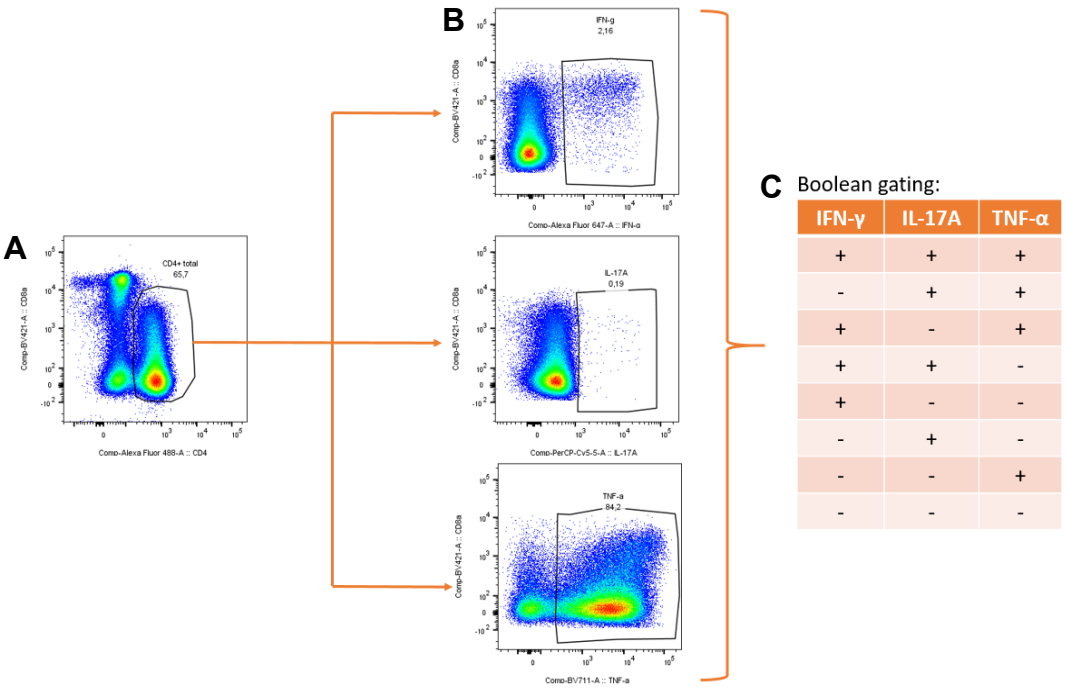

Figure 13: Gating strategies for the intracellular CD4 panel. (A) First it was gated for the total of $CD4^+$ lymphocytes. **(B)** From this, all cells positive for IFN-γ, IL-17A or TNF-α were identified. **(C)** These were used to define single, double or triple positive respectively total negative subsets by Boolean gating.

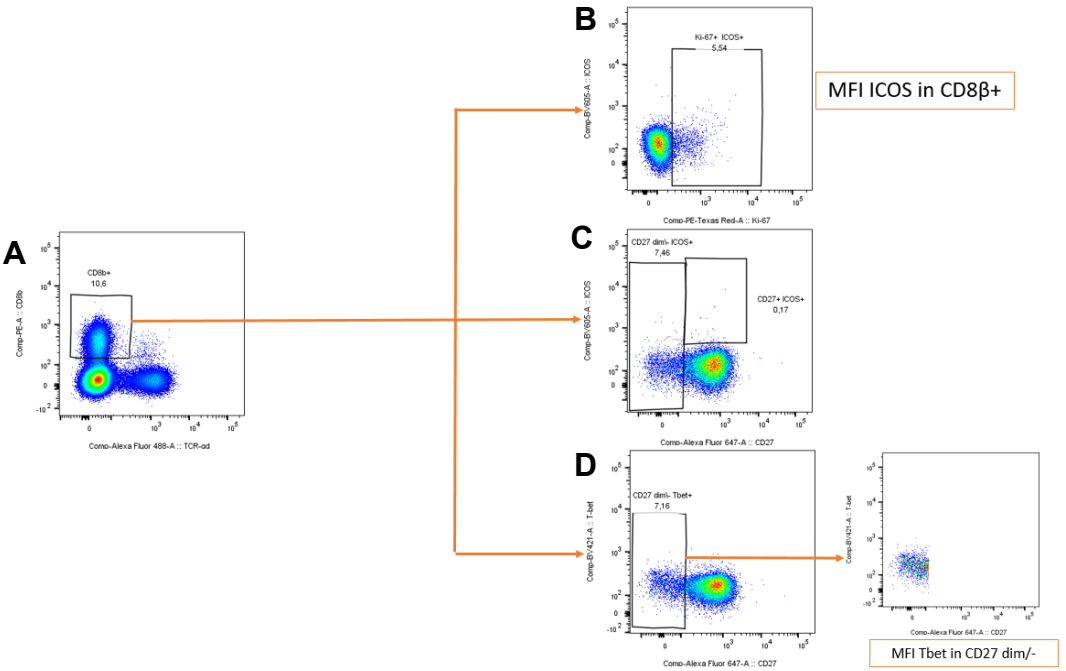

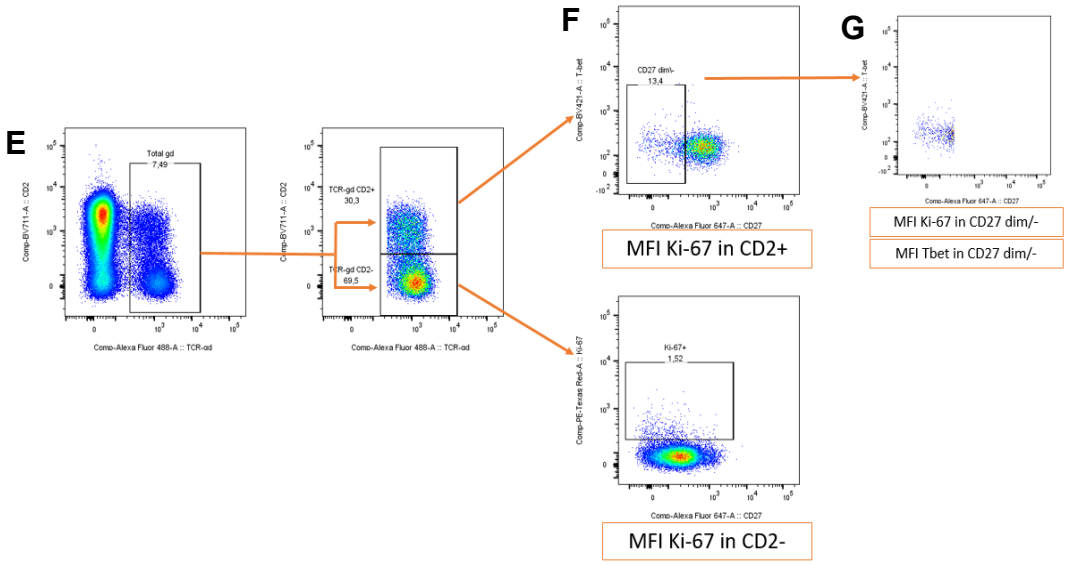

Figure 14: Gating strategies for the *ex vivo* CD8β and γδ panel. **(A)** First cytotoxic T cells, characterized as $CD8\beta^+$, were assessed. **(B)** Cells positive for Ki-67 and ICOS were analysed for their MFI of ICOS. **(C)** Effector cells were identified as $CD27^{dim/-}$ whereas naive cells showed a $CD27^+$ phenotype. **(D)** The effector cells were further tested for T-bet. **(E)** The TCR-γδ was used to mark $\gamma\delta^+$ T cells. These were further distinguished in a CD2 positive and negative subset. **(F)** The proliferative potential of both was investigated by the MFI of Ki-67. **(G)** For the $CD2^+CD27^{dim/-}$ subset this value as well as the MFI for T-bet was calculated.

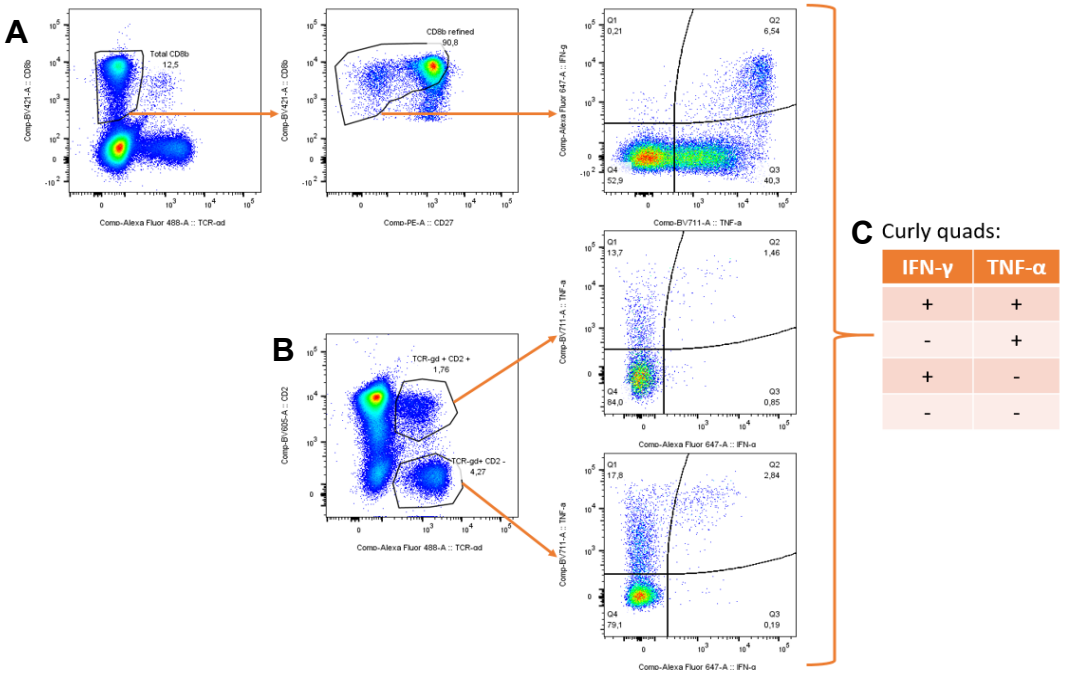

Figure 15: Gating strategies for the intracellular CD8β and γδ panel. (A) $CD8\beta^+$ cells were refined by plotting for CD27 and $CD8\beta^+$. **(B)** $\gamma\delta^+$ T cells were again divided into $CD2^+$ and $CD2^-$. **(C)** For all subsets curly quads for IFN-γ and TNF-α were performed to identify single and double positive as well as negative cells. IL-17A had to be excluded from the analysis because too few cells could be measured.

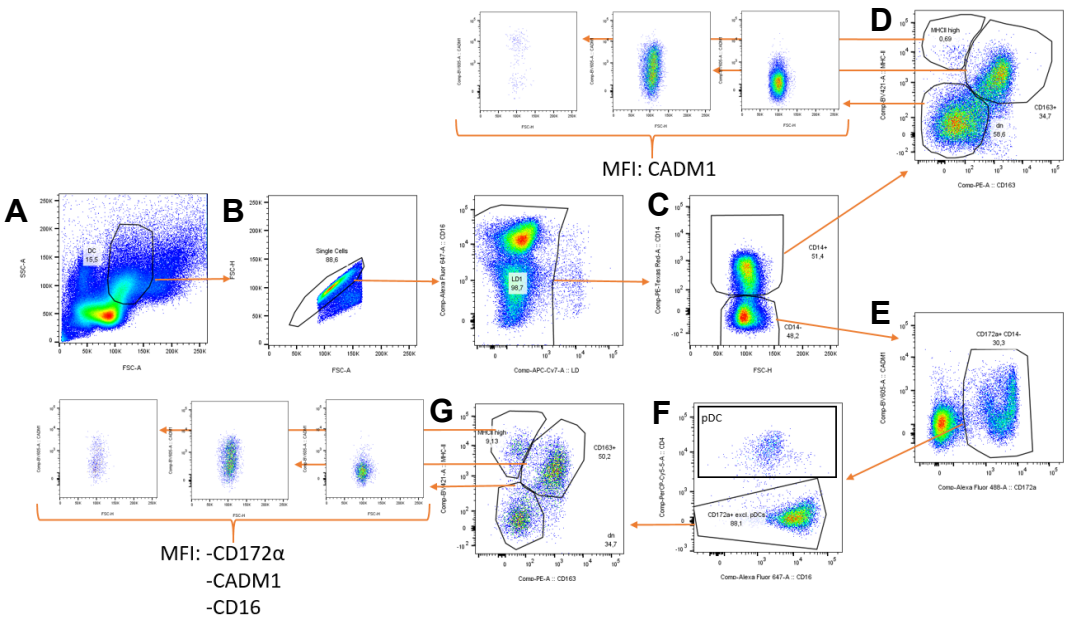

Figure 16: Starting gates and gating strategies for the myeloid cell panel. (A) Myeloid cells were gated as big cells. **(B)** The exclusion of cell aggregates and dead cells was done accordingly to lymphocytes. **(C)** The cells were distinguished as $CD14^+$ monocytes and $CD14^-$ dendritic cells. **(D)** Plotting for CD163 and MHC-II revealed three subsets ($MHC\text{-}II^{high}$, $CD163^+$, double negative). For each the MFI of CADM1 was calculated. **(E)** Typical subpopulations of conventional dendritic cells could not be identified by gating for CD172a and CADM1. Therefore $CD172a^+$ cells were further assessed. **(F)** Plasmacytoid DC were characterized as $CD172a^+$ $CD4^+$. The $CD4^-$ subset was further analysed. **(G)** Again the subpopulations $MHC\text{-}II^{high}$, $CD163^+$ and double negative could be found by plotting this for CD163 and MHC-II. For each the MFI of CD172a, CADM1 as well as CD16 was quantified.

3.4. Histological analyses

3.4.1. Tissue fixation and slice preparation

Tissue samples for the purpose of histological analyses were immediately transferred into 4% formalin solution and fixed for 24 to 32 hours. Thereafter they were processed in the Excelsior AS according to the steps in Table 8.

Procedure	Reagent	Time
Dehydration	EtOH 70% EtOH 90% EtOH 90% EtOH 100%	2 x 1.5 h 1.5 h 1 h 2 x 1 h
Intermedium	Xylol	3 x 1 h
Infiltration	Paraffin Paraffin	2 x 1.75 h 2 h

Table 8: Tissue embedding in Excelsior AS.

Paraffin embedding was done with the TES 99 embedding system and samples were cut into 1 µm thick paraffin sections by Mr. Maximilian Moraw (Klinikum rechts der Isar, TU Munich, Germany) using the Microm HM 325 microtome. Sections were mounted on Star Frost® slices and stored at 37°C until staining.

3.4.2. HE Staining

Procedure	Reagent	Time
Deparaffination	Xylol	20 min
Rehydration	2x EtOH 100% 2x EtOH 96% EtOH 70%	2 min each
Washing	Aqua bidest.	2 min
Staining	Mayer´s Hemalum	5 min
Rinsing	Floating warm tap water	5 min
Differentiation	0.5% HCl- EtOH	1-2 s
Rinsing	Floating warm tap water	5 min
Counterstaining	1% Eosin	2 min
Washing	Aqua bidest.	2 min
Dehydration	EtOH 70% 2x EtOH 96% 2x EtOH 100%	2 min each
Clearing	Xylol	5 min
Mounting	Histokit	

Table 9: Standard protocol for HE staining.

3.4.3. Picro-sirius red staining for fibrosis

Procedure	Reagent	Time
Deparaffination	Xylol	20 min
Rehydration	2x EtOH 100% 2x EtOH 96% EtOH 70%	2 min each
Washing	Aqua bidest.	2 min
Counterstaining	Weigert´s Hematoxylin	8 min
Rinsing	Floating warm tap water	10 min
Staining	Picro-sirius red	60 min
Differentiation	2x 0.5% Acetic acid	3-5 s each
Dehydration	3x EtOH 100%	2 min each
Clearing	2x Xylol	10 min each
Mounting	Histokit	

Table 10: Standard protocol for Picro-sirius red staining.

3.4.4. IHC staining

Procedure	Reagent	Time
Deparaffination	Xylol	20 min
Rehydration	2x EtOH 100% 2x EtOH 96% EtOH 70%	2 min each
Washing	Aqua bidest.	2 min
Heat antigen retrieval	Buffer	20 min in microwave
Cool down		20 min
Washing	TBS	5 min
Blocking	3% H_2O_2	15 min
Washing	TBS	10 min
Biotin blocking	Blocking Buffer + 2.5% normal serum + 50 µl/ml Avidin	30 min
Washing	TBS	1 min
Primary antibody	Blocking Buffer + 2.5% normal serum + 50 µl/ ml Biotin + Primary antibody	Stored at 4°C over night
Washing	TBS	10 min
Secondary antibody	Blocking Buffer + 2.5% normal serum + Secondary antibody	60 min
Washing	TBS	10 min
Avidin-biotin complex	Blocking Buffer + 2.5% normal serum + 1:100 ABC	30 min
Washing	TBS	10 min
Reaction	DAB	Max. 5 min
Rinsing	Floating tap water	5 min
Counterstaining	1:10 diluted Hemalum	10 s
Rinsing	Floating tap water	5 min
Washing	Aqua bidest.	2 min
Dehydration	EtOH 70% 2x EtOH 96% 2x EtOH 100%	2 min each
Clearing	Xylol	10 min
Mounting	Histokit	

Table 11: Standard protocol for immunohistochemical staining.

Immunohisto-chemistry	Buffer for Heat antigen retrieval	Normal serum added to TU Buffer	Primary antibody	Secondary antibody
CD3	Tris/EDTA	Goat	Polyclonal Rabbit Anti-Human CD3 1:100	Goat Anti-Rabbit IgG, biot. 1:200
IBA1	Citrat	Rabbit	Anti-Iba1 antibody 1:500	Rabbit Anti-Goat IgG, biot. 1:200
Neutrophils	Citrat	Goat	Neutrophils, mouse anti porcine, clone PM1 1:100	Goat Anti-Mouse, biot. 1:200

Table 12: Reagents for immunohistochemical staining.

3.4.5. Analyses of Picro-sirius red and immunohistochemical staining

Picro-sirius red and IHC staining was analysed with the help of Prof. Andreas Parzefall (Institute for Veterinary Pathology, LMU Munich, Germany) in a random systematic sampling procedure. As a first step, all 36 tissue samples of the LV were taken and processed in the same way. Sections and staining of all 36 pieces were prepared as described above and then microscoped. Leica DMi8 microscope with Thunder Imaging System (Leica Microsystems) features a function that present a predefined and not necessarily imaged area as a grid of visual fields. In this way, all tiles from LV part 1 to 36 were counted in 10x magnification. A picture of every 180^{th} was taken blinded, starting with a random first one given by an online random generator. It was defined in principle to exclude marginal tiles, which were not covered with tissue completely to avoid potential problems in the subsequent programme-based evaluation due to staining artefacts or empty areas. In this cases, the next closest further in was recorded. Histological studies were performed in two distinct ways. Global evaluations of the entire left ventricle were compared to measurements obtained only in the tissue affected by the ischemic damage. For the latter the next step was to select for analysis only those images that derived from LV pieces that were identified as infarct area or AAR. In terms of the IHC, this classification was based on the macroscopic assessment of each segment during sampling, whereas due to the stronger background staining, for Picro-sirius red this could be complemented by the microscopic judgement of each image. All pictures were in the following processed by ImageJ to calculate the amount of for staining positive pixels as shown in Figure 17. The analysis procedure was kindly provided

by Mr. Martin Kraetzl (Chair for Molecular Animal Breeding and Biotechnology, LMU Munich, Germany). Thereby each image was first split into its red, green and blue channel and the one with the best contrast for the respective staining was selected. In case of the IHC this was the blue one, while for Picro-sirius red the subtraction of the green from red was used. Positive pixels were subsequently counted in these processed pictures applying the same autotreshold method for each to ensure comparability. The percentage of staining of the total or affected left ventricle was then calculated from the quotient of the sum of positive pixels in all analysed pictures of an animal by the sum of all pixels of these pictures.

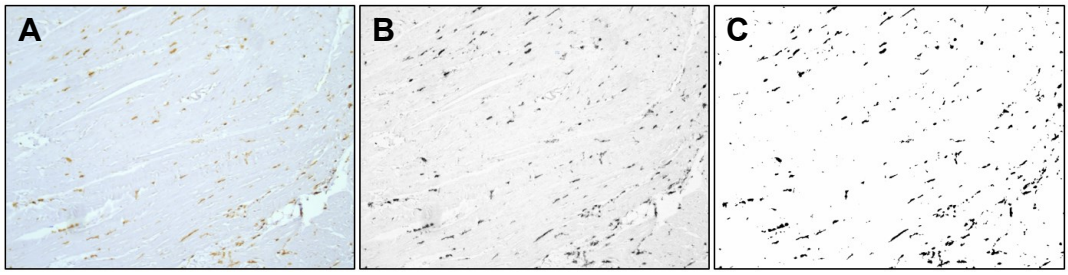

Figure 17: Histological staining analysis via ImageJ. (A) IBA1 staining of 11911_LV24_26 as it is seen in the microscope with the blue, red and green channel merged. **(B)** The same picture, blue channel only. **(C)** The same picture after processing in ImageJ showing the pixels detected and counted as positive.

3.5. Statistical analyses

For statistical analyses ANOVA- with subsequent Tukey´s Multiple Comparison Test as well as unpaired two- tailed- t test were performed with Prism 5 or Microsoft Excel. Effects were considered significant at $p < 0.05$ (*) or high significant in the case of $p < 0.01$ (**) respectively $p < 0.001$ (***). Presented results are specified as mean ± standard error of the mean (SEM).

IV. RESULTS

1. Validation of a catheter-based myocardial infarction model in LEA29Y transgenic pigs

1.1. Breeding program

Animals were generated by mating hemizygous LEA29Y with wildtype pigs. In 6 litters, a total of 56 piglets could be produced, among these, 26 (58%) were identified as LEA29Y transgenic in an endpoint PCR (Figure 18). This corresponds closely to the expected transgenic offspring of 50% according to Mendel's laws. Eleven LEA29Y and seven WT animals were selected as experimental animals in which catheter-based myocardial infarction was induced or which served as controls (Table 13).

Sow	Boar	Delivery date	piglets total	LEA29Y	Experi-mental LEA29Y	Experi-mental WT
LEA29Y	WT	27.05.21	4	4	11910 11911	0
WT	LEA29Y	30.07.21	8 (2†)	4	12100	0
WT	LEA29Y	19.09.21	13 (1†)	5	12321 12325 12327 12330	12322 12323 12324
WT	WT	16.10.21	11	/	/	12382 12383 12384
WT	LEA29Y	24.11.21	11 (1†)	9	12514 12515 12517 12518	0
WT	LEA29Y	26.11.21	9 (1†)	4	0	12551
Σ in 6 litters			**56 (5†)**	**26**	**11**	**7**

Table 13: Breeding program for experimental animals. (†: Stillborn or peripartal dead piglets).

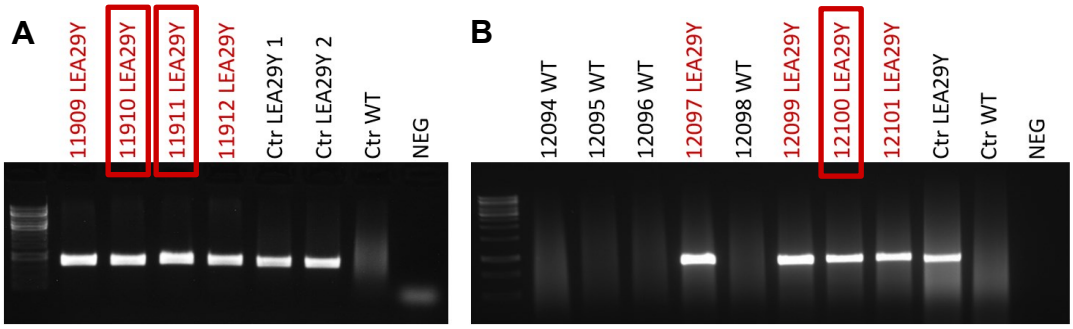

Figure 18: PCR results of animals selected for intervention and as control. (A) Litter delivered on 27.05.21. **(B)** Litter delivered on 30.07.21.

1.2. CTLA4-ELISA

The expression of CTLA4 in transgenic pigs was evaluated with a newly established sandwich ELISA to measure LEA29Y in the blood. Initially this was performed with an ELISA detecting the Fc part of the human IgG domain. But since this showed cross-reactions with porcine immunoglobulin G it was not applicable for a quantitative determination of the fusion protein. The new method targets CTLA4 as a specific epitope and thus enables the precise calculation of concentration in serum. The development has included the testing of various settings until the optimal conditions has been identified (Figure 19B). LEA29Y samples diluted 1:2000 and 1:4000 were added to wells coated with 0.5 µg of the first anti-CTLA4 antibody (abcam) and measured with a 1:1000 dilution of the HRP-conjugated second one (abcam). Mixing of the standard in wildtype serum was performed as a spike assessment to ensure there were no interactions with different diluents. Transgenic animals produced fluctuating results between 3730 and 11495 ng/ml, while the ELISA was negative for all wildtypes tested (Figure 19D). In the hulgG-ELISA, LEA29Y animals obtained values higher by a factor 10^2 and WT were also positive (Figure 19C).

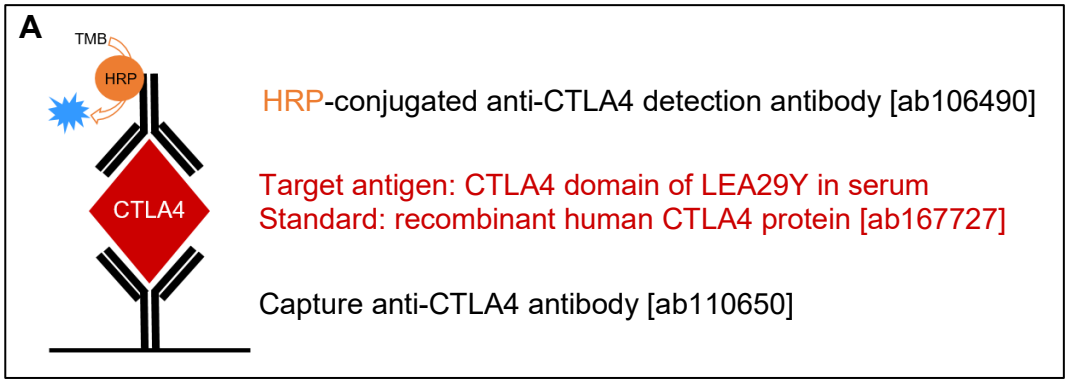

B

Conc. Standard	Conc. Capture Ab	Conc. Detection Ab	Dilution neg. ctr (WT serum)	Dilution samples (LEA29Y serum)	Reaction time TMB
6 ng/ml-0.25 ng/ml 16 ng/ml-1 ng/ml 1 µl/ml-1 ng/ml	0.25 µg 0.5 µg	1:2000 1:1000 1:500	1:1000 1:100 1:20 1:10	1:100000 1:1000 1:50000 1:500 1:10000 1:100 1:5000 1:50 1:4000 1:10 1:2000	3.5 min 5 min 5.5 min

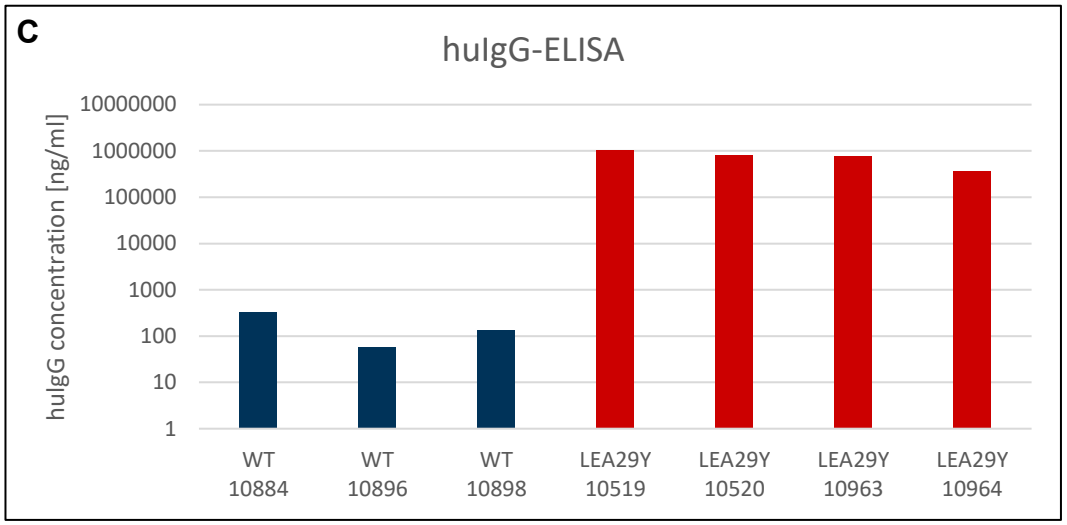

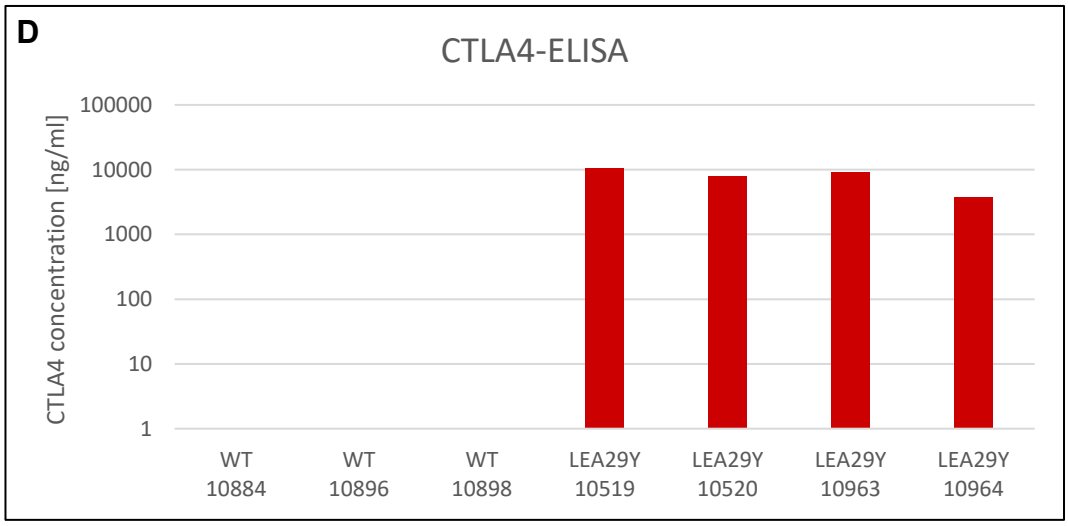

Figure 19: CTLA4-ELISA. (A) Reaction principle and used reagents (abcam, UK) of the sandwich ELISA. **(B)** Settings tested and selected as optimal during development. **(C)** Results of transgenic and WT animals in the hulgG-ELISA. **(D)** Results of transgenic and WT animals in the CTLA4-ELISA.

1.3. Catheter-based induction of myocardial infarction

Myocardial infarction with subsequent reperfusion was performed by percutaneous transluminal coronary angioplasty in 12 pigs. A sheath was used as arterial access for a Judkins catheter, through which a guide wire was placed into the left anterior descending artery. A balloon catheter was then advanced over the guidewire into the LAD and inflated to produce temporary ischemia. One single animal had to be

euthanized during the intervention due to an unstoppable bleeding upon the insertion of the arterial sheath. All other pigs underwent balloon catheter-induced MI and presented with ventricular extrasystoles within the ischemia time of 45 or 60 minutes. These went into ventricular fibrillation in three cases, which required defibrillation and brief deflation of the catheter but could successfully be treated. Complications following the intervention occurred in a single animal after 9 days. In total, myocardial infarction was successfully reproduced in 11 animals that were examined at different time points after MI and compared with another 6 pigs that were considered untreated controls.

Group	Animal		Ischemia duration [min]	Complications during intervention	Complications post intervention
	#	Genotype			
3 days	**12327**	**LEA29Y**	45	VES	/
	12330	**LEA29Y**	45	VES	/
	12514	**LEA29Y**	60	2x VF, defibrillation, deflation balloon, manual reanimation	/
	12515	**LEA29Y**	60	VES	/
	12382	**WT**	45	VES, SVES	/
	12383	**WT**	45	VES	/
	12384	**WT**	45	VF, defibrillation, deflation balloon	/
9 days	**11911**	**LEA29Y**	45	VES, blood pressure ↓	Day 9: circulatory disorder front leg
	12517	**LEA29Y**	60	VF, defibrillation, deflation balloon	/
	12518	**WT**	60	Unstoppable bleeding during insertion of arterial sheath → intraoperative euthanasia	
	12551	**WT**	60	VES	/
14 days	**11910**	**LEA29Y**	45	VES, blood pressure ↓	/

Table 14: Outcome of catheter-based induction of MI in 12 pigs. (VES: ventricular extrasystoles, SVES: supraventricular extrasystoles, VF: ventricular fibrillation, ↓: decrease).

2. Functional effects of the myocardial infarction

Various diagnostic means were performed in order to assess the effect of the myocardial infarction on cardiac function.

2.1. Echocardiography

Echocardiography was carried out to determine functional changes in the heart as a non-invasive examination of wall motion. Loops of short- and long-axis views at the end of the follow-up period were compared with baseline tests taken before MI was induced. Hypomotile wall movement and impaired contractibility could be observed for all animals. Depending on the extent and location of the ischemia and the quality of the echocardiography, they were recognisable as signs of damage to varying degrees.

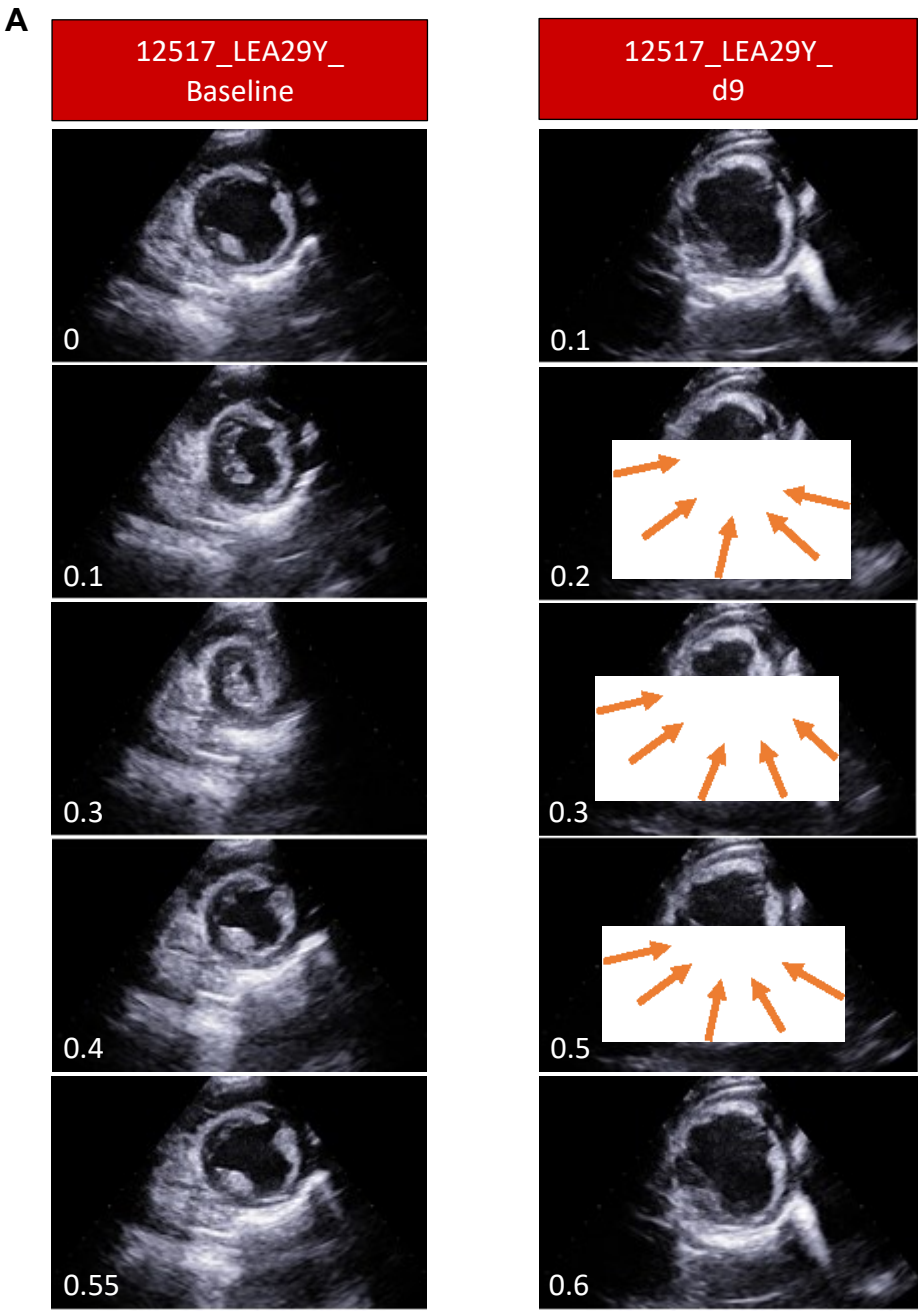

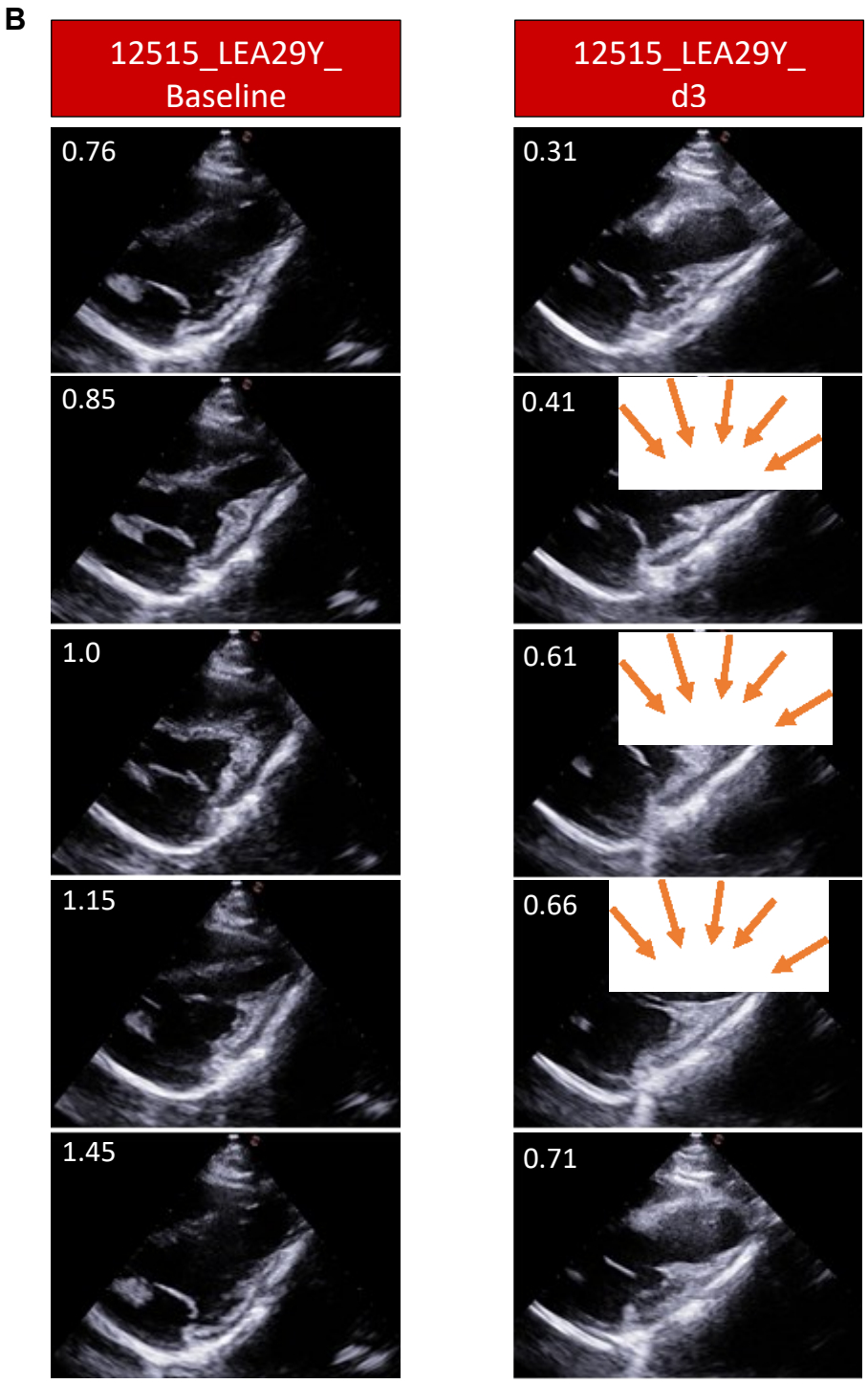

Figure 20: Echocardiographic loop images. The small numbers on the left indicate seconds after start of the loop, → refer to hypomotile wall sections compared to baseline measurements. **(A)** Short-axis view of LEA29Y pig 12517 before MI and at the end of the experiment 9 days later. The left anterior wall appeared affected. **(B)** Long-axis view of LEA29Y pig 12515 after 3 days. In this case, both the septum and the apex were impaired in their contractile function.

2.2. Left ventricular angiography

Ejection fraction (EF) was evaluated from LV angiography. For this, contrast agent was injected into the left ventricle over 2-3 heart cycles to visualize blood flow. Before myocardial infarction all animals showed an EF between 42 and 50% with no distinction between LEA29Y and WT animals. These baseline values were compared to LV angiographies obtained immediately after MI. The ischemia led to an instantaneous reduction in EF by an average of -10.3 ($\Delta EF_{\text{post MI-Baseline}}$ LEA29Y: -10.9±1.45, WT: -9.174±0.8362, p=0.4232) to 32-43%. This impairment even worsened over the follow-up period, as measurements at the end of each experiment showed a further decrease of ejection fraction in almost all animals. Only WT 12382 and 12384 as well as LEA29Y 12517 presented a slight recovery (Figure 21A) but in general, final EF was lower than before the myocardial infarction in each case (Figure 21B). The reduction varied between -17.2 (LEA29Y 12327) and -4.5 for wildtype 12384. The low loss of function in this animal was due to a brief deflation of the PCTA catheter during ischemia because of severe cardiac arrhythmias, causing ischemic preconditioning. This phenomenon depicts the beneficial effects of previous non-persistent oxygen deficiencies on the outcome of a severe myocardial infarction and is also known to positively affect global heart function (KEVIN et al., 2003). LEA29Y pigs demonstrated a significantly higher post ischemic impairment of EF than the wildtypes after three days as shown in Figure 21C. Including also the animals of the 9- and 14-day groups suggested that this effect could only be determined in the first phase after myocardial infarction ($\Delta EF_{\text{Final-Baseline}}$ (all animals) LEA29Y: -13.14±1.258, WT: -9.269±2.167, p= 0.1286).

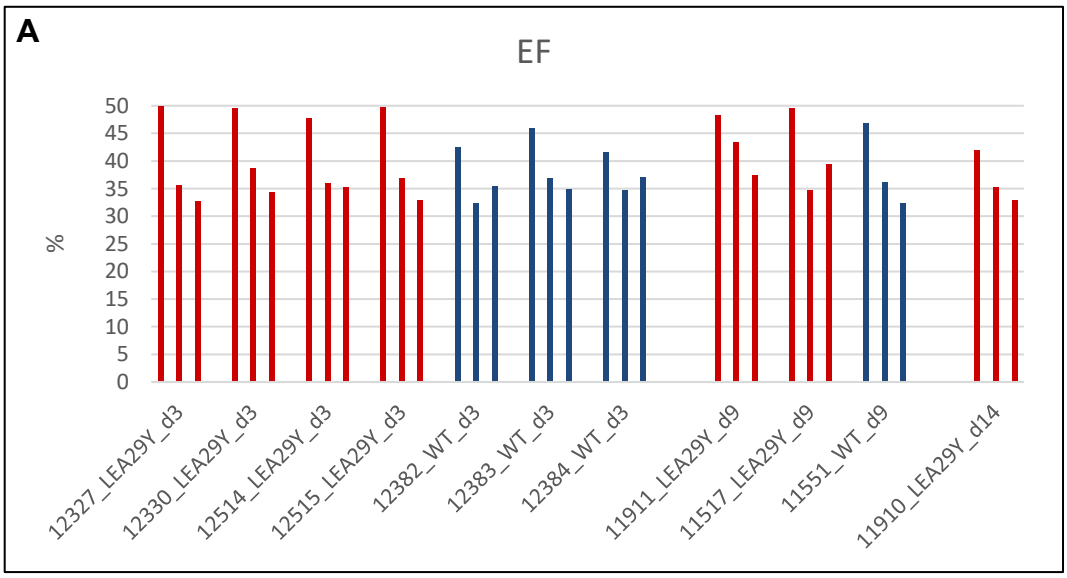

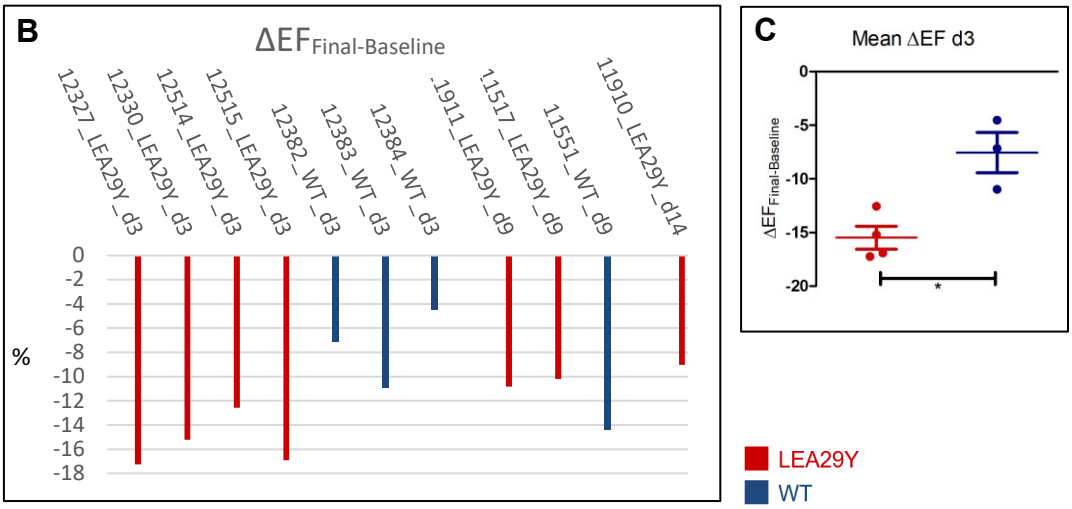

Figure 21: Analyses of ejection fraction. (A) All values for each pig. The first bar symbolises the measurement before MI, the second the one directly obtained afterwards and the third the final EF before euthanasia. **(B)** $\Delta EF_{Final\text{-}Baseline}$ for each animal. **(C)** Mean $\Delta EF_{Final\text{-}Baseline}$ of the 3-day trial group. LEA29Y: -15.48±1.069, WT: -7.554±1.873, p=0.011.

2.3. Electrocardiography

Electrocardiography was used as another qualitative method to characterise the functional effects of myocardial infarction. ST-elevations and depressions in the 6-channel ECG were observed directly after the ischemia. In some animals not only an anterior wall infarction (ST-elevation in lead I, aVL) could be detected, but involvement of the posterior wall (ST-elevation in lead II, III, aVF) was also suggested. ECG changes persisted until the end of the follow-up period nearly in each pig and were usually most evident in the final measurements of the 3-day group, but again wildtype 12384 displayed smaller effects (Figure 22A/B), as ischemic preconditioning can also positively influence arrhythmia development (VEGH et al., 1995). Only LEA29Y 12514 and WT 12551 had normalised electrocardiograms at the end of the experiments after 3, respectively 9, days. Overall, apart from severe alterations and clear arrhythmias of the transgenic pig 12515 at 72 hours, no differences between LEA29Y and wildtype animals could be detected in terms of rhythm, morphology and elevations or depressions following MI (Figure 22C).

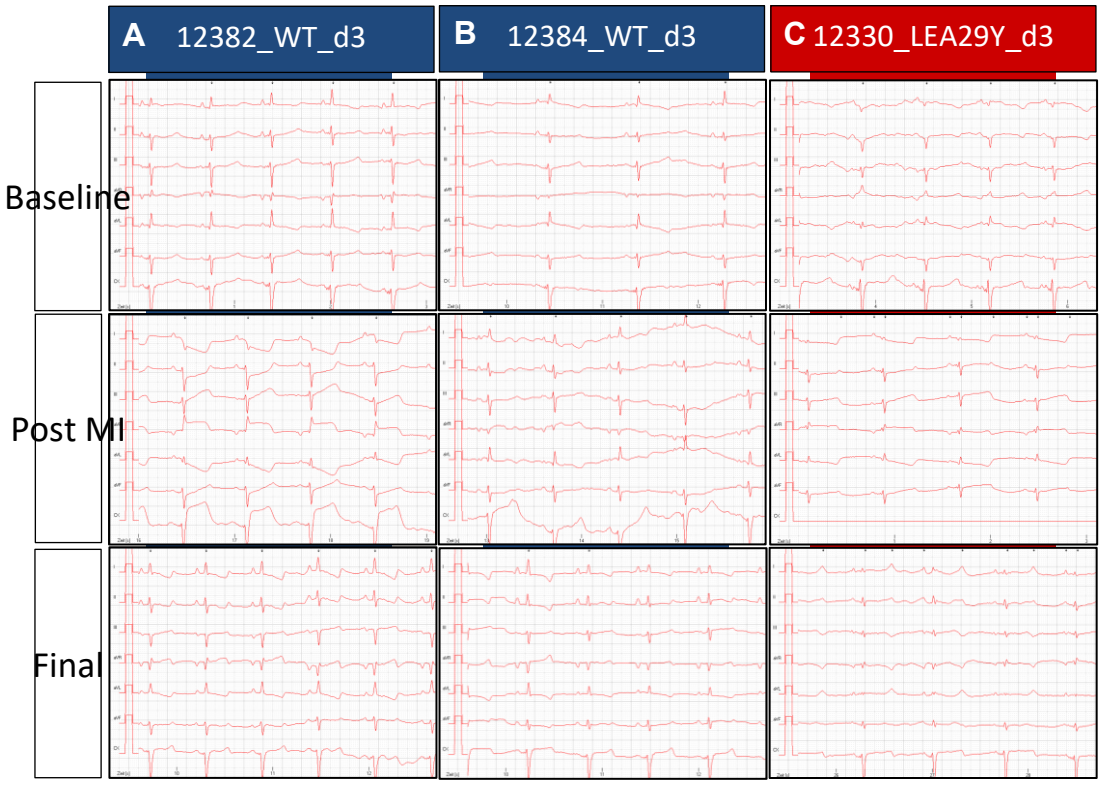

Figure 22: 6 channel ECG. (A) WT 12382. Immediately after ischemia, marked elevations (lead: III, aVR, aVF, CX) and depressions (I, II, aVL) were observed, which were still detectable after 3 days. **(B)** WT 12384. Similar changes were also detectable in this animal at both times after the infarction, but less pronounced. **(C)** LEA29Y 12330. This transgenic animal displayed ST-elevations in lead II, III, aVR and aVF as well as depressions in I and aVL (CX was not evaluated due to a technical problem). Although these were no longer clear after 72 h, small QRS complexes and negative T waves were signs of a post infarction stage.

2.4. Insertable cardiac monitor

For longitudinal observation of heart function, an insertable cardiac monitor (ICM) was subcutaneously implanted in each pig after MI as shown in Figure 23A. This offered the opportunity to monitor heart function over the entire follow-up period. The devices measure heart rate and recognize arrhythmias based on a specific algorithm. The monitoring revealed heavily fluctuating heart rates for all animals in a range from 50 to 300 bpm (Figure 23D) with numerous episodes sensed as sinus tachycardia. Usually during these periods, nearly all pigs showed ventricular extrasystoles (VES), mostly already on the first day after the MI, suggesting that myocardial infarction had caused significant damage. These VES occurred in various forms such as bigemini, duplets, triplets and up to salves. In a total of 5 transgenic and only one WT pig, they even turned into non-sustained ventricular tachycardia (VT) at rates of up to 150 bpm (Figures 23B/C). VT could mostly be

observed from day 3 onwards, in LEA29Y pigs 12515 and 12517 this was already the case on the first day after the myocardial infarction. Another quite unexpected observation was that many tachycardia episodes were recorded at night. Elevated heart rates are usually related to the catecholamine and cortisol release associated with handling or feeding. At night, however, external influences such as these could be ruled out to stress the animals.

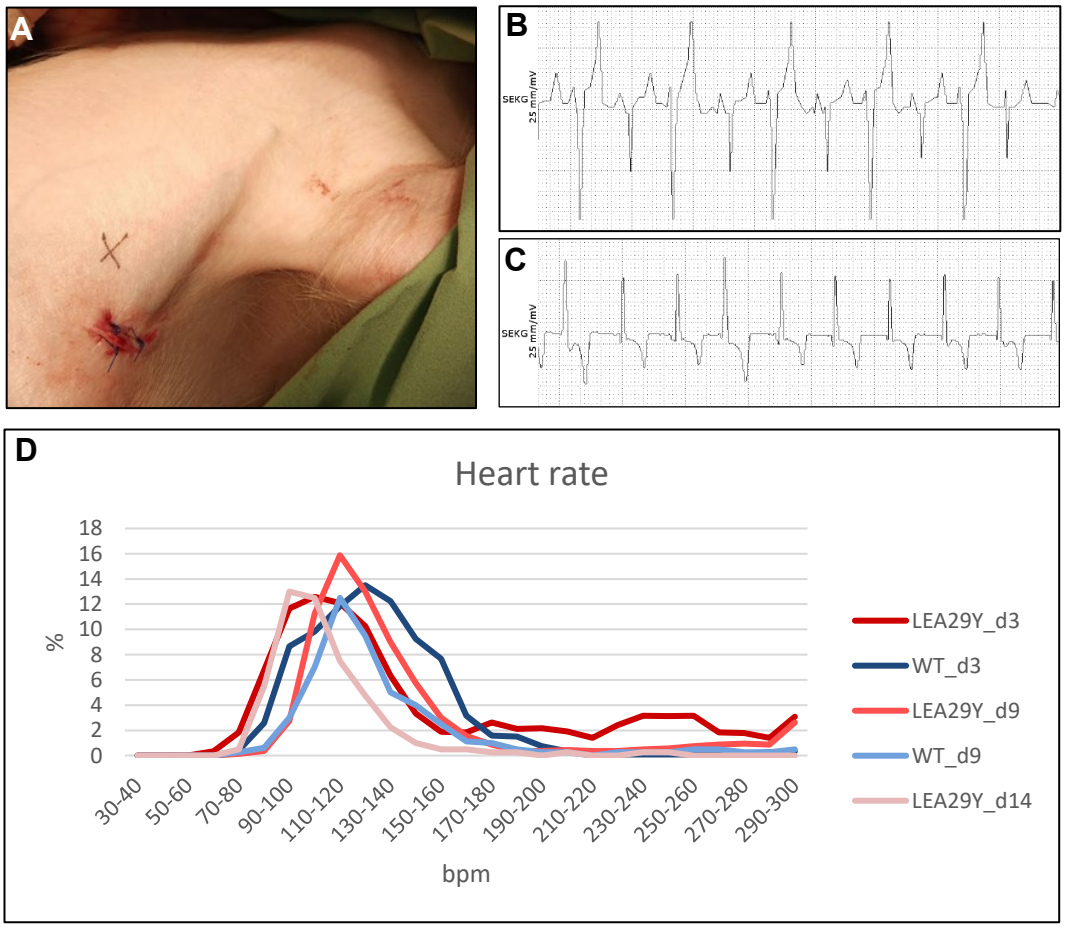

Figure 23: Insertable cardiac monitors. (A) The BIOMONITOR III subcutaneously implanted on the left side of the thorax. The pig is in a supine position and the head is at the top right corner of the picture. **(B)** Bigeminus rhythm of WT 12384 one day after MI. **(C)** A sequence of non-sustained VT of LEA29Y 11910 on day eight. **(D)** Analyses of the heart rate of the experimental groups. Transgenic LEA29Y animals seemed to show a higher range and more often heart rates >200 bpm compared to WT.

2.5. Infarct size

Upon completion of the experimental follow-up period, animals were euthanized and the heart was explanted and evaluated macroscopically. An infarct could be clearly detected in each animal. Infarct size was calculated as proportion of area as

well as circumference of the left ventricle and yielded values ranging from 14 to 36% of LV for surface assessment and between 12 and 43% when analysing the perimeter (Figure 24A/B). For both methods no significant difference could be detected between the experimental groups. In the 3-day group, wildtype 12384 showed the smallest infarct of only 18% or 12% of LV due to the deflation of the PCTA catheter and the thereby caused ischemic preconditioning that leads to less tissue damage (VAN DEN BOS et al., 2005).

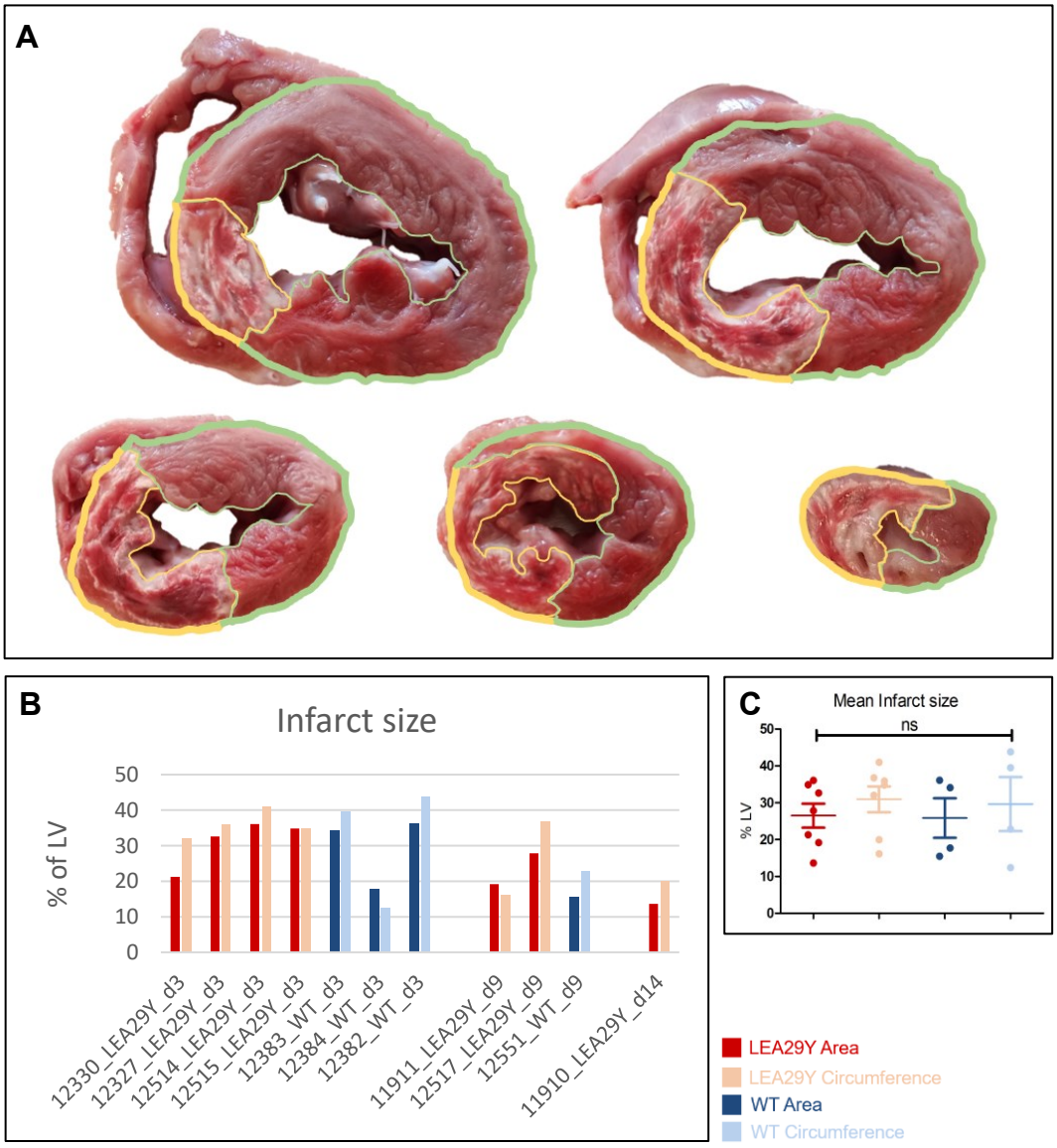

Figure 24: Infarct size. (A) Calculation of the infarct size of LEA29Y 12327. **(B)** Results of both methods for every animal. In the 3-day group, a mean infarct size of 30% (area) respectively 34% (circumference) of the LV was determined. Smaller values were measured after 9 and 14 days, which was consistent with the expected course of a scar contraction. **(C)** Mean infarct sizes between 26% and 31% showed neither a significant difference between the analysis techniques nor in the animals.

3. Systemic immune cell profiling

Isolated PBMC were used to study the effect of myocardial infarction and subsequent reperfusion on circulating immune cells. They were examined at different time points during the experiment and compared to values obtained before MI as the baseline condition. Table 15 lists the respective sample numbers used for the analyses. It must be taken into account that populations were not calculated as absolute numbers but as a proportion of the parent one so that any increases or reductions may be the result of shifts in other subpopulations.

Time point	Baseline	Post MI	Post 24h	Post 48h	Post 72h	Post 9d	Post 14d
LEA29Y	7; ICS:6	7	2	4; ICS:3	5	2	1
WT	3	3	3	4	4	1	1

Table 15: Analysed sample numbers in flow cytometry. Particular measurements were excluded due to insufficient cell numbers, as it was the case twice for the intracellular staining (ICS). Different sample sizes were also caused by systemic problems in blood collection or cell isolation. For the 14-day group blood from an additional WT animal was analysed.

Of special interest here were T cells, since this leukocyte subset is particularly affected by the pathway underlying the immunosuppressive model of LEA29Y. The transgenic animals showed a higher proportion of T cells in total leucocytes compared to wildtype pigs as shown in Figure 25.

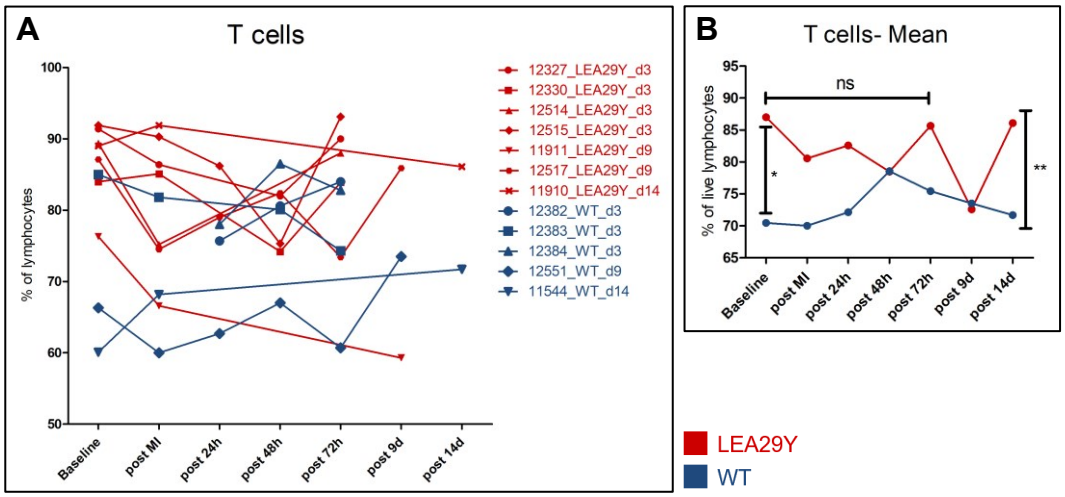

Figure 25: T cells. (A) Individual results of all animals. **(B)** The mean values of all measurements. These were checked for differences between LEA29Y and WT pigs at the individual time points and in the overall course as well as for changes within a group during the first 72h. The proportion of T cells was significantly higher in LEA29Y animals (LEA29Y: 87.01%±2.051, WT: 70.47%±7.484, p=0.0172)

before myocardial infarction and this was even more striking when looking at the entire study period (LEA29Y:81.86%±1.941, WT: 73.12%±1.144, p=0.0022). There were no clear in- or decreases in the courses within the individual groups.

3.1. CD4$^+$ T cells

Within the T lymphocytes, the LEA29Y pigs also showed a greater proportion of CD4$^+$ cells (Figure 26A). However, a closer look at several subsets revealed further differences in the composition of this T cell population. The percentages of type 1 T helper cells (Th1) as well as regulatory T (Tregs) were significantly higher in WT (Figure 26B/C). This was also the case for cells with a phenotype positive for CD8α, which is considered as a swine-specific activation marker. Furthermore their capacity to proliferate or express the inducible T cell costimulator (ICOS) as a further expansion signal was at a lower level in the transgenic animals (Figure 26C-E). Additionally, the lymphocytes were examined regarding their cytokine (co-) production of IFN-γ, IL-17A and TNF-α. Thereby the subset of TNF-α-single-positive cells was the only one found more frequently in LEA29Y pigs (Figure 26F).

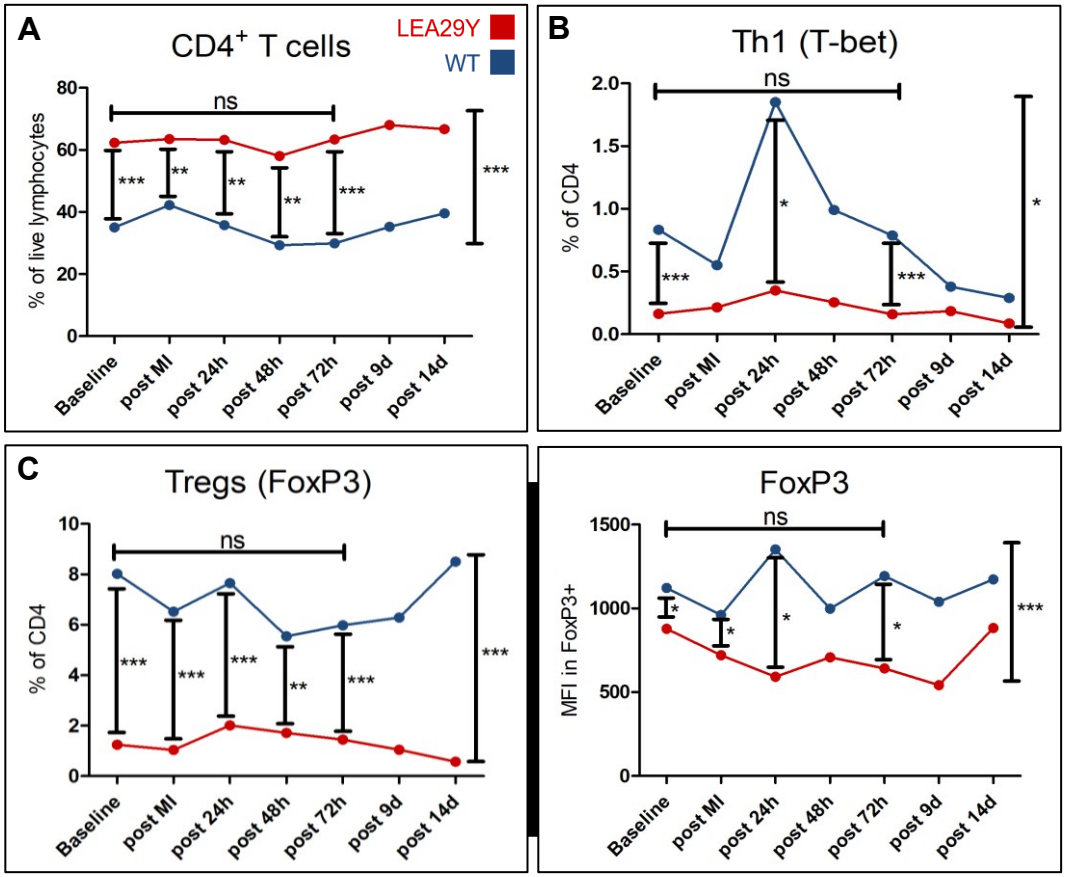

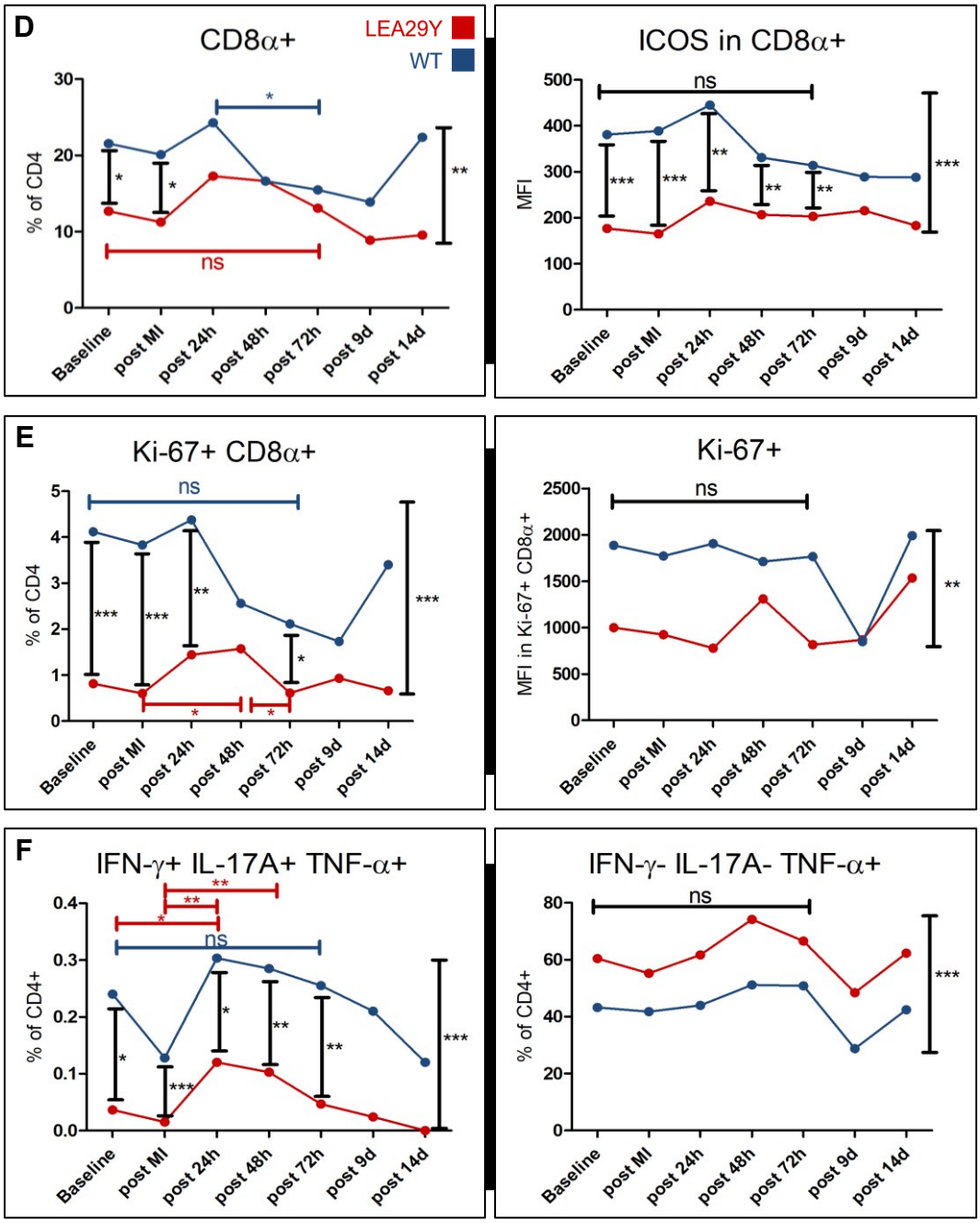

Figure 26: CD4⁺ T cells. (A) Frequency of $CD4^+$ within live lymphocytes. These appeared stable but with 63.58%±1.21 in a significantly higher percentage in LEA29Y pigs compared to 35.29%±1.77 in WT over the entire time course ($p<0.0001$). **(B)** Proportion of type 1 T helper cells within $CD4^+$ cells. Th1 occurred more often in WT (LEA29Y: 0.2018%±0.03158, WT: 0.8115%±0.1975, $p=0.0101$). Only for this genotype an increase after 72h was detected but it was not statistically relevant. **(C)** Frequency and median fluorescence intensity (MFI) of regulatory T cells. The proportion of Tregs within $CD4^+$ cells was about five times lower in transgenic pigs (LEA29Y: 1.295%±0.1798, WT: 6.930%±0.4248, $p<0.0001$) and showed also a lower MFI (LEA29Y: 709.1±50.05, WT: 1120±50.88, WT: $p<0.0001$). **(D)** Proportion of $CD8\alpha^+$ cells and their MFI of ICOS. $CD8\alpha^+$ cells were significantly more frequent in $CD4^+$ cells derived from WT pigs (LEA29Y: 12.77%±1.22, WT: 19.2%±1.47, $p=0.0057$). For this group a clear decrease between day 1 and day 3 as well as higher MFI values of ICOS were

observed (LEA29Y: 198±9.273, WT: 348±22.2, p<0.0001). **(E)** Frequency and MFI of Ki-67. The percentage of Ki-67$^+$ CD8α$^+$ within CD4$^+$ was about four folds lower in LEA29Y animals before and shortly after MI. Despite a relevant increase it stayed significantly under the level of WT (LEA29Y: 0.9481%±0.1520, WT: 3.162%±0.3905, p=0.0002). The MFI of Ki-67 within this subpopulation was also lower in transgenic pigs (LEA29Y: 1032±107.0, WT: 1697±146.0, p=0.0032). **(F)** Cytokine (co-)production of CD4$^+$ cells. Triple-positive cells showed similar courses in both groups, with a significant increase in LEA29Y during the first 3 days but with a higher proportion within wildtype derived CD4$^+$ cells (LEA29Y: 0.04936%±0.01707, WT: 0.2201%±0.02735, p=0.0002). This was also the case for almost all other (co-)producing subpopulations. Only TNF-α-single-positive cells were more frequent in the transgenic animals (LEA29Y: 61.26%±3.078, WT: 43.17%±2.815, p=0.001).

3.2. Cytotoxic T cells

In contrast to CD4$^+$ cells, there were no significant differences in the percentages of CD8β$^+$ T lymphocytes (Figure 27A). The production levels of IFN-γ and TNF-α were also similar in both genotypes. Only for Ki-67$^+$ (LEA29Y: 5.196%±0.4964, WT: 8.44%±1.307) as well as for ICOS$^+$ naive CD8β$^+$ cells a higher frequency within the cytotoxic T lymphocytes of wildtype pigs could be detected (Figure 27B).

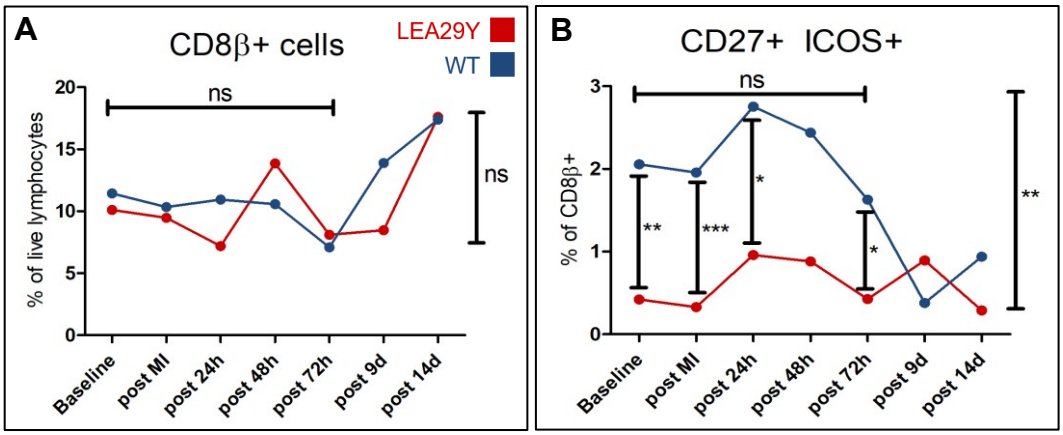

Figure 27: CD8β$^+$ T cells. (A) Frequency of CD8β$^+$ as percentage of live lymphocytes. This analysis showed similar results for both groups (LEA29Y: 10.69%±1.41, WT: 11.67%±1.218, p=0.6073). **(B)** Proportion of naive CD27$^+$ ICOS$^+$ cells within the CD8β$^+$ population. Especially before and during the first days after MI, this subset was much smaller in transgenic animals (LEA29Y: 0.6008%±0.1121, WT: 1.736%±0.3148, p=0.0053).

3.3. γδ$^+$ T cells

The distinct T lymphocyte subclass of γδ$^+$ cells in pigs showed higher frequencies in wildtype animals (Figure 28A) while the CD2$^+$ was more prominent for LEA29Y

(Figure 28B), but with lower amounts of proliferating CD27$^{dim/-}$ effector cells (LEA29Y: 165.5±14.58, WT: 257.4±36.5, p=0.0376), as well as less cytokine production (Figure 28C/D). Exactly the opposite results were obtained with the CD2^{-} subset. Here, a higher percentage of Ki-67^{+} (LEA29Y: 6.483%±0.7941, WT: 3.084%±0.3351, p=002) and TNF-α^{+} IFN-γ^{+} cells could be measured for LEA29Y (LEA29Y: 0.1522%±0.1908, WT: 0.1346%±0.01673, p<0.0001).

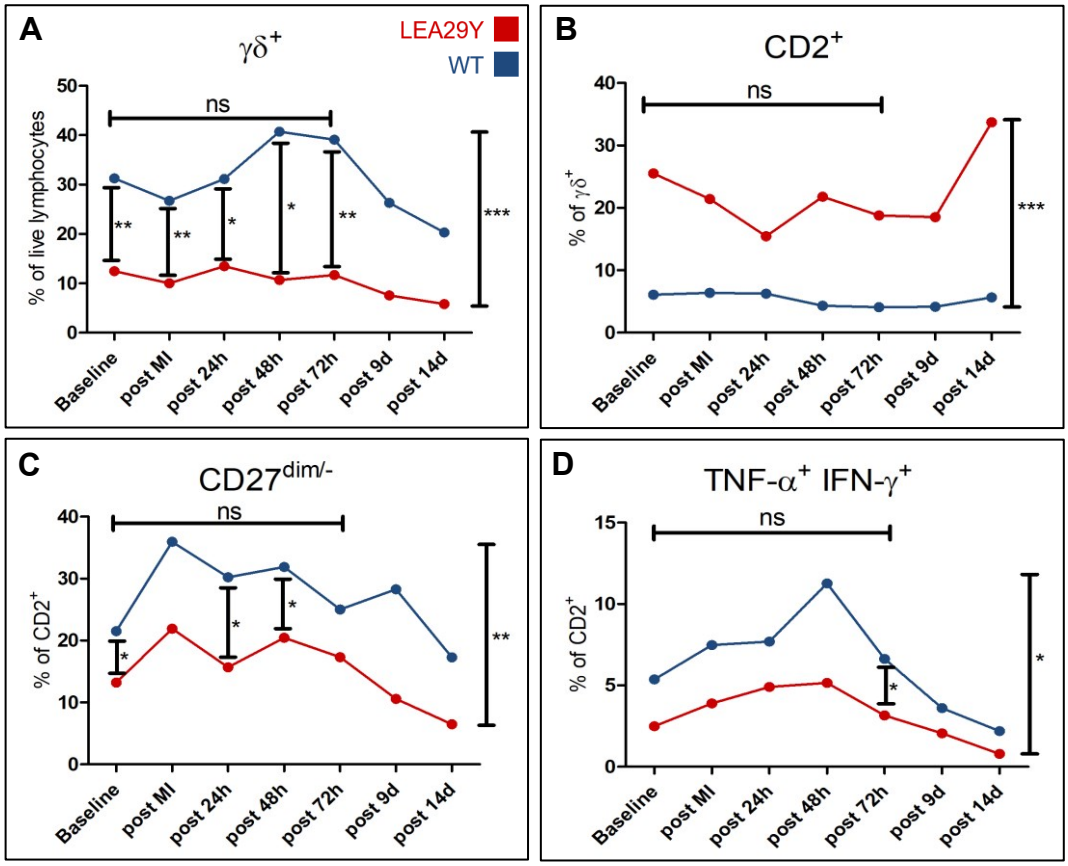

Figure 28: γδ^{+} T cells. (A) Frequency of γδ^{+} as percentage of live lymphocytes. WT showed significantly higher levels of this T lymphocyte subclass (LEA29Y: 10.25%±1.031, WT: 30.8%±2.738, p<0.0001). **(B)** Proportion of the CD2^{+} phenotype. This was more prominent in immunosuppressed pigs. (LEA29Y: 22.17%±2.263, WT: 5.27%± 0.3959, p<0.0001). **(C)** Percentage of CD27$^{dim/-}$ cells within CD2^{+}. The effector cells, however, were again more abundantly found in WT (LEA29Y: 15.1%±2.063, WT: 27.17%±2.407, p=0.0025). **(D)** Frequency of TNF-α^{+}IFN-γ^{+} producing cells. These were also more prominent in the wildtype pigs (LEA29Y: 3.209%±0.5945, WT: 6.32%±1.125, p=0.0309).

3.4. Myeloid cells

In order to investigate the immune system as comprehensively as possible, myeloid cells were also examined by flow cytometry in addition to lymphocytes. It was found that the proportion of monocytes (CD14^{+}CD163^{+}) was significantly higher in LEA29Y pigs (Figure 29A) and that subpopulations of these also expressed more

cell adhesion molecule 1 (CADM1) as a cell surface protein important for contact and signal transmission between cells (Figure 29B). Monocytes can further develop into dendritic cells (DC), which in turn are divided into conventional (cDC) and plasmacytoid (pDC) subclasses. For the latter, no statistically relevant difference comparing the transgenic with WT animals was detected (Figure 29C) except for one case of higher values of CADM1 in LEA29Y, that also applied to cDC similar subsets of $CD14^{-}CD172a^{+}CADM1^{+}CD4^{-}$ cells (Figure 29D). However, the described clear subpopulations of cDC1 and cDC2 could not be identified.

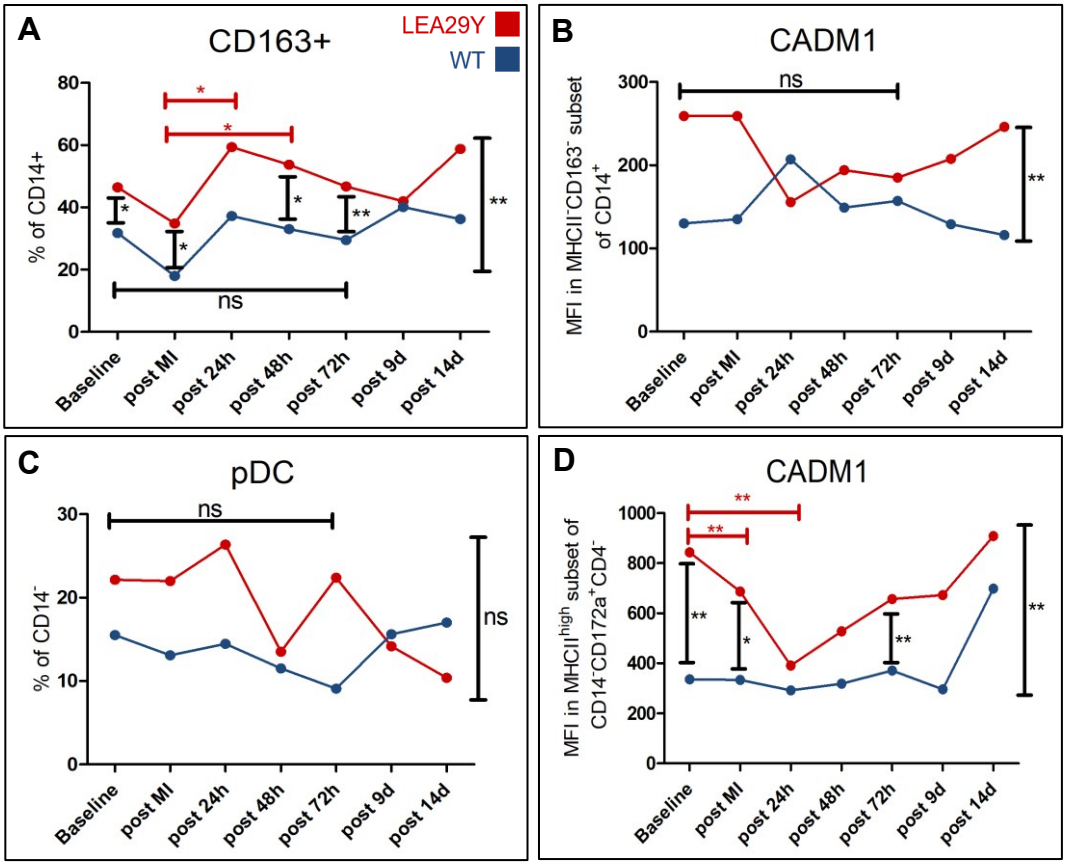

Figure 29: Myeloid cells. (A) Frequency of $CD163^{+}$ monocytes within $CD14^{+}$ myeloid cells. LEA29Y animals showed a significant increase during the first two days after MI and generally higher levels (LEA29Y: 48.82%±3.409, WT: 32.25%±2.735, p=0.0026). **(B)** MFI of CADM1 in monocyte subset. The molecule was more expressed in transgenic pigs (LEA29Y: 215.1±15.25, WT: 146.1±11.36, p=0.0035). **(C)** Percentage of pDC in $CD14^{-}$ cells. This population revealed no significant differences (LEA29Y: 18.71%±2.241, WT: 13.75%±1.031, p=0.0677). **(D)** MFI of CADM1 in cDC subset. Again higher amounts were detected in the immunosuppressed pigs (LEA29Y: 669.8±66.55, WT: 379.1±54.43, p=0.0053).

Overall, analysis of PBMC at different time points after myocardial infarction demonstrated distinct differences between LEA29Y and WT pigs in their systemic

immune cell profiles. Transgenic animals showed a higher proportion of $CD163^+$ monocytes and a more abundant expression of the cell adhesion molecule 1 (CADM1) within the subset of myeloid cells. T lymphocytes per se, but in particular the $CD4^+$ subclass was also found in higher percentages at LEA29Y, whereas Tregs and Th1 were more prevalent in wildtypes. In general, the immunosuppressed animals showed less activated ($CD8\alpha^+$, ICOS, $CD27^{dim/-}$) as well as proliferating (Ki-67) cells and were in most cases also inferior to WT in cytokine production.

4. Local histological assessment

Complementary to the functional and systemic investigations, the tissue of the left ventricle of each pig was examined histologically.

4.1. Hematoxylin and Eosin staining

Hematoxylin and eosin staining was performed to obtain a general overview of the local processes in the heart at different time points following reperfused MI. At day 3 the myocardial tissue was clearly affected by infarct-typical damage. It appeared loosened and dead cardiomyocytes showed core pyknosis or no nuclei at all. Particularly striking was the huge amount of infiltrating cells at this stage that seemed to encircle the infarcted area like a wall (Fig. 30A/B). This was clearly changed on the ninth day. Cells had spread throughout the necrotic region and had already scavenged most of it. Thus, the predominant impression in the infarct area was a mixture of dead and immune cells as well as already developing granulation tissue (Figure 30C). Two weeks after MI, this was even more pronounced as a sign of progressive remodelling and scarring (Figure 30D). All these findings were observed equally in LEA29Y transgenic and wildtype pigs.

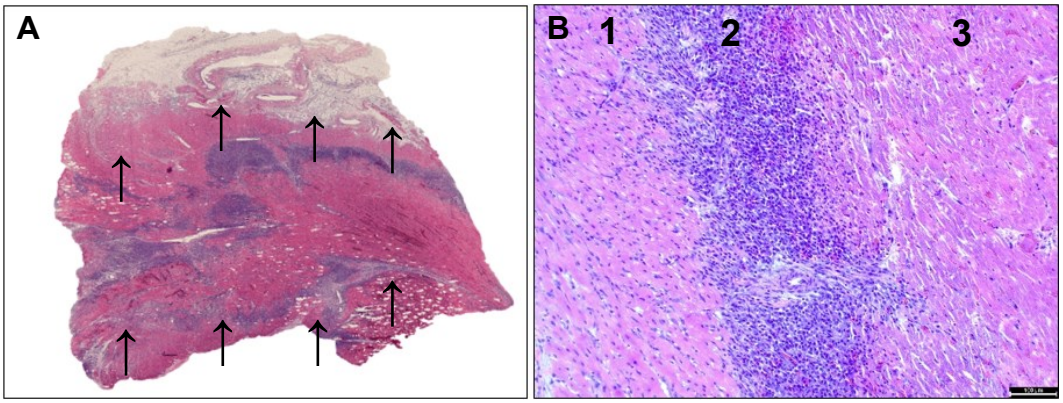

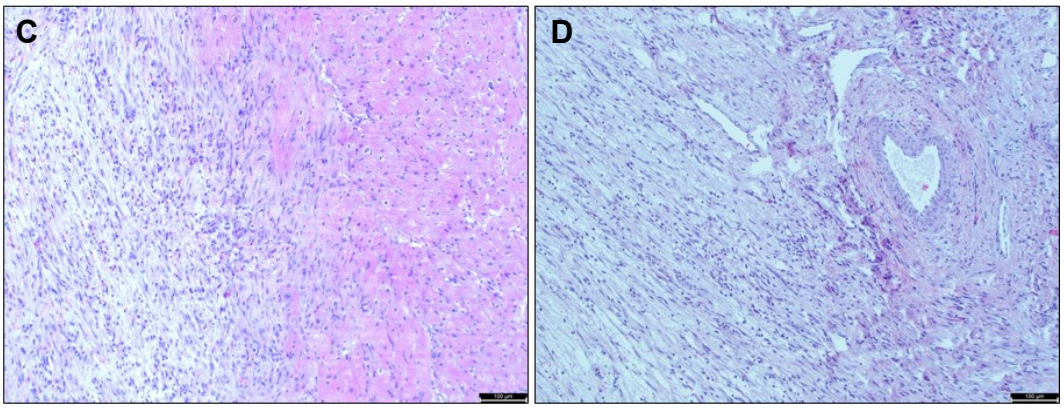

Figure 30: HE staining. (A) Merged overview of LEA29Y 12330 LV piece 11 on day 3. Hyperaemia in the damaged tissue is clearly surrounded by attracted cells (↑). **(B)** The same section in 10x magnification. A wall of infiltrating cells (2) separates still intact myocardium (1) from necrosis (3). **(C)** WT 12551 LV10 on day 9 (10x magnification). **(D)** LEA29Y 11910 LV9 on day 14 (10x magnification).

4.2. Immunohistochemistry

Immunohistochemistry was performed for a more detailed examination of the infiltrating cells. Three different staining protocols were carried out to identify neutrophils, T lymphocytes and macrophages as the described subclasses involved in the immune reaction after MI. The quantitative assessment of their amounts was achieved through random systematic sampling and analysis with ImageJ. The entire LV was sampled as 36 defined pieces. Each of those was stained and microscoped, with a picture of every 180th tile taken blinded. For a global analysis of the entire left ventricle, each image acquired randomly in this way was examined. This was compared to a more specific local assessment of the affected area alone, in which only images of LV parts macroscopically defined as MI or AAR were selected for analysis.

4.2.1. Neutrophils

As previously mentioned, neutrophil granulocytes are the cells that are the first to be attracted to the damaged tissue after myocardial infarction and decrease again after a short time frame. This could also be observed in the immunohistochemical heart staining (Figure 31A). With values of 0.09% versus 0.02% of LV neutrophils were significantly higher in the untreated heart of an immunosuppressed animal compared to the wildtype control ($p=0.0002$), suggesting that these cells are generally more abundant in the LEA29Y tissue. Both genotypes showed a clear increase (LEA29Y: $p=0.0459$, WT: $p=0.0044$) to 0.29% respectively 0.36% of the

left ventricle on day 3 before the number of neutrophils in the tissue dropped again significantly (LEA29Y: p=0.0162, WT: p=0.0131) to the levels comparable to the baseline conditions (LEA29Y: 0.1% LV, WT: 0.03% LV, p<0.0001).

This course was the same if only the affected LV areas were analysed (Figure 31B). The rise after 72 hours was more pronounced (LE29Y: 0.38% affected LV, p=0.0128; WT: 0.55% affected LV, p=0.0002) but the decrease at day 9 resulted in similar values (LEA29Y: 0.1%, WT: 0.03% affected LV; p=0.0001).

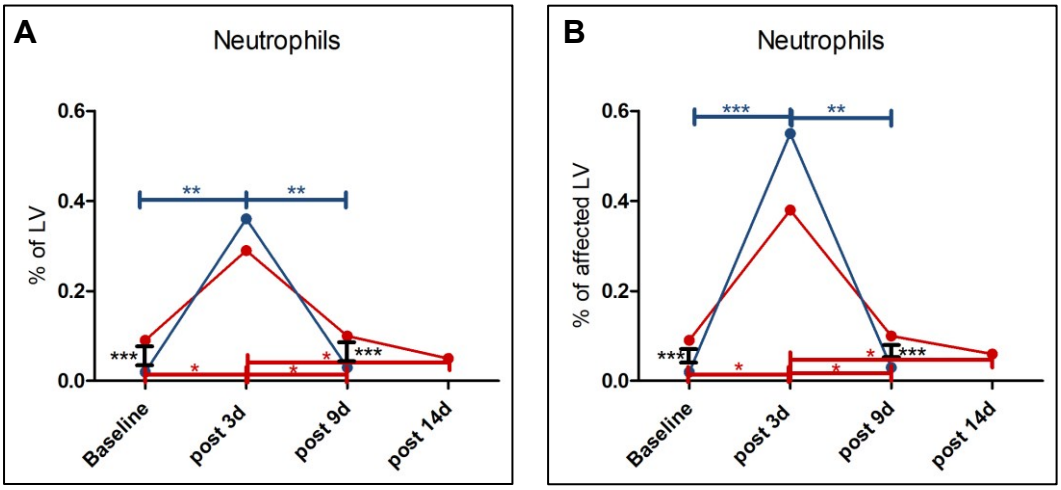

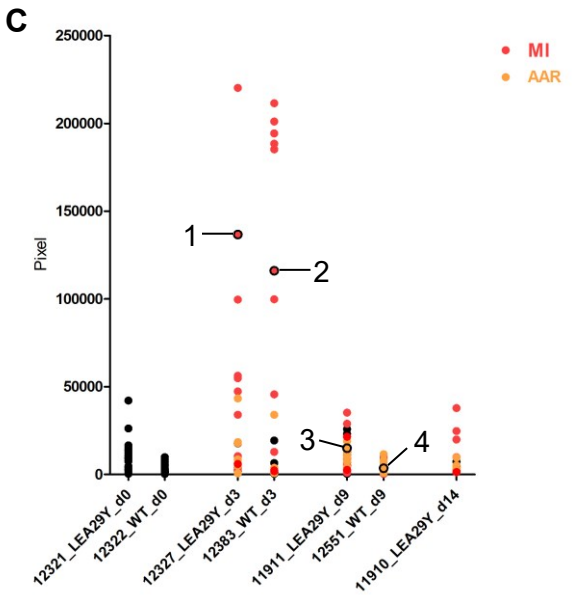

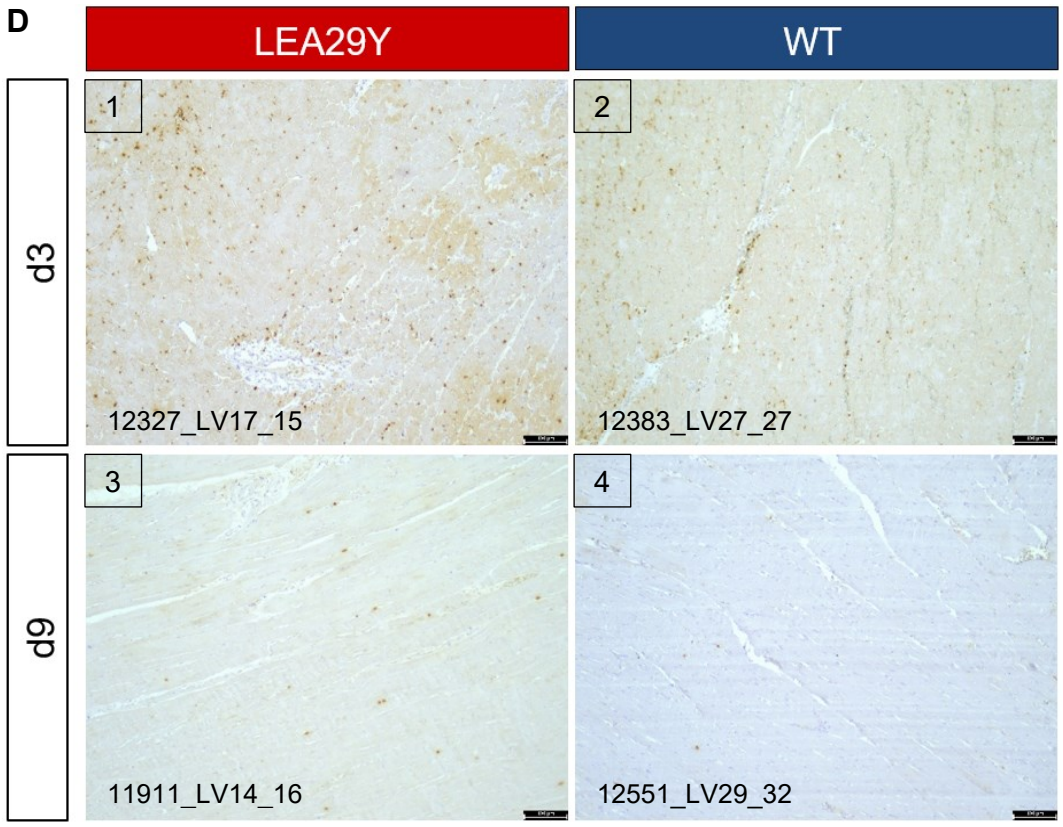

Figure 31: IHC staining for neutrophils. (A) Dynamic of neutrophils analysed globally as percentage of the total LV. **(B)** Dynamic of neutrophils analysed locally as percentage of the affected LV only. **(C)** Amount of positive pixels of all randomly taken pictures. Red and orange mark parts of the defined MI region respectively AAR. The numbers refer to representative example images of the different groups at day 3 and 9, shown in **(D)**.

4.2.2. T lymphocytes

In line with the peripheral immune cell profiling, the T cells as by LEA29Y affected cells were also of particular interest for local histological assessment. These showed a baseline level similar to the neutrophils in the immunosuppressed pig (0.05%) but were five times higher for the WT (0.25%, $p<0.0001$). Also in this case a distinct enlargement of the proportion of cells in the entire left ventricle could be detected on day 3 (LEA29Y: 0.15% LV, $p=0.0115$), although this was not statistically effective in wildtype (0.36% LV, $p=0.323$). T lymphocytes were still present 9 days after the myocardial infarction (LEA29Y: 0.11% LV, WT: 0.34% LV, $p=0.0021$) and remained higher than the initial values after two weeks (LEA29Y: 0.12%, $p=0.0453$). Overall, T cells showed the same course in both groups but were generally more abundant in the WT group ($p=0.0026$; Figure 32A).

This was also the case for the evaluation of infarct area and AAR (p=0.0065; Figure 32B). The increase was more evident after 72 h (LEA29Y: 0.16% affected LV, p=0.0068; WT: 0.43% affected LV) and 9 days (LEA29Y: 0.13% affected LV, WT: 0.42%, p=0.0076), which in this analysis was significant for wildtype (p=0.0363). The same percentage was calculated for day 14 but was not statistically relevant here (LEA29Y: 0.12%, p=0.0514).

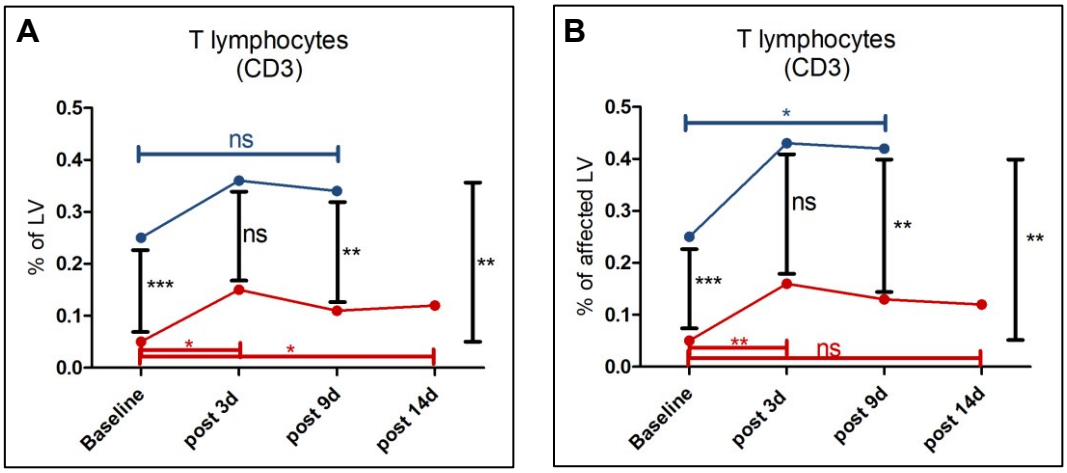

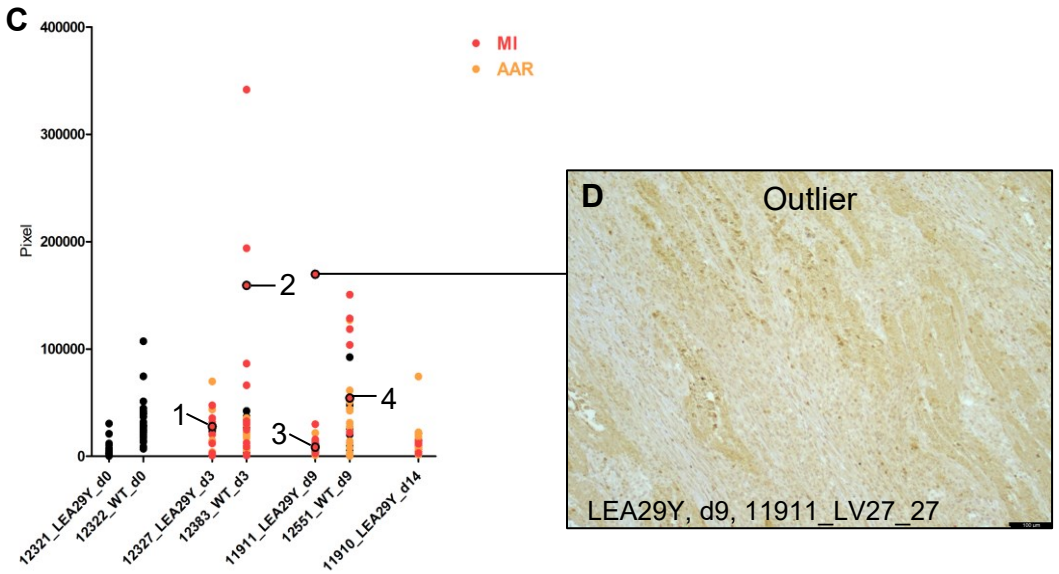

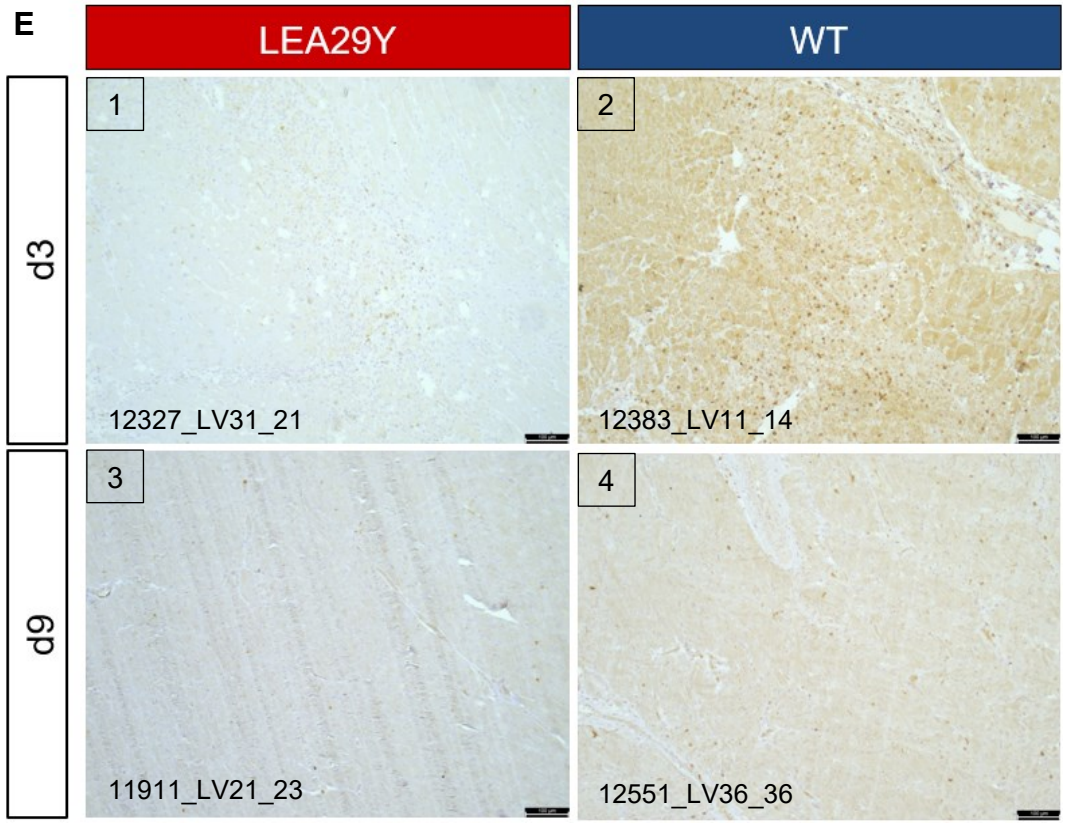

Figure 32: IHC staining for T lymphocytes. (A) Dynamic of T cells as percentage of the total LV. **(B)** Dynamic of T cells analysed locally as percentage of the affected LV only. **(C)** Amount of positive pixels of all randomly taken pictures. Red and orange mark again parts of the defined MI region respectively AAR. **(D)** For animal 11911 an outlier occurred and was checked for its correct processing in the ImageJ analysis. **(E)** Typical example pictures of the 3- and 9-day groups. The numbers correspond to the respective pixel measurement in (C).

4.2.3. Macrophages

The third population studied by IHC was the immune cell subset of macrophages that is described as the most prominent subclass of resident cells in the heart. An untreated LEA29Y pig presented 0.89% macrophages in the LV tissue, which was similar to the 1.08% obtained in the WT ($p=0.3791$) and above the levels of neutrophils and T cells. Macrophages within the wildtype group showed a distinct increase on the third day after MI up to 4.12% of the left ventricle ($p=0.0037$). This was significantly higher ($p=0.0215$) than 1.5% of LV in LEA29Y. The enlargement in these only became noticeable on the ninth day ($p=0.0333$), but could not reach the level of WT, although it was not statistically determinable (LEA29Y: 3.22% LV, WT: 4.23% LV, $p=0.4358$). This was followed by a clear decrease in LEA29Y to 1.15% of LV ($p=0.0485$; Figure 33A).

Local analysis of only the affected tissue also showed a later and not so strong accumulation of macrophages in the transgenic animals (Figure 33B). Again the increase was more pronounced. Wildtypes reached 5.11% (p=0.0005) and 6.32% of affected left ventricle (p<0.0001) at day 3 and day 9, respectively. In LEA29Y transgenic animals 1.56% (p=0.1302) and 4.14% macrophages (p=0.0139) could be detected in affected LV. The drop to 1.5% of affected left ventricle after two weeks what statistically not significant (p=0.1381).

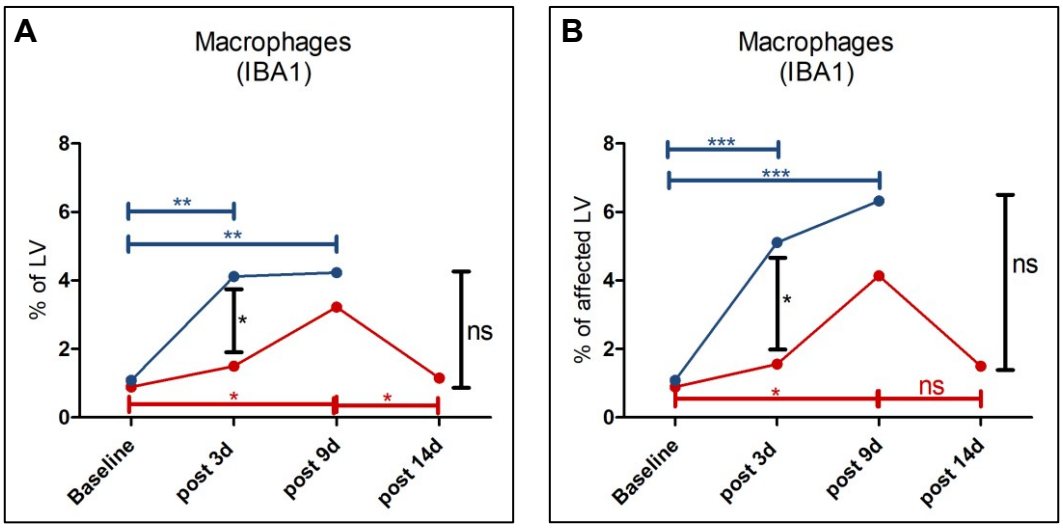

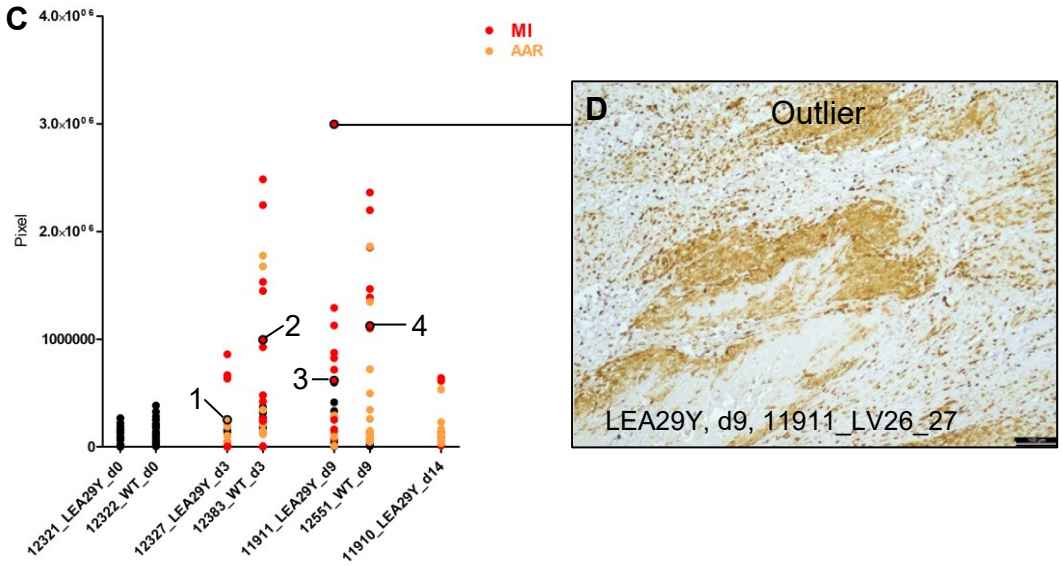

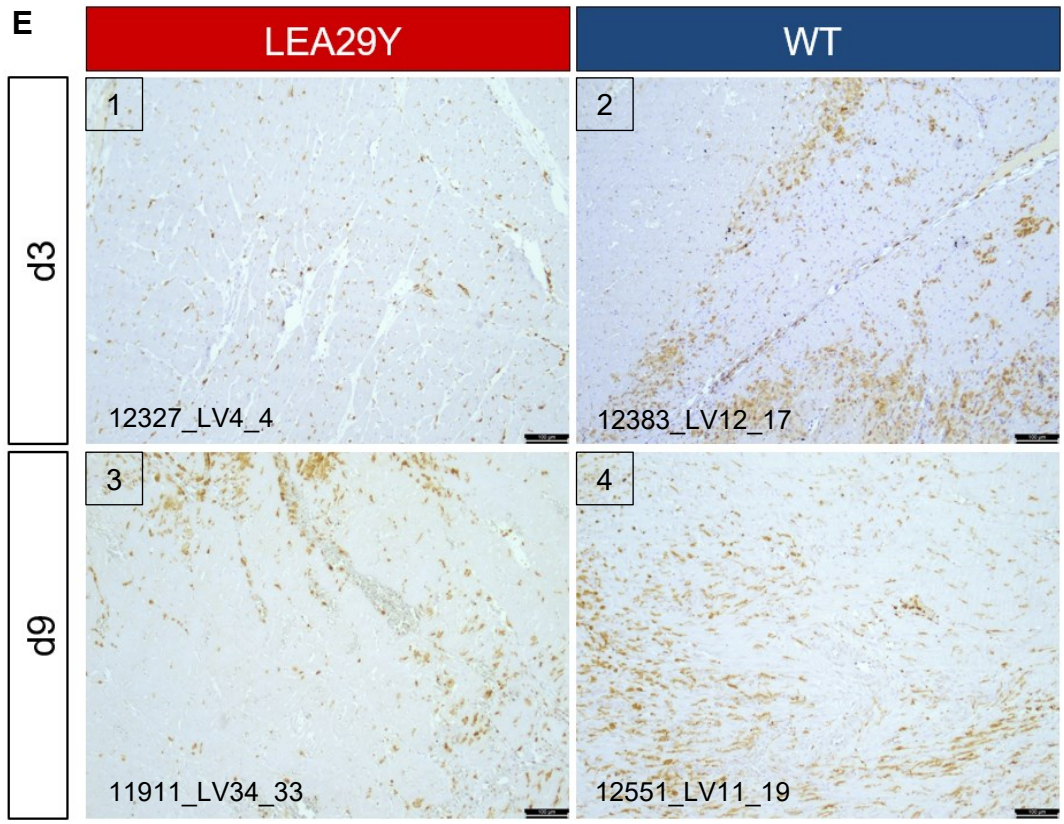

Figure 33: IHC staining for macrophages. (A) Dynamic of macrophages as percentage of the total LV. **(B)** Dynamic of macrophages analysed locally as percentage of the affected LV only. **(C)** Amount of positive pixels of all randomly taken pictures. **(D)** An outlier again occurred for LEA29Y 11911. The correct analysis by ImageJ could be confirmed. **(E)** Representative example images of the different groups at day 3 and 9 whose positive pixels are indicated by the numbers in (C).

4.3. Picro-sirius red staining for fibrosis

Picro-sirius red staining as a method of fibrosis visualisation was carried out to check the tissue for later occurring remodelling processes and scarring. The amount of collagen was compared to values obtained in untreated control animals. As with IHC stainings, it was calculated globally as the percentage of the whole left ventricle (Figure 34A) as well as locally as the proportion of only affected myocardial areas (Figure 34B). Due to the clearer staining in this method, the selection of the corresponding pictures was not only based on macroscopic classification as MI or AAR but was additionally complemented by microscopic assessment of the tissue. Both LEA29Y and wildtype pigs showed values similar to the control animals (LEA29Y: 2.3% LV±1.253, WT: 2.6% LV±0.3756, p=0.4032) on day 3 (LEA29Y: 2.1% LV±0.2483, WT: 2.2% LV±0.2862, p=0.6566). After

nine days, a significant increase of collagen (LEA29Y: 4.8% LV±0.695, p<0.0001; WT: 3.8% LV, p=0.0074) was observed in both groups (p=0.3035), which continued also after two weeks in LEA29Y (7.07% LV, p<0.0001).

The same development of fibrosis was observed in the evaluation of the infarct areas and AAR only. The results after 72 hours were quite similar (LEA29Y: 2% affected LV±0.1455, WT: 1.9% affected LV±0.2451, p=0.7255), whereas the elevation of collagen on day nine was more distinct (LEA29Y: 7.4% affected LV±0.98, p<0.0001; WT: 8.06%, p<0.0001) for both genotypes (p=0.8639). This was also the case for fibrosis on day 14 (LEA29Y: 13.76% affected LV, p<0.0001).

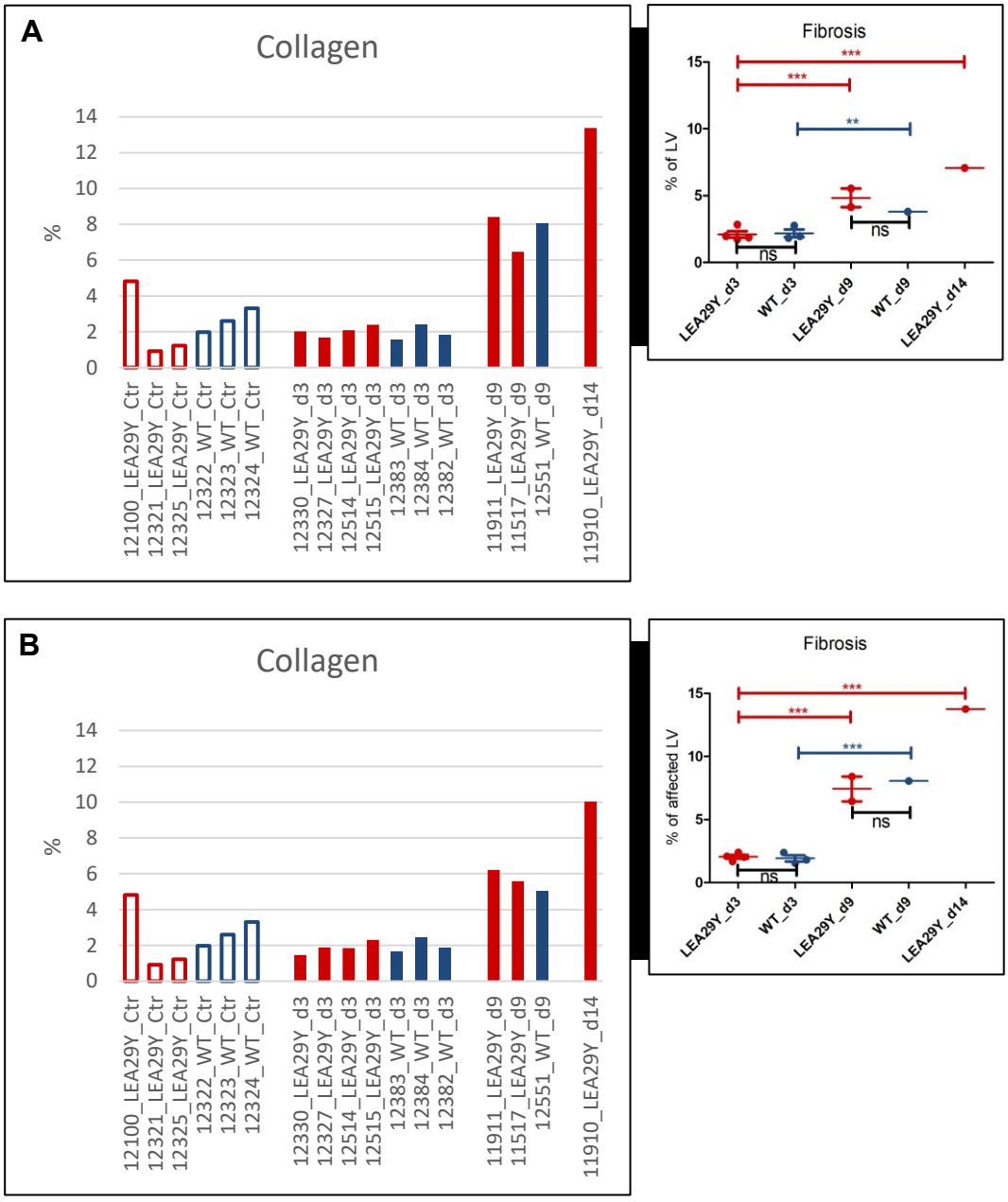

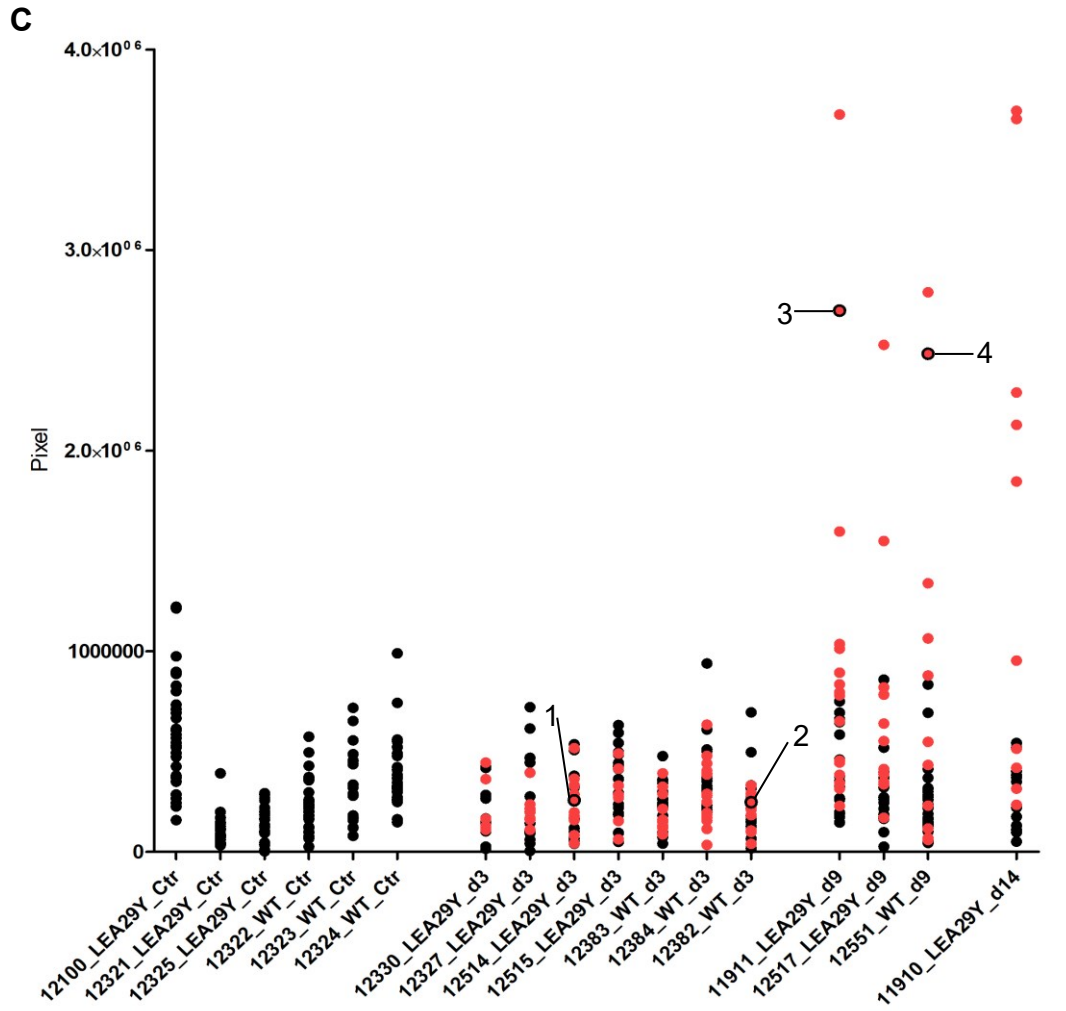
C
4.0×10^06
3.0×10^06
2.0×10^06
1000000
0
Pixel
1
2
3
4
12100_LEA29Y_Ctr
12321_LEA29Y_Ctr
12325_LEA29Y_Ctr
12322_WT_Ctr
12323_WT_Ctr
12324_WT_Ctr
12330_LEA29Y_d3
12327_LEA29Y_d3
12514_LEA29Y_d3
12515_LEA29Y_d3
12383_WT_d3
12384_WT_d3
12382_WT_d3
11911_LEA29Y_d9
12517_LEA29Y_d9
12551_WT_d9
11910_LEA29Y_d14

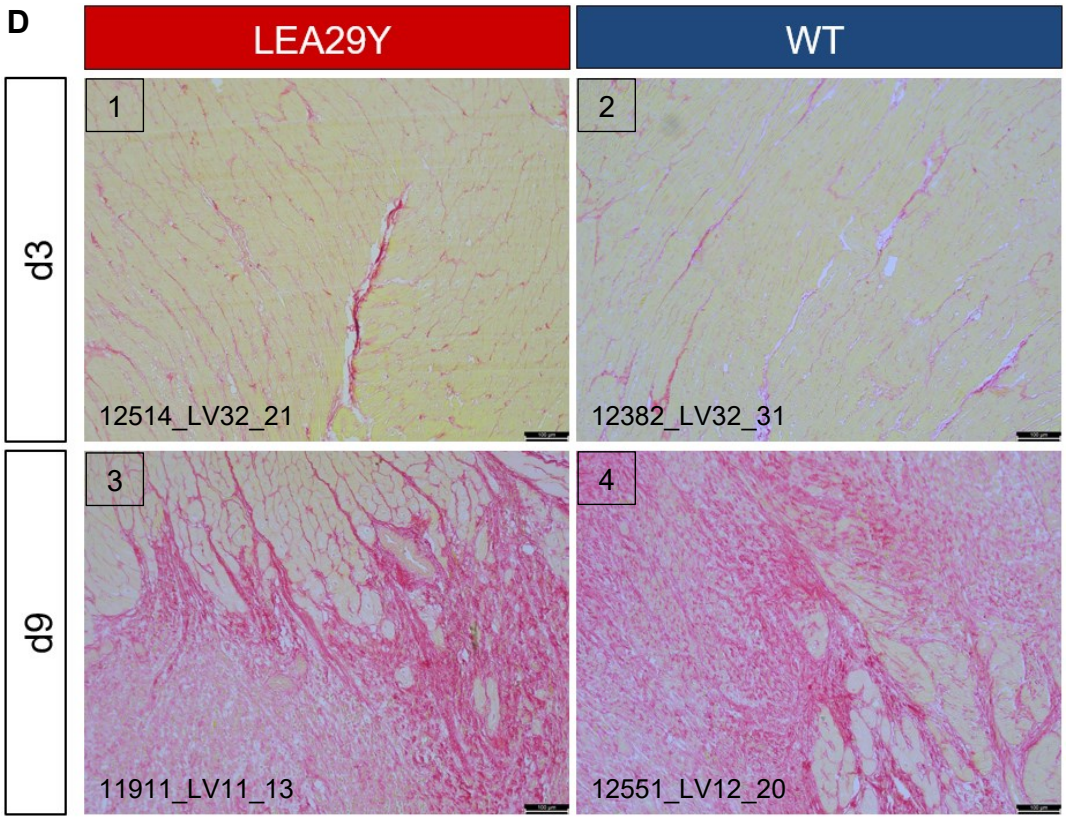
D
LEA29Y
WT
d3
d9
1
2
3
4
12514_LV32_21
12382_LV32_31
11911_LV11_13
12551_LV12_20

Figure 34: Picro-sirius red staining. (A) Results and statistical evaluation of collagen assessment in the entire left ventricle. **(B)** Results and statistical evaluation of collagen assessment in the affected LV. **(C)** Overview of positive pixels of all measured images (affected LV parts are marked in red). The numbers refer to exemplary pictures in **(D)**.

Histological evaluation complemented the study of the effects of myocardial infarction followed by reperfusion in immunocompromised pigs by local assessment of the affected myocardium. Various functional measurements demonstrated the impairment of the heart due to the damage caused and revealed a significantly higher loss of function after 3 days in the transgenic animals compared to WT. Further differences between the two genotypes were also identified in the analysis of isolated PBMCs. LEA29Y demonstrated lower proportions of activated and proliferating immune cells, but generally had higher percentages of T lymphocytes and monocytes in the circulation. Histological assessment showed that these cell subsets reach the affected heart tissue in the transgenic pigs only with a delay and in lower amounts, while fibrosis was detected equally in both groups from day 9 onwards.

V. DISCUSSION

Myocardial infarction is still one of the most common causes of death worldwide (GBD 2017 CAUSES OF DEATH COLLABORATORS, 2018). A great deal of research is therefore being carried out in this field and many insights into pathogenesis, prevention and therapy have been gained to date. Nevertheless, the lack of data on MI in immunocompromised patients shows that further efforts are still needed to provide the best possible care for such special cases. To that end, this thesis offers the opportunity to identify abnormalities in healing after MI in individuals with impaired T cell activation and to investigate the role of these lymphocytes in the complex immune response following reperfused myocardial infarction at the most translational level possible.

Due to its similarity to humans in terms of size and the cardiovascular system, the pig as an experimental model enables the use of equipment and measurements like those used in patients. The functional observations performed in our study correspond to the management procedures for MI in clinics, as electrocardiography in particular is one of the most significant diagnostic techniques (IBANEZ et al., 2018). Six channel ECG revealed ST-elevations and depressions in various leads immediately after the myocardial infarction and could prove these to be persistent, when repeated at the end of the follow-up period. For longitudinal monitoring in the meantime, human insertable cardiac monitors were implanted into the experimental animals. Originally, these devices have been developed to identify unclear arrhythmias in patients with non-specific cardiac symptoms (GIANCATERINO et al., 2018). In pigs, they also offer the rare opportunity to longitudinally screen the ECG on non-anaesthetized animals moving freely in their familiar environment and behaving normally in groups. This makes the ICM an excellent option for biotelemetry, where various physical parameters can be recorded remotely. Especially in the field of laboratory animals, this method is becoming increasingly important and is considered to be a good opportunity for Reduction and Refinement in the sense of the three Rs strategy for animal welfare (HAWKINS, 2014). Up to now they have been applied in different species such as sheep (KLATT et al., 2016), guinea pigs (WOULFE et al., 2018) as well as even in hibernating bears (LASKE et al., 2014). In our study, the devices of the company Biotronik were used. The set-up is quite simple and can be directly followed by the

actual surgery, without any further narcosis for the animal. The BIOMONITOR III in particular is a very small device that can be easily placed subcutaneously with the help of the insertion tool. The skin incision required for this is only short and if implantation is carried out under sterile conditions, there are no wound healing disturbances. The battery life of a Biomonitor is about three years in total. This means that the ICM can be used in the long term without any additional handling or stress for the animal, because once all settings have been made, the data is stored and, in the newer systems, sent daily to a home monitoring cloud via mobile phone network. The monitor can detect tachycardia, bradycardia, asystole, atrial fibrillation as well as sudden drop in rate, but saves only the past, most recent and longest episodes of each according to an algorithm. The limitation that not each event can be recorded prevents a quantitative evaluation of the results. For example, ventricular tachycardia was usually not detected until the third day, but it is possible that it occurred earlier not only in animals 12515 and 12517, but also in other pigs, for which the corresponding sequences were not memorized. It is also advisable to check the data individually, because it must be considered that the devices have been constructed for the use in humans. Discrepancies in the electrical axis of the heart can interfere with the detection of arrhythmias and the setting limits for the heart rate are not suitable for the large fluctuations in pigs. The cutoff for normal rates can only be extended to a maximum of 200 bpm with the Biomonitors. In LEA29Y and WT animals, much higher frequencies were detected, so that many episodes of apparent tachycardia were perceived. Of course, it cannot be ruled out that in isolated cases the system may measure incorrectly if the ECG is not stored and can be verified. But fast heart rates have already been described by other groups with long term ECG measurements in awake pigs (ROMAGNUOLO et al., 2019) and the available episodes were checked for accurate analysis. Based on the time stamps, it was possible to prove that animals were doing well during these events and that some could be associated with handling or feeding times by day. But what could not be explained were the high heart frequencies at night. Although many believe that all mammals dream (MANGER & SIEGEL, 2020), due to the sometimes very long and frequent occurrence, it seems very unlikely that this alone would explain the findings. Nevertheless, further examination of the ECG revealed regular sinus rhythm in almost all cases of recorded tachycardia and the detection of VT in the remaining confirmed that the Biomonitors are definitely suitable for qualitative rhythm diagnosis in swine. Another disadvantage of this monitoring

method is, however, the high cost of equipment but it is possible to re-sterilize previously implanted devices and reuse them in several animals. There are also other telemetric possibilities, such as full implants with multiple sensors to check not only the ECG but also, for example, blood pressure or core body temperature. The major drawback of these systems is their highly invasive insertion, where the individual electrodes and leads have to be placed directly in the heart or vessels in complex surgical procedures (CHOY et al., 2014; MARKERT et al., 2018). On the other hand, there are also non-invasive alternatives available. Devices to measure the ECG can simply be stuck on the thorax like patches (BRLOŽNIK et al., 2019) or can be worn as chest strap (DE GROOT et al., 2012). The ease of use of these methods is at the same time their biggest disadvantage for application in swine. Pigs are very curious and explorative and would tear down and destroy even strongly attached objects of this kind in no time at all. Therefore the Biomonitors were the perfect intermediate solution to perform biotelemetry in a not too burdensome but reliable way for monitoring the ECG during the follow-up period after myocardial infarction.

Impairments in the functional measurements as the observed electrophysiological changes in the electrocardiography proved the damage caused by myocardial infarction, which was further investigated on a histological level. Therefore a random systematic sampling procedure was performed to examine immunohistochemical as well as Picro-sirius red staining of the left ventricle. This required uniform processing of the tissue samples, from cutting to staining and up to microscoping (ALBL et al., 2016), whereby all 36 pieces obtained from an animal were studied in sequence, taking a picture of every 180^{th} tile blinded. Each image was then analysed using the same settings in ImageJ to further avoid any bias. Hence, this method of a random systematic sampling enabled the generation of highly randomised samples of best quality in terms of reliability and comparability. Consequently, we expected to be able to obtain representative results for the entire left ventricle with the analysis of the images of every 180^{th} visual field. However, we could identify a limitation of this procedure in case of Picro-sirius red staining. This is a very sensitive and often used method for detecting collagen not only in fibrosis but also in connective tissue, based on the birefringent property of the dye molecule (RITTIÉ, 2017). The heart as a well perfused organ is pervaded by a dense network of blood vessels (DEWEY et al., 2020). Coronary

arteries originate from the bulbus aortae and branch out in a vascular tree, particularly at the base of the heart (KASSAB, 2000). These are embedded in connective tissue, which is essential for their undisturbed movement and supply (BOU-GHARIOS et al., 2004), but causes an inhomogeneous collagen distribution in the left ventricle. Some random images were therefore produced with (parts of) large vessels present and the perivascular collagen influencing the fibrosis evaluation. The lower the number of pictures, the greater the impact of this was leading us to two possibilities to overcome this issue. The first option was to increase the number of visual fields analysed. The other was to eliminate the scatter by excluding corresponding images, which we decided to do. All tiles with a large artery or vein were identified again microscopically on the respective slice and in each case the one on the right or, if it represented a marginal visual field, the one below it was taken instead. The decision on whether to replace them was based on if the vessel significantly influenced the overall macroscopic impression of collagen in the picture. The random systematic sampling could therefore still be used for the quantification of fibrosis following myocardial infarction. In accordance with the described remodeling processes of the heart with the onset of proliferation and maturation after several days (SWIRSKI & NAHRENDORF, 2018; KOLOGRIVOVA et al., 2021), an increase of fibrosis could not be observed after 72 hours but was significant to the same extent from day 9 onwards in LEA29Y transgenic and wildtype animals.

Aside from the limitation that random systematic sampling can only be performed in homogeneous tissues without further restrictions, this global assessment of the entire left ventricle carried the risk to mitigate possible local effects, which is certainly the case for the damage caused by myocardial infarction. This was tested by comparing it with the analysis of affected areas only, examining exclusively images obtained in LV pieces classified as MI or AAR. For IHC, this categorisation was based solely on the macroscopic evaluation during sampling, whereas for Picro-sirius red staining it was complemented by microscopic findings. The local analysis produced results similar to the global study with the same trends for all stainings. Only on two occasions, evaluation of the entire LV revealed a significance that was not mathematically ascertainable when examining just the affected tissue. Conversely, although some of them were more pronounced, pre-selection for MI and AAR, based on macroscopic or microscopic classification, did

not produce any significant differences that could not be recognised in the evaluation of the whole left ventricle. Thus, it could be demonstrated that the random systematic sampling requires adaptations for the application in inhomogeneous organs, but also reliably detects local effects despite the maximum randomisation.

The procedure was thereby proven as a robust analysis method to further investigate initially obtained functional measurements. In addition to electrophysiological alterations, these demonstrated a significantly higher loss of ejection fraction in the LEA29Y pigs compared to WT after three days. The greater impairment in the transgenic animals may be related to the varying local processes in the heart. Although immunohistochemical staining could show a similar level of infiltration with neutrophils, this was not the case for other cells important for the immune response. T lymphocytes have been described as crucial for the healing after myocardial infarction and have been detected in the peri-infarct tissue within the first few days of damage (CURATO et al., 2010). Especially Tregs are responsible for the switch from the inflammatory to the maturation phase. Insufficient activation of T cells or deficiency of the $Foxp3^+$ subclass therefore results in deteriorated cardiac function and shortened survival due to compromised scarring and left ventricular rupture (HOFMANN et al., 2012; SAXENA et al., 2014). Histological examinations in our experiments have confirmed an increase of T lymphocytes in the heart following myocardial infarction for LEA29Y and WT animals. Although the trend was the same in both genotypes, the number of cells was significantly lower in the immunosuppressed pigs. In the case of also investigated macrophages, the discrepancy was even more pronounced. While in contrast to T cells, which were generally less present in cardiac tissue of LEA29Y, resident macrophages in untreated hearts were similar in both groups, the accumulation of these cells in the transgenic animals occurred considerably later and not to the same extent as in the WT. As previously described, macrophages are also attributed great importance in healing after MI, as on the one hand their Ly-$6C^{high}$ subset is required for phagocytosis of degraded cells (KOLOGRIVOVA et al., 2021) and to promote the initial response by secretion of pro-inflammatory cytokines (SHAPOURI-MOGHADDAM et al., 2018). On the other hand, M2 (Ly-$6C^{low}$) are essential for the following reparative and proliferative phase to prevent an excessive immune reaction and ensure sufficient scar formation

(NAHRENDORF et al., 2007). Since there was hardly any increase of macrophages in LEA29Y after three days and their quantity, although not statistically relevant, in general remains below that of WT, the question naturally arises which effect the absence of these cells had and which phenotype was recruited at all. Because the M1 subtype is usually attracted first (SWIRSKI et al., 2009) and represents the predominant monocyte fraction between day one and four before the ratio changes in favor of M2 (NAHRENDORF et al., 2007), it seems more likely that the infiltrating macrophages belonged to the Ly-6C^{low} subclass. This would also be consistent with the mentioned results of the Picro-sirius red staining, which demonstrated that scarring was not affected in the transgenic compared to wildtype animals.

In general, immunohistochemical stainings showed a reduced amount of T lymphocytes and macrophages in the tissue of the left ventricle of LEA29Y pigs. One possible reason for this could have been that the ubiquitous blocking of the T cell costimulation affected the immune system in such a way that the cells appeared in reduced numbers or did not mature. This could be ruled out by the results of the PBMC analyses by flow cytometry, which indicated even more cells of the corresponding subsets in the circulation of transgenic pigs. It should be noted, however, that these were not absolute numbers, but the respective populations were expressed as a proportion of the parent one and that increases or declines could therefore be the result of changes in other subpopulations. Nevertheless, total CD3$^+$ T lymphocytes as well as their CD4$^+$ subpopulation showed significantly higher percentages in the immunocompromised animals. These results were not obtained after the infarction, but already at baseline measurements, confirming that this was the usual steady state. Hence, the question arose why the immune cells did not target the damaged tissue, although they were present in the circulation. As mentioned, T lymphocytes need two distinct signals to be fully activated. First, the TCR recognizes a foreign epitope on the MHC complex, but secondly, to generate a sufficient immune response, costimulation by further surface receptors is required and if this does not occur, the cell enters a non-responsive state (SMITH-GARVIN et al., 2009; SZETO et al., 2020). Since the immunosuppressive effect of LEA29Y is based on blocking this additional trigger, it is obvious that cells in our transgenic pigs also displayed the described anergy of T lymphocytes. T cell anergy is defined as an active intracellular mechanism, usually in naive T cells, in which they remain

alive but do not respond effectively to antigens (SCHWARTZ, 2003; CRESPO et al., 2013), even if both activation signals have been present subsequently, as they remain refractory for restimulation (SMITH-GARVIN et al., 2009). Characteristics of this are, for example, the missing differentiation of the T lymphocytes. Although our experiments showed higher levels of $CD4^+$ cells for LEA29Y animals compared to wildtypes, the opposite was observed when gating for several evolved subclasses of these. T-bet^+ Th1 as well as Tregs and $CD8\alpha^+$ cells were detected more frequently in WT. CD8α is found on memory cells following antigen contact and is considered a porcine-specific activation marker (GERNER et al., 2015). The resulting impression that lymphocytes in immunocompromised pigs did not respond potently to stimulation was reinforced by a smaller subset of $CD27^{dim/-}$ effector cells within $\gamma\delta^+$ T cells and also the lower expression of ICOS, another costimulatory molecule. It is induced only by sufficient contact of T and antigen presenting cells (WIKENHEISER & STUMHOFER, 2016) and was also measured less in the $CD4^+$ as well as in the $CD8\beta^+$ population of the transgenic pigs. Furthermore, when examining the number of cells with a Ki-67^+ phenotype as well as the MFI value, lower proliferation rates were found for each of these two T lymphocyte subsets, which is another hallmark for anergy. Especially CTLA4 inhibits the entry into the cell cycle or causes an arrest in the G1 phase (MACIÁN et al., 2004). Also typical for this nonresponsive condition is a reduced cytokine secretion (APPLEMAN & BOUSSIOTIS, 2003). This too was observed in our myocardial infarction study, as the LEA29Y transgenic animals displayed lower numbers of cytokine (co-)producing cells in $CD4^+$ and $\gamma\delta^+$ T lymphocyte subclasses.

Moreover, it has been shown that this condition does not only affect T cells alone. Due to their close interaction, they can also influence APCs in such a way that they form inhibitory surface molecules and thus impair their ability to activate other lymphocytes (TAAMS et al., 2000; MACIÁN et al., 2004). On the other hand, they can interfere with both endothelial and epithelial cells, preventing the migration of lymphocytes as such, but also of other leukocytes, out of the blood and into the tissue (JAMES et al., 2003). This may explain our results on the $CD163^+$ monocytes. Similar to T lymphocytes, these were generally more frequent in the circulation of immunocompromised pigs and even showed a significant increase after MI, but were locally present in the affected myocardium in lower numbers

compared to WT.

In addition, it was remarkable that both these and dendritic cells contained higher MFI values for CADM1 in some subsets. According to its name, cell adhesion molecule 1 is a surface protein that promotes signal transduction encouraging direct cell contact. Therefore, it can contribute to communication within the immune system, but also enhance attachment to vascular endothelial cells, stimulating migration out of the vessels (SAWADA et al., 2020; YUAN et al., 2022). The increased expression of this molecule in LEA29Y animals suggests that this was a response to the disturbed emigration of monocytes. This would imply that the immune system was trying to compensate for the impairment and anergy of the T cells with other mechanisms, which would go along with further findings in terms of cytokine production and $\gamma\delta^+$ T cell subsets. As described, the secretion of IL-17A and IFN-γ in the transgenic pigs was generally lower than in wildtype animals, but they showed a significantly higher proportion of TNF-α releasing $CD4^+$ cells. Tumor necrosis factor alpha is an important messenger substance with various functions in the homeostasis and reaction of the immune system. Among other things, it can address T cells and support their triggering by the TCR, which is why it is also seen as a costimulatory molecule (MEHTA et al., 2018). This could be the underlying mechanism for the increased TNF-α production in LEA29Y pigs to counteract the inhibited activation of lymphocytes. CD2, a surface marker that we examined in our experiments, also contributes to a sufficient reaction after antigen contact. It can strengthen TCR binding affinity to ligands and positively reinforce weaker signals in particular, while its absence or inhibition leads to a hyporesponsive behavior of T lymphocytes similar to anergy (BINDER et al., 2020). CD2 is expressed on $\gamma\delta^+$ T cells, which appeared at a lower percentage in the circulation of the immunosuppressed animals. The $CD2^+$ subpopulation, on the contrary, was significantly larger in these, suggesting that this was again a balancing for impaired T cell reactivity.

Taking all observations of the histological examinations and the systemic immune cell profiling into account, the final conclusion is that the T lymphocytes in LEA29Y transgenic pigs were in anergy due to the lack of costimulation. Although they were present in the peripheral circulation, they obtained an inability to differentiate or proliferate as well as to migrate into injured tissue. Since macrophages showed similar distributions, this indicated an additional effect of T

cell anergy also on further immune cells. Collectively, this explained the significant higher functional impairment of the transgenic animals determined in ejection fraction measurements 72 hours after the myocardial infarction. However, the T cell anergy not only led to the inhibition of cells, but it also caused an increase in some other immune responses to counteract the inactivation. These compensatory mechanisms could contribute to the later balanced function that showed no more differences between LEA29Y and WT at day 9 and were evidence of the complexity of the immune system with the involvement of multiple cell types and correlations (SWIRSKI & NAHRENDORF, 2018).

In summary, this work can bridge the gap between myocardial infarction and immunosuppression. In a highly translational approach, devices and measurements equally used in humans were applied to induce and diagnostic MI in transgenic pigs with impaired T cell activation. Heart tissue was examined histologically in a random systematic sampling procedure and, in combination with systematic immune cell profiling, showed anergy of T cells, which also influenced macrophages and was partially compensated by further immune mechanisms. As the immunomodulation in LEA29Y is exactly the same as in humans treated with Belatacept, similar results can be expected for these patients, and therefore the insights into the function of the adaptive immune system gained in our experiments may contribute to further advances in this particular area of infarct research.

VI. SUMMARY

Impact of LEA29Y expression on myocardial infarction outcome in pigs

Myocardial infarction (MI) remains one of the leading causes of death worldwide. It is a lack of oxygen supply to the heart tissue due to a thrombotic occlusion in the coronary vessels. This leads to the death of cardiomyocytes, life-threatening arrhythmias and even heart failure. The cause is usually the eruption of an atherosclerotic plaque that has developed asymptomatically over a long period of time. Risk factors for this are a generally unhealthy lifestyle, but also psychosocial stress situations increase the danger of a heart attack. Treatment strategies aim to reperfuse the heart as quickly as possible, but due to metabolic imbalances, this can further increase the damage and intensify the necrosis caused. This triggers a multiphase reaction in which there is initially a strong inflammation, that subsequently passes into a maturation stage and finally into scar formation. The entire process of this remodeling is a complex process of the immune system, which requires very tight regulation in order to maintain the heart function as much as possible. Neutrophil granulocytes, macrophages and T lymphocytes are described as particularly important in this process. Despite intensive research in the field of myocardial infarction, there are hardly any data on the effects of a disturbed resistance system, as is the case in immunocompetent individuals, for example after organ transplantation.

The aim of this work was therefore to close this gap and to investigate the possible consequences of immunosuppression on healing and scar formation. For this purpose, an infarction model with subsequent reperfusion was replicated in transgenic pigs by means of percutaneous transluminal coronary angioplasty (PTCA). These ubiquitously expressed a fusion protein, called LEA29Y, which led to a blockade of costimulation during T cell activation and is used as a drug in patients after kidney or heart transplantation under the name Belatacept. The experiments were examined with regard to functional and histological aspects, as well as the immune cells present in the circulation at different time points after MI, and compared with the results of wildtypes.

A clear T cell anergy in the transgenic animals, characterised by absent or reduced

differentiation, proliferation and cytokine secretion could be detected. In addition, there was an inability to migrate from the vessels into the damaged tissue, which was also observed in monocytes. This resulted in significantly reduced pump function in LEA29Y pigs after 72 hours. However, by day 9, this was no longer detectable and the scarring that began at this time was not affected. Instead, the immune system appeared to develop various compensatory mechanisms to counterbalance the impaired T lymphocyte activation, highlighting the complexity of this network of different cascades, cells and molecules.

In conclusion, catheter-based induction of MI in LEA29Y transgenic pigs represents a translational model to depict healing processes in immunosuppressed patients and to support further myocardial infarction research with the study results.

VII. ZUSAMMENFASSUNG

Auswirkung der Expression von LEA29Y auf das Ergebnis eines Myokardinfarktes bei Schweinen

Der Myokardinfarkt (MI) ist nach wie vor eine der häufigsten Todesursachen weltweit. Es handelt sich dabei um eine Sauerstoffunterversorgung des Herzgewebes aufgrund eines thrombotischen Verschlusses in den Koronargefäßen. Dies führt zum Untergang von Kardiomyozyten, lebensbedrohlichen Arrhythmien und bis hin zum Herzversagen. Ursache ist meist die Eruption einer atherosklerotischen Plaque, die sich über längere Zeit asymptomatisch entwickelt hat. Risikofaktoren hierfür sind ein generell ungesunder Lebensstil, aber auch psychosoziale Stresssituationen erhöhen die Gefahr eines Herzinfarktes. Behandlungsstrategien zielen dabei auf eine möglichst schnelle Reperfusion ab, jedoch kann dadurch, aufgrund von metabolischen Imbalancen, der Schaden noch zusätzlich potenziert und die verursachte Nekrose verstärkt werden. Diese löst eine mehrphasige Reaktion aus, bei der es zunächst zu einer starken Entzündung kommt, die im Folgenden in ein Reifungsstadium und schließlich in die Narbenbildung übergeht. Der gesamte Vorgang dieses Remodelings ist komplexer Prozess des Immunsystems, der einer sehr engen Regulation bedingt, um die Herzfunktion möglichst aufrecht zu erhalten. Als besonders wichtig dabei werden neutrophile Granulozyten, Makrophagen und T Lymphozyten beschrieben. Trotz intensiver Forschung auf dem Gebiet des Myokardinfarktes, gibt es kaum Daten zu den Effekten eines gestörten Abwehrsystems, wie es in immuninkompetenten Personen, beispielsweise nach Organtransplantation, der Fall ist.

Das Ziel dieser Arbeit war es daher diese Lücke zu schließen und die möglichen Folgen einer Immunsuppression auf die Heilung und Narbenbildung zu untersuchen. Hierfür wurde mittels perkutaner transluminaler Koronarangioplastie (PTCA) ein Infarktmodell mit anschließender Reperfusion in transgenen Schweinen nachgebildet. Diese exprimierten ubiquitär ein Fusionsprotein, das sogenannte LEA29Y, das zu einer Blockade der Kostimulation während der T-Zellaktivierung führte und in Patienten nach Nieren- oder Herztransplantation unter dem Namen Belatacept als Medikament eingesetzt wird. Die Experimente wurden im Hinblick auf funktionelle und histologische Aspekte, sowie den in der

Zirkulation vorhandenen Immunzellen zu verschiedenen Zeitpunkten nach MI untersucht und mit den Ergebnissen von Wildtypen verglichen.

Dabei zeigte sich eine deutliche T-Zellanergie in den transgenen Tieren, die charakterisiert war durch fehlende oder verringerte Differenzierung, Proliferation und Zytokinsekretion. Hinzu kam die Unfähigkeit zur Migration aus den Gefäßen in das geschädigte Gewebe, welche außerdem bei Monozyten beobachtet werden konnte. Dies führte zu einer signifikant reduzierten Pumpfunktion bei LEA29Y Schweinen nach 72 Stunden. An Tag 9 war diese jedoch nicht mehr nachweisbar und auch die zu diesem Zeitpunkt beginnende Narbenbildung war nicht beeinträchtigt. Stattdessen schien das Immunsystem verschiedene Kompensationsmechanismen zum Ausgleich der gestörten T-Lymphozytenaktivierung auszubilden, was die Komplexität dieses Netzwerkes an verschiedenen Kaskaden, Zellen und Molekülen verdeutlichte.

Zusammenfassend lässt sich sagen, dass die katheterbasierte Induktion eines MI in LEA29Y transgenen Schweinen ein translationales Modell darstellt, um Heilungsvorgänge in immunsupprimierten Patienten abzubilden und mit den Untersuchungsergebnisse die weitere Herzinfarktforschung zu unterstützen.

VIII. INDEX OF FIGURES

IX. INDEX OF TABLES

X. REFERENCES

Albl B, Haesner S, Braun-Reichhart C, Streckel E, Renner S, Seeliger F, Wolf E, Wanke R, Blutke A. Tissue Sampling Guides for Porcine Biomedical Models. Toxicol Pathol 2016; 44: 414-20.

Alegre M-L, Frauwirth KA, Thompson CB. T-cell regulation by CD28 and CTLA-4. Nature Reviews Immunology 2001; 1: 220-8.

Aleman K, Noordzij JG, de Groot R, van Dongen JJ, Hartwig NG. Reviewing Omenn syndrome. Eur J Pediatr 2001; 160: 718-25.

Alsheikh MM, Alsheikh AM. Risk of Myocardial Infarction in HIV Patients: A Systematic Review. Cureus 2022; 14: e31825.

Anzai A, Anzai T, Nagai S, Maekawa Y, Naito K, Kaneko H, Sugano Y, Takahashi T, Abe H, Mochizuki S, Sano M, Yoshikawa T, Okada Y, Koyasu S, Ogawa S, Fukuda K. Regulatory role of dendritic cells in postinfarction healing and left ventricular remodeling. Circulation 2012; 125: 1234-45.

Anzai A, Choi JL, He S, Fenn AM, Nairz M, Rattik S, McAlpine CS, Mindur JE, Chan CT, Iwamoto Y, Tricot B, Wojtkiewicz GR, Weissleder R, Libby P, Nahrendorf M, Stone JR, Becher B, Swirski FK. The infarcted myocardium solicits GM-CSF for the detrimental oversupply of inflammatory leukocytes. J Exp Med 2017; 214: 3293-310.

Appleman LJ, Boussiotis VA. T cell anergy and costimulation. Immunol Rev 2003; 192: 161-80.

Arakawa K, Yasuda S, Hao H, Kataoka Y, Morii I, Kasahara Y, Kawamura A, Ishibashi-Ueda H, Miyazaki S. Significant association between neutrophil aggregation in aspirated thrombus and myocardial damage in patients with ST-segment elevation acute myocardial infarction. Circ J 2009; 73: 139-44.

Badimon L, Vilahur G. Thrombosis formation on atherosclerotic lesions and plaque rupture. J Intern Med 2014; 276: 618-32.

Baechli C, Koch D, Bernet S, Gut L, Wagner U, Mueller B, Schuetz P, Kutz A. Association of comorbidities with clinical outcomes in patients after acute myocardial infarction. Int J Cardiol Heart Vasc 2020; 29: 100558.

Bähr A, Käser T, Kemter E, Gerner W, Kurome M, Baars W, Herbach N, Witter K, Wünsch A, Talker SC, Kessler B, Nagashima H, Saalmüller A, Schwinzer R, Wolf E, Klymiuk N. Ubiquitous LEA29Y Expression Blocks T Cell Co-Stimulation but Permits Sexual Reproduction in Genetically Modified Pigs. PLoS One 2016; 11: e0155676.

Bähr A, Hornaschewitz N, Kupatt C. Myocardial Infarction in Pigs. Methods Mol Biol 2021; 2158: 43-50.

Bajpai G, Bredemeyer A, Li W, Zaitsev K, Koenig AL, Lokshina I, Mohan J, Ivey B, Hsiao HM, Weinheimer C, Kovacs A, Epelman S, Artyomov M, Kreisel D, Lavine KJ. Tissue Resident CCR2- and CCR2+ Cardiac Macrophages Differentially Orchestrate Monocyte Recruitment and Fate Specification Following Myocardial Injury. Circ Res 2019; 124: 263-78.

Barakat K, Wilkinson P, Deaner A, Fluck D, Ranjadayalan K, Timmis A. How should age affect management of acute myocardial infarction? A prospective cohort study. Lancet 1999; 353: 955-9.

Bentzon JF, Otsuka F, Virmani R, Falk E. Mechanisms of plaque formation and rupture. Circ Res 2014; 114: 1852-66.

Binder C, Cvetkovski F, Sellberg F, Berg S, Paternina Visbal H, Sachs DH, Berglund E, Berglund D. CD2 Immunobiology. Front Immunol 2020; 11: 1090.

Bolad IA. ST-Segment Elevation Myocardial Infarction in Dialysis and Renal

Transplant Patients. How Does It Compare to That in the General Population? Am J Nephrol 2016; 44: 327-8.

Bonilla FA, Oettgen HC. Adaptive immunity. J Allergy Clin Immunol 2010; 125: S33-40.

Bou-Gharios G, Ponticos M, Rajkumar V, Abraham D. Extra-cellular matrix in vascular networks. Cell Prolif 2004; 37: 207-20.

Braunwald E, Kloner RA. The stunned myocardium: prolonged, postischemic ventricular dysfunction. Circulation 1982; 66: 1146-9.

Briggs JD. Causes of death after renal transplantation. Nephrol Dial Transplant 2001; 16: 1545-9.

Brložnik M, Likar Š, Krvavica A, Avbelj V, Domanjko Petrič A. Wireless body sensor for electrocardiographic monitoring in dogs and cats. J Small Anim Pract 2019; 60: 223-30.

Cadenas S, Aragonés J, Landázuri MO. Mitochondrial reprogramming through cardiac oxygen sensors in ischaemic heart disease. Cardiovasc Res 2010; 88: 219-28.

Cahill TJ, Choudhury RP, Riley PR. Heart regeneration and repair after myocardial infarction: translational opportunities for novel therapeutics. Nat Rev Drug Discov 2017; 16: 699-717.

Camacho P, Fan H, Liu Z, He JQ. Large Mammalian Animal Models of Heart Disease. J Cardiovasc Dev Dis 2016; 3

Cameron JS, Gaide MS, Goad PL, Altman CB, Cuevas J, Myerburg RJ, Bassett AL. Enhanced adverse electrophysiologic effects of histamine after myocardial infarction in guinea pigs. J Pharmacol Exp Ther 1985; 232: 480-4.

Canto JG, Rogers WJ, Goldberg RJ, Peterson ED, Wenger NK, Vaccarino V, Kiefe CI, Frederick PD, Sopko G, Zheng ZJ. Association of age and sex with myocardial infarction symptom presentation and in-hospital mortality. Jama 2012; 307: 813-22.

Cavagnaro J, Silva Lima B. Regulatory acceptance of animal models of disease to support clinical trials of medicines and advanced therapy medicinal products. Eur J Pharmacol 2015; 759: 51-62.

Chapman AR, Adamson PD, Shah ASV, Anand A, Strachan FE, Ferry AV, Lee KK, Berry C, Findlay I, Cruikshank A, Reid A, Gray A, Collinson PO, Apple F, McAllister DA, Maguire D, Fox KAA, Vallejos CA, Keerie C, Weir CJ, Newby DE, Mills NL. High-Sensitivity Cardiac Troponin and the Universal Definition of Myocardial Infarction. Circulation 2020; 141: 161-71.

Chen L, Flies DB. Molecular mechanisms of T cell co-stimulation and co-inhibition. Nat Rev Immunol 2013; 13: 227-42.

Chen L, Li S, Zhu J, You A, Huang X, Yi X, Xue M. Mangiferin prevents myocardial infarction-induced apoptosis and heart failure in mice by activating the Sirt1/FoxO3a pathway. J Cell Mol Med 2021; 25: 2944-55.

Choi YJ, Lee K, Park WJ, Kwon DN, Park C, Do JT, Song H, Cho SK, Park KW, Brown AN, Samuel MS, Murphy CN, Prather RS, Kim JH. Partial loss of interleukin 2 receptor gamma function in pigs provides mechanistic insights for the study of human immunodeficiency syndrome. Oncotarget 2016; 7: 50914-26.

Choi YJ, Kim E, Reza A, Hong K, Song H, Park C, Cho SK, Lee K, Prather RS, Kim JH. Recombination activating gene-2(null) severe combined immunodeficient pigs and mice engraft human induced pluripotent stem cells differently. Oncotarget 2017; 8: 69398-407.

Chong JJ, Yang X, Don CW, Minami E, Liu YW, Weyers JJ, Mahoney WM, Van Biber B, Cook SM, Palpant NJ, Gantz JA, Fugate JA, Muskheli V, Gough GM,

Vogel KW, Astley CA, Hotchkiss CE, Baldessari A, Pabon L, Reinecke H, Gill EA, Nelson V, Kiem HP, Laflamme MA, Murry CE. Human embryonic-stem-cell-derived cardiomyocytes regenerate non-human primate hearts. Nature 2014; 510: 273-7.

Chou CH, Hung CS, Liao CW, Wei LH, Chen CW, Shun CT, Wen WF, Wan CH, Wu XM, Chang YY, Wu VC, Wu KD, Lin YH. IL-6 trans-signalling contributes to aldosterone-induced cardiac fibrosis. Cardiovasc Res 2018; 114: 690-702.

Choy JS, Zhang ZD, Pitsillides K, Sosa M, Kassab GS. Longitudinal hemodynamic measurements in swine heart failure using a fully implantable telemetry system. PLoS One 2014; 9: e103331.

Coillard A, Segura E. In vivo Differentiation of Human Monocytes. Front Immunol 2019; 10: 1907.

Corrales-Medina VF, Madjid M, Musher DM. Role of acute infection in triggering acute coronary syndromes. Lancet Infect Dis 2010; 10: 83-92.

Corrales-Medina VF, Alvarez KN, Weissfeld LA, Angus DC, Chirinos JA, Chang CC, Newman A, Loehr L, Folsom AR, Elkind MS, Lyles MF, Kronmal RA, Yende S. Association between hospitalization for pneumonia and subsequent risk of cardiovascular disease. Jama 2015; 313: 264-74.

Crespo J, Sun H, Welling TH, Tian Z, Zou W. T cell anergy, exhaustion, senescence, and stemness in the tumor microenvironment. Curr Opin Immunol 2013; 25: 214-21.

Curato C, Slavic S, Dong J, Skorska A, Altarche-Xifró W, Miteva K, Kaschina E, Thiel A, Imboden H, Wang J, Steckelings U, Steinhoff G, Unger T, Li J. Identification of noncytotoxic and IL-10-producing CD8+AT2R+ T cell population in response to ischemic heart injury. J Immunol 2010; 185: 6286-93.

Dal Canto E, Ceriello A, Rydén L, Ferrini M, Hansen TB, Schnell O, Standl E, Beulens JW. Diabetes as a cardiovascular risk factor: An overview of global trends of macro and micro vascular complications. Eur J Prev Cardiol 2019; 26: 25-32.

Daseke MJ, 2nd, Valerio FM, Kalusche WJ, Ma Y, DeLeon-Pennell KY, Lindsey ML. Neutrophil proteome shifts over the myocardial infarction time continuum. Basic Res Cardiol 2019; 114: 37.

De Groot D, Slieker R, Van Loo P, Verheij E, Lorentsen H, Laursen M, Markert M, Masse F, Bouwens F. Integrative Wireless Monitoring of Minipigs. Newsletter 2012; 38: 11-7.

De Villiers C, Riley PR. Mouse models of myocardial infarction: comparing permanent ligation and ischaemia-reperfusion. Dis Model Mech 2020; 13

DeBerge M, Glinton K, Subramanian M, Wilsbacher LD, Rothlin CV, Tabas I, Thorp EB. Macrophage AXL receptor tyrosine kinase inflames the heart after reperfused myocardial infarction. J Clin Invest 2021; 131

Dewey M, Siebes M, Kachelrieß M, Kofoed KF, Maurovich-Horvat P, Nikolaou K, Bai W, Kofler A, Manka R, Kozerke S, Chiribiri A, Schaeffter T, Michallek F, Bengel F, Nekolla S, Knaapen P, Lubberink M, Senior R, Tang MX, Piek JJ, van de Hoef T, Martens J, Schreiber L. Clinical quantitative cardiac imaging for the assessment of myocardial ischaemia. Nat Rev Cardiol 2020; 17: 427-50.

Deutsches Zentrum für Herz- Kreislauf- Forschung e.V. https://dzhk.de/herz-kreislauf-erkrankungen/herz-kreislauf-erkrankungen/herzinfarkt/. 10.01.2023.

Du Toit E, Hofmann D, McCarthy J, Pineda C. Effect of levosimendan on myocardial contractility, coronary and peripheral blood flow, and arrhythmias during coronary artery ligation and reperfusion in the in vivo pig model. Heart 2001; 86: 81-7.

Ekelund U, Ward HA, Norat T, Luan J, May AM, Weiderpass E, Sharp SJ, Overvad K, Østergaard JN, Tjønneland A, Johnsen NF, Mesrine S, Fournier A, Fagherazzi G, Trichopoulou A, Lagiou P, Trichopoulos D, Li K, Kaaks R, Ferrari P, Licaj I, Jenab M, Bergmann M, Boeing H, Palli D, Sieri S, Panico S, Tumino R, Vineis P, Peeters PH, Monnikhof E, Bueno-de-Mesquita HB, Quirós JR, Agudo A, Sánchez MJ, Huerta JM, Ardanaz E, Arriola L, Hedblad B, Wirfält E, Sund M, Johansson M, Key TJ, Travis RC, Khaw KT, Brage S, Wareham NJ, Riboli E. Physical activity and all-cause mortality across levels of overall and abdominal adiposity in European men and women: the European Prospective Investigation into Cancer and Nutrition Study (EPIC). Am J Clin Nutr 2015; 101: 613-21.

Ertl G, Frantz S. Healing after myocardial infarction. Cardiovasc Res 2005; 66: 22-32.

Ertl G, Frantz S. Adverse cardiac remodeling: phosphoinositide 3-kinase, another unique factor in a multifactorial condition. Circulation 2012; 126: 2175-6.

Esensten JH, Helou YA, Chopra G, Weiss A, Bluestone JA. CD28 Costimulation: From Mechanism to Therapy. Immunity 2016; 44: 973-88.

Falk E. Pathogenesis of atherosclerosis. J Am Coll Cardiol 2006; 47: C7-12.

Frangogiannis NG, Youker KA, Rossen RD, Gwechenberger M, Lindsey MH, Mendoza LH, Michael LH, Ballantyne CM, Smith CW, Entman ML. Cytokines and the microcirculation in ischemia and reperfusion. J Mol Cell Cardiol 1998; 30: 2567-76.

Frank A, Bonney M, Bonney S, Weitzel L, Koeppen M, Eckle T. Myocardial ischemia reperfusion injury: from basic science to clinical bedside. Semin Cardiothorac Vasc Anesth 2012; 16: 123-32.

Furtado MB, Nim HT, Boyd SE, Rosenthal NA. View from the heart: cardiac fibroblasts in development, scarring and regeneration. Development 2016; 143: 387-97.

GBD 2017 Causes of Death Collaborators. Global, regional, and national age-sex-specific mortality for 282 causes of death in 195 countries and territories, 1980-2017: a systematic analysis for the Global Burden of Disease Study 2017. Lancet 2018; 392: 1736-88.

Gerner W, Talker SC, Koinig HC, Sedlak C, Mair KH, Saalmüller A. Phenotypic and functional differentiation of porcine αβ T cells: current knowledge and available tools. Mol Immunol 2015; 66: 3-13.

Giancaterino S, Lupercio F, Nishimura M, Hsu JC. Current and Future Use of Insertable Cardiac Monitors. JACC Clin Electrophysiol 2018; 4: 1383-96.

Giugliano GR, Giugliano RP, Gibson CM, Kuntz RE. Meta-analysis of corticosteroid treatment in acute myocardial infarction. Am J Cardiol 2003; 91: 1055-9.

Glanz K. Patient and public education for cholesterol reduction: a review of strategies and issues. Patient Educ Couns 1988; 12: 235-57.

Gomoll AW. Cardioprotection associated with preconditioning in the anesthetized ferret. Basic Res Cardiol 1996; 91: 433-43.

Gulati R, Behfar A, Narula J, Kanwar A, Lerman A, Cooper L, Singh M. Acute Myocardial Infarction in Young Individuals. Mayo Clin Proc 2020; 95: 136-56.

Gwechenberger M, Mendoza LH, Youker KA, Frangogiannis NG, Smith CW, Michael LH, Entman ML. Cardiac myocytes produce interleukin-6 in culture and in viable border zone of reperfused infarctions. Circulation 1999; 99: 546-51.

Halade GV, Kain V, Ingle KA. Heart functional and structural compendium of cardiosplenic and cardiorenal networks in acute and chronic heart failure pathology. Am J Physiol Heart Circ Physiol 2018; 314: H255-h67.

Hanes DW, Wong ML, Jenny Chang CW, Humphrey S, Grayson JK, Boyd WD, Griffiths LG. Embolization of the first diagonal branch of the left anterior descending coronary artery as a porcine model of chronic trans-mural myocardial infarction. J Transl Med 2015; 13: 187.

Hausenloy DJ, Yellon DM. Myocardial ischemia-reperfusion injury: a neglected therapeutic target. J Clin Invest 2013; 123: 92-100.

Hawkins P. Refining Housing, Husbandry and Care for Animals Used in Studies Involving Biotelemetry. Animals (Basel) 2014; 4: 361-73.

Heidt T, Courties G, Dutta P, Sager HB, Sebas M, Iwamoto Y, Sun Y, Da Silva N, Panizzi P, van der Laan AM, Swirski FK, Weissleder R, Nahrendorf M. Differential contribution of monocytes to heart macrophages in steady-state and after myocardial infarction. Circ Res 2014; 115: 284-95.

Heusch G, Boengler K, Schulz R. Inhibition of mitochondrial permeability transition pore opening: the Holy Grail of cardioprotection. Basic Res Cardiol 2010; 105: 151-4.

Heusch G, Skyschally A, Schulz R. The in-situ pig heart with regional ischemia/reperfusion - ready for translation. J Mol Cell Cardiol 2011; 50: 951-63.

Hilgendorf I, Gerhardt LM, Tan TC, Winter C, Holderried TA, Chousterman BG, Iwamoto Y, Liao R, Zirlik A, Scherer-Crosbie M, Hedrick CC, Libby P, Nahrendorf M, Weissleder R, Swirski FK. Ly-6Chigh monocytes depend on Nr4a1 to balance both inflammatory and reparative phases in the infarcted myocardium. Circ Res 2014; 114: 1611-22.

Hinkel R, Boekstegers P, Kupatt C. Adjuvant early and late cardioprotective therapy: access to the heart. Cardiovasc Res 2012; 94: 226-36.

Hirano A, Fujita J, Kanazawa H, Kawaguchi S, Handa N, Yamada Y, Okuda S,

Hishikawa S, Teratani T, Kunita S, Tohyama S, Seki T, Tabei R, Nakajima K, Kishino Y, Okada M, Okamoto K, Shimizu H, Kobayashi E, Fukuda K. Cryoinjury-induced acute myocardial infarction model and ameroid constrictor-induced ischemic heart disease model in adult micro-mini pigs for preclinical studies. Translational Medicine Communications 2017; 2: 1.

Hoffmann J, Fiser K, Weaver J, Dimmick I, Loeher M, Pircher H, Martin-Ruiz C, Veerasamy M, Keavney B, von Zglinicki T, Spyridopoulos I. High-throughput 13-parameter immunophenotyping identifies shifts in the circulating T-cell compartment following reperfusion in patients with acute myocardial infarction. PLoS One 2012; 7: e47155.

Hoffmann J, Shmeleva EV, Boag SE, Fiser K, Bagnall A, Murali S, Dimmick I, Pircher H, Martin-Ruiz C, Egred M, Keavney B, von Zglinicki T, Das R, Todryk S, Spyridopoulos I. Myocardial ischemia and reperfusion leads to transient CD8 immune deficiency and accelerated immunosenescence in CMV-seropositive patients. Circ Res 2015; 116: 87-98.

Hofmann U, Beyersdorf N, Weirather J, Podolskaya A, Bauersachs J, Ertl G, Kerkau T, Frantz S. Activation of CD4+ T lymphocytes improves wound healing and survival after experimental myocardial infarction in mice. Circulation 2012; 125: 1652-63.

Hofmann U, Frantz S. Role of T-cells in myocardial infarction. Eur Heart J 2016; 37: 873-9.

Holmes DR, Jr., Berger PB, Hochman JS, Granger CB, Thompson TD, Califf RM, Vahanian A, Bates ER, Topol EJ. Cardiogenic shock in patients with acute ischemic syndromes with and without ST-segment elevation. Circulation 1999; 100: 2067-73.

Holmes JW, Yamashita H, Waldman LK, Covell JW. Scar remodeling and transmural deformation after infarction in the pig. Circulation 1994; 90: 411-20.

Horckmans M, Ring L, Duchene J, Santovito D, Schloss MJ, Drechsler M, Weber C, Soehnlein O, Steffens S. Neutrophils orchestrate post-myocardial infarction healing by polarizing macrophages towards a reparative phenotype. Eur Heart J 2017; 38: 187-97.

Huang J, Guo X, Fan N, Song J, Zhao B, Ouyang Z, Liu Z, Zhao Y, Yan Q, Yi X, Schambach A, Frampton J, Esteban MA, Yang D, Yang H, Lai L. RAG1/2 knockout pigs with severe combined immunodeficiency. J Immunol 2014; 193: 1496-503.

Ibanez B, Fuster V, Jiménez-Borreguero J, Badimon JJ. Lethal myocardial reperfusion injury: a necessary evil? Int J Cardiol 2011; 151: 3-11.

Ibanez B, James S, Agewall S, Antunes MJ, Bucciarelli-Ducci C, Bueno H, Caforio ALP, Crea F, Goudevenos JA, Halvorsen S, Hindricks G, Kastrati A, Lenzen MJ, Prescott E, Roffi M, Valgimigli M, Varenhorst C, Vranckx P, Widimský P. 2017 ESC Guidelines for the management of acute myocardial infarction in patients presenting with ST-segment elevation: The Task Force for the management of acute myocardial infarction in patients presenting with ST-segment elevation of the European Society of Cardiology (ESC). Eur Heart J 2018; 39: 119-77.

Iqbal MA, Hong K, Kim JH, Choi Y. Severe combined immunodeficiency pig as an emerging animal model for human diseases and regenerative medicines. BMB Rep 2019; 52: 625-34.

Ishida M, Miyagawa S, Saito A, Fukushima S, Harada A, Ito E, Ohashi F, Watabe T, Hatazawa J, Matsuura K, Sawa Y. Transplantation of Human-induced Pluripotent Stem Cell-derived Cardiomyocytes Is Superior to Somatic Stem Cell Therapy for Restoring Cardiac Function and Oxygen Consumption in a Porcine Model of Myocardial Infarction. Transplantation 2019; 103: 291-8.

Ishikawa K, Watanabe S, Hammoudi N, Aguero J, Bikou O, Fish K, Hajjar RJ. Reduced longitudinal contraction is associated with ischemic mitral regurgitation after posterior MI. Am J Physiol Heart Circ Physiol 2018; 314: H322-h9.

Itoh M, Mukae Y, Kitsuka T, Arai K, Nakamura A, Uchihashi K, Toda S, Matsubayashi K, Oyama JI, Node K, Kami D, Gojo S, Morita S, Nishida T, Nakayama K, Kobayashi E. Development of an immunodeficient pig model allowing long-term accommodation of artificial human vascular tubes. Nat Commun 2019; 10: 2244.

James MJ, Belaramani L, Prodromidou K, Datta A, Nourshargh S, Lombardi G, Dyson J, Scott D, Simpson E, Cardozo L, Warrens A, Szydlo RM, Lechler RI, Marelli-Berg FM. Anergic T cells exert antigen-independent inhibition of cell-cell interactions via chemokine metabolism. Blood 2003; 102: 2173-9.

Jin Y, Kang EH, Brill G, Desai RJ, Kim SC. Cardiovascular (CV) Risk after Initiation of Abatacept versus TNF Inhibitors in Rheumatoid Arthritis Patients with and without Baseline CV Disease. J Rheumatol 2018; 45: 1240-8.

Jugdutt BI. The dog model of left ventricular remodeling after myocardial infarction. J Card Fail 2002; 8: S472-5.

Kang EH, Jin Y, Brill G, Lewey J, Patorno E, Desai RJ, Kim SC. Comparative Cardiovascular Risk of Abatacept and Tumor Necrosis Factor Inhibitors in Patients With Rheumatoid Arthritis With and Without Diabetes Mellitus: A Multidatabase Cohort Study. J Am Heart Assoc 2018; 7

Kassab GS. The coronary vasculature and its reconstruction. Ann Biomed Eng 2000; 28: 903-15.

Kawaguchi M, Takahashi M, Hata T, Kashima Y, Usui F, Morimoto H, Izawa A, Takahashi Y, Masumoto J, Koyama J, Hongo M, Noda T, Nakayama J, Sagara J, Taniguchi S, Ikeda U. Inflammasome activation of cardiac fibroblasts is essential for myocardial ischemia/reperfusion injury. Circulation 2011; 123: 594-604.

Keller K, Hobohm L, Schmitt VH, Engelhardt M, Wenzel P, Post F, Münzel T, Gori T, Friedmann-Bette B. Total numbers and in-hospital mortality of patients with myocardial infarction in Germany during the FIFA soccer world cup 2014. Sci

Rep 2021; 11: 11330.

Kevin LG, Camara AK, Riess ML, Novalija E, Stowe DF. Ischemic preconditioning alters real-time measure of O2 radicals in intact hearts with ischemia and reperfusion. Am J Physiol Heart Circ Physiol 2003; 284: H566-74.

Kim JH, Chung HS, Antonisamy P, Lee SR, Bae H. Cardioprotective effect of rhizomes of Acorus gramineus against isoproterenol-induced cardiac damage in pigs. Cardiovasc Toxicol 2014; 14: 183-92.

Klatt N, Scherschel K, Schad C, Lau D, Reitmeier A, Kuklik P, Muellerleile K, Yamamura J, Zeller T, Steven D, Baldus S, Schäffer B, Jungen C, Eickholt C, Wassilew K, Schwedhelm E, Willems S, Meyer C. Development of nonfibrotic left ventricular hypertrophy in an ANG II-induced chronic ovine hypertension model. Physiol Rep 2016; 4

Klintmalm GB, Feng S, Lake JR, Vargas HE, Wekerle T, Agnes S, Brown KA, Nashan B, Rostaing L, Meadows-Shropshire S, Agarwal M, Harler MB, Garcia-Valdecasas JC. Belatacept-based immunosuppression in de novo liver transplant recipients: 1-year experience from a phase II randomized study. Am J Transplant 2014; 14: 1817-27.

Kloner RA, King KS, Harrington MG. No-reflow phenomenon in the heart and brain. Am J Physiol Heart Circ Physiol 2018; 315: H550-h62.

Kologrivova I, Shtatolkina M, Suslova T, Ryabov V. Cells of the Immune System in Cardiac Remodeling: Main Players in Resolution of Inflammation and Repair After Myocardial Infarction. Front Immunol 2021; 12: 664457.

Krug A, Du Mesnil de R, Korb G. Blood supply of the myocardium after temporary coronary occlusion. Circ Res 1966; 19: 57-62.

Kumar M, Kasala ER, Bodduluru LN, Dahiya V, Sharma D, Kumar V, Lahkar M.

Animal models of myocardial infarction: Mainstay in clinical translation. Regul Toxicol Pharmacol 2016; 76: 221-30.

Larsen CP, Pearson TC, Adams AB, Tso P, Shirasugi N, Strobert E, Anderson D, Cowan S, Price K, Naemura J, Emswiler J, Greene J, Turk LA, Bajorath J, Townsend R, Hagerty D, Linsley PS, Peach RJ. Rational development of LEA29Y (belatacept), a high-affinity variant of CTLA4-Ig with potent immunosuppressive properties. Am J Transplant 2005; 5: 443-53.

Laske TG, Garshelis DL, Iaizzo PA. Big data in wildlife research: remote web-based monitoring of hibernating black bears. BMC Physiol 2014; 14: 13.

Laslett LJ, Alagona P, Jr., Clark BA, 3rd, Drozda JP, Jr., Saldivar F, Wilson SR, Poe C, Hart M. The worldwide environment of cardiovascular disease: prevalence, diagnosis, therapy, and policy issues: a report from the American College of Cardiology. J Am Coll Cardiol 2012; 60: S1-49.

Latek R, Fleener C, Lamian V, Kulbokas E, 3rd, Davis PM, Suchard SJ, Curran M, Vincenti F, Townsend R. Assessment of belatacept-mediated costimulation blockade through evaluation of CD80/86-receptor saturation. Transplantation 2009; 87: 926-33.

Ledwoch J, Schneider A, Leidgschwendner K, Kraxenberger J, Krauth A, Schneider V, Martens E, Müller A, Laugwitz KL, Kupatt C. Diagnostic Accuracy of High-Sensitive Troponin for the Identification of Myocardial Infarction in Patients Presenting with Acute Heart Failure. J Emerg Med 2022; 62: 359-67.

Leonard WJ, Lin JX, O'Shea JJ. The γ(c) Family of Cytokines: Basic Biology to Therapeutic Ramifications. Immunity 2019; 50: 832-50.

Li RK, Weisel RD, Mickle DA, Jia ZQ, Kim EJ, Sakai T, Tomita S, Schwartz L, Iwanochko M, Husain M, Cusimano RJ, Burns RJ, Yau TM. Autologous porcine heart cell transplantation improved heart function after a myocardial infarction. J Thorac Cardiovasc Surg 2000; 119: 62-8.

Liang S, Zhang J, Ning R, Du Z, Liu J, Batibawa JW, Duan J, Sun Z. The critical role of endothelial function in fine particulate matter-induced atherosclerosis. Part Fibre Toxicol 2020; 17: 61.

Libby P, Ridker PM, Hansson GK. Progress and challenges in translating the biology of atherosclerosis. Nature 2011; 473: 317-25.

Lindsey ML, Bolli R, Canty JM, Jr., Du XJ, Frangogiannis NG, Frantz S, Gourdie RG, Holmes JW, Jones SP, Kloner RA, Lefer DJ, Liao R, Murphy E, Ping P, Przyklenk K, Recchia FA, Schwartz Longacre L, Ripplinger CM, Van Eyk JE, Heusch G. Guidelines for experimental models of myocardial ischemia and infarction. Am J Physiol Heart Circ Physiol 2018; 314: H812-h38.

Lindsey ML, Brunt KR, Kirk JA, Kleinbongard P, Calvert JW, de Castro Brás LE, DeLeon-Pennell KY, Del Re DP, Frangogiannis NG, Frantz S, Gumina RJ, Halade GV, Jones SP, Ritchie RH, Spinale FG, Thorp EB, Ripplinger CM, Kassiri Z. Guidelines for in vivo mouse models of myocardial infarction. Am J Physiol Heart Circ Physiol 2021a; 321: H1056-h73.

Lindsey ML, de Castro Brás LE, DeLeon-Pennell KY, Frangogiannis NG, Halade GV, O'Meara CC, Spinale FG, Kassiri Z, Kirk JA, Kleinbongard P, Ripplinger CM, Brunt KR. Reperfused vs. nonreperfused myocardial infarction: when to use which model. Am J Physiol Heart Circ Physiol 2021b; 321: H208-h13.

Lontchi-Yimagou E, Sobngwi E, Matsha TE, Kengne AP. Diabetes mellitus and inflammation. Curr Diab Rep 2013; 13: 435-44.

Lozahic C, Maddock H, Sandhu H. Anti-cancer Therapy Leads to Increased Cardiovascular Susceptibility to COVID-19. Front Cardiovasc Med 2021; 8: 634291.

Ma Y, Yabluchanskiy A, Lindsey ML. Neutrophil roles in left ventricular remodeling following myocardial infarction. Fibrogenesis Tissue Repair 2013; 6: 11.

Macián F, Im SH, García-Cózar FJ, Rao A. T-cell anergy. Curr Opin Immunol 2004; 16: 209-16.

Makkar RR, Price MJ, Lill M, Frantzen M, Takizawa K, Kleisli T, Zheng J, Kar S, McClelan R, Miyamota T, Bick-Forrester J, Fishbein MC, Shah PK, Forrester JS, Sharifi B, Chen PS, Qayyum M. Intramyocardial injection of allogenic bone marrow-derived mesenchymal stem cells without immunosuppression preserves cardiac function in a porcine model of myocardial infarction. J Cardiovasc Pharmacol Ther 2005; 10: 225-33.

Manfroi WC, Peukert C, Berti CB, Noer C, Gutierres Dde A, Silva FT. Acute myocardial infarction: the first manifestation of ischemic heart disease and relation to risk factors. Arq Bras Cardiol 2002; 78: 392-5.

Manger PR, Siegel JM. Do all mammals dream? J Comp Neurol 2020; 528: 3198-204.

Manning AS, Hearse DJ. Reperfusion-induced arrhythmias: mechanisms and prevention. J Mol Cell Cardiol 1984; 16: 497-518.

Manolis AA, Manolis TA, Melita H, Manolis AS. Takotsubo Syndrome and Sudden Cardiac Death. Angiology 2023; 74: 105-28.

Markert M, Trautmann T, Krause F, Cioaga M, Mouriot S, Wetzel M, Guth BD. A new telemetry-based system for assessing cardiovascular function in group-housed large animals. Taking the 3Rs to a new level with the evaluation of remote measurement via cloud data transmission. J Pharmacol Toxicol Methods 2018; 93: 90-7.

Matsumoto K, Ogawa M, Suzuki J, Hirata Y, Nagai R, Isobe M. Regulatory T lymphocytes attenuate myocardial infarction-induced ventricular remodeling in mice. Int Heart J 2011; 52: 382-7.

McManus DD, Gore J, Yarzebski J, Spencer F, Lessard D, Goldberg RJ. Recent trends in the incidence, treatment, and outcomes of patients with STEMI and NSTEMI. Am J Med 2011; 124: 40-7.

Mehta AK, Gracias DT, Croft M. TNF activity and T cells. Cytokine 2018; 101: 14-8.

Mendis S, Thygesen K, Kuulasmaa K, Giampaoli S, Mähönen M, Ngu Blackett K, Lisheng L. World Health Organization definition of myocardial infarction: 2008-09 revision. Int J Epidemiol 2011; 40: 139-46.

Mensah GA, Moran AE, Roth GA, Narula J. The global burden of cardiovascular diseases, 1990-2010. Glob Heart 2014; 9: 183-4.

Milani-Nejad N, Janssen PM. Small and large animal models in cardiac contraction research: advantages and disadvantages. Pharmacol Ther 2014; 141: 235-49.

Miller V, Mente A, Dehghan M, Rangarajan S, Zhang X, Swaminathan S, Dagenais G, Gupta R, Mohan V, Lear S, Bangdiwala SI, Schutte AE, Wentzel-Viljoen E, Avezum A, Altuntas Y, Yusoff K, Ismail N, Peer N, Chifamba J, Diaz R, Rahman O, Mohammadifard N, Lana F, Zatonska K, Wielgosz A, Yusufali A, Iqbal R, Lopez-Jaramillo P, Khatib R, Rosengren A, Kutty VR, Li W, Liu J, Liu X, Yin L, Teo K, Anand S, Yusuf S. Fruit, vegetable, and legume intake, and cardiovascular disease and deaths in 18 countries (PURE): a prospective cohort study. Lancet 2017; 390: 2037-49.

Mitsis A, Gragnano F. Myocardial Infarction with and without ST-segment Elevation: a Contemporary Reappraisal of Similarities and Differences. Curr Cardiol Rev 2021; 17: e230421189013.

Mostofsky E, Chahal HS, Mukamal KJ, Rimm EB, Mittleman MA. Alcohol and Immediate Risk of Cardiovascular Events: A Systematic Review and Dose-Response Meta-Analysis. Circulation 2016; 133: 979-87.

Nahrendorf M, Swirski FK, Aikawa E, Stangenberg L, Wurdinger T, Figueiredo JL, Libby P, Weissleder R, Pittet MJ. The healing myocardium sequentially mobilizes two monocyte subsets with divergent and complementary functions. J Exp Med 2007; 204: 3037-47.

Newton K, Dixit VM. Signaling in innate immunity and inflammation. Cold Spring Harb Perspect Biol 2012; 4

Nielsen M, Andersson C, Gerds TA, Andersen PK, Jensen TB, Køber L, Gislason G, Torp-Pedersen C. Familial clustering of myocardial infarction in first-degree relatives: a nationwide study. Eur Heart J 2013; 34: 1198-203.

Notohamiprodjo S, Nekolla SG, Robu S, Villagran Asiares A, Kupatt C, Ibrahim T, Laugwitz KL, Makowski MR, Schwaiger M, Weber WA, Varasteh Z. Imaging of cardiac fibroblast activation in a patient after acute myocardial infarction using (68)Ga-FAPI-04. J Nucl Cardiol 2022; 29: 2254-61.

Okura H, Saga A, Soeda M, Miyagawa S, Sawa Y, Daimon T, Ichinose A, Matsuyama A. Intracoronary artery transplantation of cardiomyoblast-like cells from human adipose tissue-derived multi-lineage progenitor cells improve left ventricular dysfunction and survival in a swine model of chronic myocardial infarction. Biochem Biophys Res Commun 2012; 425: 859-65.

Ozen G, Pedro S, Michaud K. The Risk of Cardiovascular Events Associated With Disease-modifying Antirheumatic Drugs in Rheumatoid Arthritis. J Rheumatol 2021; 48: 648-55.

Pabst R. The pig as a model for immunology research. Cell Tissue Res 2020; 380: 287-304.

Panizzi P, Swirski FK, Figueiredo JL, Waterman P, Sosnovik DE, Aikawa E, Libby P, Pittet M, Weissleder R, Nahrendorf M. Impaired infarct healing in atherosclerotic mice with Ly-6C(hi) monocytosis. J Am Coll Cardiol 2010; 55: 1629-38.

Paradies G, Petrosillo G, Pistolese M, Di Venosa N, Federici A, Ruggiero FM. Decrease in mitochondrial complex I activity in ischemic/reperfused rat heart: involvement of reactive oxygen species and cardiolipin. Circ Res 2004; 94: 53-9.

Pedrinelli R, Ballo P, Fiorentini C, Denti S, Galderisi M, Ganau A, Germanò G, Innelli P, Paini A, Perlini S, Salvetti M, Zacà V. Hypertension and acute myocardial infarction: an overview. J Cardiovasc Med (Hagerstown) 2012; 13: 194-202.

Petrosillo G, Ruggiero FM, Di Venosa N, Paradies G. Decreased complex III activity in mitochondria isolated from rat heart subjected to ischemia and reperfusion: role of reactive oxygen species and cardiolipin. Faseb j 2003; 17: 714-6.

Potz BA, Scrimgeour LA, Pavlov VI, Sodha NR, Abid MR, Sellke FW. Extracellular Vesicle Injection Improves Myocardial Function and Increases Angiogenesis in a Swine Model of Chronic Ischemia. J Am Heart Assoc 2018; 7

Powell EJ, Cunnick JE, Tuggle CK. SCID pigs: An emerging large animal NK model. J Rare Dis Res Treat 2017; 2: 1-6.

Prabhu SD, Frangogiannis NG. The Biological Basis for Cardiac Repair After Myocardial Infarction: From Inflammation to Fibrosis. Circ Res 2016; 119: 91-112.

Ramos GC, van den Berg A, Nunes-Silva V, Weirather J, Peters L, Burkard M, Friedrich M, Pinnecker J, Abeßer M, Heinze KG, Schuh K, Beyersdorf N, Kerkau T, Demengeot J, Frantz S, Hofmann U. Myocardial aging as a T-cell-mediated phenomenon. Proc Natl Acad Sci U S A 2017; 114: E2420-e9.

Reimer KA, Lowe JE, Rasmussen MM, Jennings RB. The wavefront phenomenon of ischemic cell death. 1. Myocardial infarct size vs duration of coronary occlusion in dogs. Circulation 1977; 56: 786-94.

Ren J, Yu D, Wang J, Xu K, Xu Y, Sun R, An P, Li C, Feng G, Zhang Y, Dai X,

Zhao H, Wang Z, Han Z, Zhu H, Ding Y, You X, Liu X, Wu M, Luo L, Li Z, Yang YG, Hu Z, Wei HJ, Ge L, Hai T, Li W. Generation of immunodeficient pig with hereditary tyrosinemia type 1 and their preliminary application for humanized liver. Cell Biosci 2022; 12: 26.

Ribichini F, Ferrero V, Wijns W. Reperfusion treatment of ST-elevation acute myocardial infarction. Prog Cardiovasc Dis 2004; 47: 131-57.

Ritchie DM, Kelliher GJ, MacMillan A, Fasolak W, Roberts J, Mansukhani S. The cat as a model for myocardial infarction. Cardiovasc Res 1979; 13: 199-206.

Rittié L. Method for Picrosirius Red-Polarization Detection of Collagen Fibers in Tissue Sections. Methods Mol Biol 2017; 1627: 395-407.

Roffi M, Patrono C, Collet JP, Mueller C, Valgimigli M, Andreotti F, Bax JJ, Borger MA, Brotons C, Chew DP, Gencer B, Hasenfuss G, Kjeldsen K, Lancellotti P, Landmesser U, Mehilli J, Mukherjee D, Storey RF, Windecker S. 2015 ESC Guidelines for the management of acute coronary syndromes in patients presenting without persistent ST-segment elevation: Task Force for the Management of Acute Coronary Syndromes in Patients Presenting without Persistent ST-Segment Elevation of the European Society of Cardiology (ESC). Eur Heart J 2016; 37: 267-315.

Romagnuolo R, Masoudpour H, Porta-Sánchez A, Qiang B, Barry J, Laskary A, Qi X, Massé S, Magtibay K, Kawajiri H, Wu J, Valdman Sadikov T, Rothberg J, Panchalingam KM, Titus E, Li RK, Zandstra PW, Wright GA, Nanthakumar K, Ghugre NR, Keller G, Laflamme MA. Human Embryonic Stem Cell-Derived Cardiomyocytes Regenerate the Infarcted Pig Heart but Induce Ventricular Tachyarrhythmias. Stem Cell Reports 2019; 12: 967-81.

Rudd CE, Taylor A, Schneider H. CD28 and CTLA-4 coreceptor expression and signal transduction. Immunol Rev 2009; 229: 12-26.

Sakaguchi G, Sakakibara Y, Tambara K, Lu F, Premaratne G, Nishimura K,

Komeda M. A pig model of chronic heart failure by intracoronary embolization with gelatin sponge. Ann Thorac Surg 2003; 75: 1942-7.

Sawada Y, Mashima E, Saito-Sasaki N, Nakamura M. The Role of Cell Adhesion Molecule 1 (CADM1) in Cutaneous Malignancies. Int J Mol Sci 2020; 21

Saxena A, Dobaczewski M, Rai V, Haque Z, Chen W, Li N, Frangogiannis NG. Regulatory T cells are recruited in the infarcted mouse myocardium and may modulate fibroblast phenotype and function. Am J Physiol Heart Circ Physiol 2014; 307: H1233-42.

Schwartz RH. T cell anergy. Annu Rev Immunol 2003; 21: 305-34.

Shapouri-Moghaddam A, Mohammadian S, Vazini H, Taghadosi M, Esmaeili SA, Mardani F, Seifi B, Mohammadi A, Afshari JT, Sahebkar A. Macrophage plasticity, polarization, and function in health and disease. J Cell Physiol 2018; 233: 6425-40.

Sharir R, Semo J, Shimoni S, Ben-Mordechai T, Landa-Rouben N, Maysel-Auslender S, Shaish A, Entin-Meer M, Keren G, George J. Experimental myocardial infarction induces altered regulatory T cell hemostasis, and adoptive transfer attenuates subsequent remodeling. PLoS One 2014; 9: e113653.

Sharma A, Gupta I, Venkatesh U, Singh AK, Golamari R, Arya P. E-cigarettes and myocardial infarction: A systematic review and meta-analysis. Int J Cardiol 2023; 371: 65-70.

Sharma D, Sharma N. A potential drug in the armamentarium of post-cardiac transplantation immunosuppression: belatacept. Indian J Thorac Cardiovasc Surg 2020; 36: 625-8.

Shi C, Jia T, Mendez-Ferrer S, Hohl TM, Serbina NV, Lipuma L, Leiner I, Li MO, Frenette PS, Pamer EG. Bone marrow mesenchymal stem and progenitor cells induce monocyte emigration in response to circulating toll-like receptor ligands.

Immunity 2011; 34: 590-601.

Shin HS, Shin HH, Shudo Y. Current Status and Limitations of Myocardial Infarction Large Animal Models in Cardiovascular Translational Research. Front Bioeng Biotechnol 2021; 9: 673683.

Silverman HS, Pfeifer MP. Relation between use of anti-inflammatory agents and left ventricular free wall rupture during acute myocardial infarction. Am J Cardiol 1987; 59: 363-4.

Singh V, Cohen MG. Therapy in ST-elevation myocardial infarction: reperfusion strategies, pharmacology and stent selection. Curr Treat Options Cardiovasc Med 2014; 16: 302.

Sjaastad I, Grund F, Ilebekk A. Effects on infarct size and on arrhythmias by controlling reflow after myocardial ischaemia in pigs. Acta Physiol Scand 2000; 169: 195-201.

Skyschally A, Hagelschuer H, Kleinbongard P, Heusch G. Larger infarct size but equal protection by ischemic conditioning in septum and anterior free wall of pigs with LAD occlusion. Physiol Rep 2019; 7: e14236.

Smith-Garvin JE, Koretzky GA, Jordan MS. T cell activation. Annu Rev Immunol 2009; 27: 591-619.

Solomon DH, Avorn J, Katz JN, Weinblatt ME, Setoguchi S, Levin R, Schneeweiss S. Immunosuppressive medications and hospitalization for cardiovascular events in patients with rheumatoid arthritis. Arthritis Rheum 2006; 54: 3790-8.

Sundaram V, Rothnie K, Bloom C, Zakeri R, Sahadevan J, Singh A, Nagai T, Potts J, Wedzicha J, Smeeth L, Simon D, Timmis A, Rajagopalan S, Quint JK. Impact of comorbidities on peak troponin levels and mortality in acute myocardial infarction. Heart 2020; 106: 677-85.

Swirski FK, Nahrendorf M, Etzrodt M, Wildgruber M, Cortez-Retamozo V, Panizzi P, Figueiredo JL, Kohler RH, Chudnovskiy A, Waterman P, Aikawa E, Mempel TR, Libby P, Weissleder R, Pittet MJ. Identification of splenic reservoir monocytes and their deployment to inflammatory sites. Science 2009; 325: 612-6.

Swirski FK, Nahrendorf M. Cardioimmunology: the immune system in cardiac homeostasis and disease. Nat Rev Immunol 2018; 18: 733-44.

Szeto C, Lobos CA, Nguyen AT, Gras S. TCR Recognition of Peptide-MHC-I: Rule Makers and Breakers. Int J Mol Sci 2020; 22

Taams LS, Boot EP, van Eden W, Wauben MH. 'Anergic' T cells modulate the T-cell activating capacity of antigen-presenting cells. J Autoimmun 2000; 14: 335-41.

The World Health Organization. https://www.who.int/news-room/fact-sheets/detail/the-top-10-causes-of-death. 10.01.2023.

Théry C, Amigorena S. The cell biology of antigen presentation in dendritic cells. Curr Opin Immunol 2001; 13: 45-51.

Thygesen K, Alpert JS, White HD. Universal definition of myocardial infarction. J Am Coll Cardiol 2007; 50: 2173-95.

Thygesen K, Alpert JS, Jaffe AS, Chaitman BR, Bax JJ, Morrow DA, White HD. Fourth Universal Definition of Myocardial Infarction (2018). J Am Coll Cardiol 2018; 72: 2231-64.

Timmers L, Lim SK, Hoefer IE, Arslan F, Lai RC, van Oorschot AA, Goumans MJ, Strijder C, Sze SK, Choo A, Piek JJ, Doevendans PA, Pasterkamp G, de Kleijn DP. Human mesenchymal stem cell-conditioned medium improves cardiac function following myocardial infarction. Stem Cell Res 2011; 6: 206-14.

Timmis A, Townsend N, Gale C, Grobbee R, Maniadakis N, Flather M, Wilkins E,

Wright L, Vos R, Bax J, Blum M, Pinto F, Vardas P. European Society of Cardiology: Cardiovascular Disease Statistics 2017. Eur Heart J 2018; 39: 508-79.

van den Bos EJ, Mees BM, de Waard MC, de Crom R, Duncker DJ. A novel model of cryoinjury-induced myocardial infarction in the mouse: a comparison with coronary artery ligation. Am J Physiol Heart Circ Physiol 2005; 289: H1291-300.

van der Bijl P, Abou R, Goedemans L, Gersh BJ, Holmes DR, Jr., Ajmone Marsan N, Delgado V, Bax JJ. Left Ventricular Post-Infarct Remodeling: Implications for Systolic Function Improvement and Outcomes in the Modern Era. JACC Heart Fail 2020; 8: 131-40.

Vegh A, Papp JG, Parratt JR. Pronounced antiarrhythmic effects of preconditioning in anaesthetized dogs: is adenosine involved? J Mol Cell Cardiol 1995; 27: 349-56.

Vincenti F, Rostaing L, Grinyo J, Rice K, Steinberg S, Gaite L, Moal MC, Mondragon-Ramirez GA, Kothari J, Polinsky MS, Meier-Kriesche HU, Munier S, Larsen CP. Belatacept and Long-Term Outcomes in Kidney Transplantation. N Engl J Med 2016; 374: 333-43.

Waide EH, Dekkers JC, Ross JW, Rowland RR, Wyatt CR, Ewen CL, Evans AB, Thekkoot DM, Boddicker NJ, Serão NV, Ellinwood NM, Tuggle CK. Not All SCID Pigs Are Created Equally: Two Independent Mutations in the Artemis Gene Cause SCID in Pigs. J Immunol 2015; 195: 3171-9.

Wan E, Yeap XY, Dehn S, Terry R, Novak M, Zhang S, Iwata S, Han X, Homma S, Drosatos K, Lomasney J, Engman DM, Miller SD, Vaughan DE, Morrow JP, Kishore R, Thorp EB. Enhanced efferocytosis of apoptotic cardiomyocytes through myeloid-epithelial-reproductive tyrosine kinase links acute inflammation resolution to cardiac repair after infarction. Circ Res 2013; 113: 1004-12.

Wang TY, Zhang M, Fu Y, Armstrong PW, Newby LK, Gibson CM, Moliterno DJ, Van de Werf F, White HD, Harrington RA, Roe MT. Incidence, distribution, and prognostic impact of occluded culprit arteries among patients with non-ST-

elevation acute coronary syndromes undergoing diagnostic angiography. Am Heart J 2009; 157: 716-23.

Wang Y, Beydoun MA. The obesity epidemic in the United States--gender, age, socioeconomic, racial/ethnic, and geographic characteristics: a systematic review and meta-regression analysis. Epidemiol Rev 2007; 29: 6-28.

Watanabe M, Nakano K, Matsunari H, Matsuda T, Maehara M, Kanai T, Kobayashi M, Matsumura Y, Sakai R, Kuramoto M, Hayashida G, Asano Y, Takayanagi S, Arai Y, Umeyama K, Nagaya M, Hanazono Y, Nagashima H. Generation of interleukin-2 receptor gamma gene knockout pigs from somatic cells genetically modified by zinc finger nuclease-encoding mRNA. PLoS One 2013; 8: e76478.

Weirather J, Hofmann UD, Beyersdorf N, Ramos GC, Vogel B, Frey A, Ertl G, Kerkau T, Frantz S. Foxp3+ CD4+ T cells improve healing after myocardial infarction by modulating monocyte/macrophage differentiation. Circ Res 2014; 115: 55-67.

Weiss A, Manger B, Imboden J. Synergy between the T3/antigen receptor complex and Tp44 in the activation of human T cells. J Immunol 1986; 137: 819-25.

Wekerle T, Grinyó JM. Belatacept: from rational design to clinical application. Transpl Int 2012; 25: 139-50.

Wikenheiser DJ, Stumhofer JS. ICOS Co-Stimulation: Friend or Foe? Front Immunol 2016; 7: 304.

Woulfe KC, Wilson CE, Nau S, Chau S, Phillips EK, Zang S, Tompkins C, Sucharov CC, Miyamoto SD, Stauffer BL. Acute isoproterenol leads to age-dependent arrhythmogenesis in guinea pigs. Am J Physiol Heart Circ Physiol 2018; 315: H1051-h62.

Xiong Q, Ye L, Zhang P, Lepley M, Swingen C, Zhang L, Kaufman DS, Zhang J.

Bioenergetic and functional consequences of cellular therapy: activation of endogenous cardiovascular progenitor cells. Circ Res 2012; 111: 455-68.

Yang Y, Gruwel ML, Dreessen de Gervai P, Sun J, Jilkina O, Gussakovsky E, Kupriyanov V. MRI study of cryoinjury infarction in pig hearts: i. Effects of intrapericardial delivery of bFGF/VEGF embedded in alginate beads. NMR Biomed 2012; 25: 177-88.

Yokota T, McCourt J, Ma F, Ren S, Li S, Kim TH, Kurmangaliyev YZ, Nasiri R, Ahadian S, Nguyen T, Tan XHM, Zhou Y, Wu R, Rodriguez A, Cohn W, Wang Y, Whitelegge J, Ryazantsev S, Khademhosseini A, Teitell MA, Chiou PY, Birk DE, Rowat AC, Crosbie RH, Pellegrini M, Seldin M, Lusis AJ, Deb A. Type V Collagen in Scar Tissue Regulates the Size of Scar after Heart Injury. Cell 2020; 182: 545-62.e23.

Yoshimura C, Nagasaka A, Kurose H, Nakaya M. Efferocytosis during myocardial infarction. J Biochem 2020; 168: 1-6.

Yuan J, Kihara T, Kimura N, Yamasaki T, Yoshida M, Isozaki K, Ito A, Hirota S. CADM1 promotes adhesion to vascular endothelial cells and transendothelial migration in cultured GIST cells. Oncol Lett 2022; 23: 86.

Yusuf S, Hawken S, Ounpuu S, Dans T, Avezum A, Lanas F, McQueen M, Budaj A, Pais P, Varigos J, Lisheng L. Effect of potentially modifiable risk factors associated with myocardial infarction in 52 countries (the INTERHEART study): case-control study. Lancet 2004; 364: 937-52.

Zhang T, Zhang Y, Cui M, Jin L, Wang Y, Lv F, Liu Y, Zheng W, Shang H, Zhang J, Zhang M, Wu H, Guo J, Zhang X, Hu X, Cao CM, Xiao RP. CaMKII is a RIP3 substrate mediating ischemia- and oxidative stress-induced myocardial necroptosis. Nat Med 2016; 22: 175-82.

Zhao H, Ye W, Guo J, Wang J, Jiao D, Xu K, Yang C, Chen S, Jamal MA, Bai Z, Wei T, Cai J, Nguyen TD, Qing Y, Cheng W, Jia B, Li H, Zhao HY, Chen Q, Wei

HJ. Development of RAG2 (-/-) IL2Rγ (-/Y) immune deficient FAH-knockout miniature pig. Front Immunol 2022; 13: 950194.

Zweier JL, Flaherty JT, Weisfeldt ML. Direct measurement of free radical generation following reperfusion of ischemic myocardium. Proc Natl Acad Sci U S A 1987; 84: 1404-7.

XI. ACKNOWLEDGEMENTS

First, I would like to thank Prof. Dr. Eckhard Wolf for accepting this external thesis and hosting me as a guest scientist at the Chair for Molecular Animal Breeding and Biotechnology, LMU Munich.

I would also like to thank Prof. Dr. Christian Kupatt for the opportunity to do my doctoral thesis in his group at the department of Internal Medicine I at the Klinikum rechts der Isar, TU Munich. This offered me the opportunity to experience the field of first-class research and to develop personally in it.

Sincere thanks to my mentor Dr. Andrea Bähr for introducing me to the field of preclinical research, her support and her personal understanding.

Thank you also to Prof. Dr. Nikolai Klymiuk for his scientific advice and input.

Further I would like to thank Dr. Wilhelm Gerner and his group for the great opportunity to analyse my PBMC samples at the Pirbright Institute, UK, as well as Prof. Andreas Parzefall (Institute for Veterinary Pathology, LMU Munich) and his team for their support with the histological examinations.

In this context also a big thanks to my colleague Martin Kraetzl (Chair for Molecular Animal Breeding and Biotechnology, LMU Munich) who provided me the analysis method for these and also to Maximilian Moraw (Klinikum rechts der Isar, TU Munich) who prepared all histological sections.

Thank you also to Lisa Oberberger for her help with the animal breeding and in general a thank you to all colleagues in our group, at the Moorversuchsgut, the ZPF and the German Heart Centre for the great working relationship with always an open ear and help.

Finally, I would like to sincerely thank my beloved family, my mum and all my friends for their continued encouragement and belief in me. My special thanks thereby is for my partner Maximilian who always supported me with his understanding, patience and a hug just at the right time.